MONASH University

EXPERIMENTAL AND SIMULATION STUDY ON PARTICLE CLUSTERING BEHAVIOR IN THE FAST FLUIDIZED BED

By

Dailin Chen

A THESIS SUBMITTED FOR THE DEGREE

OF

DOCTOR OF PHILOSOPHY

IN THELABORATORY FOR SIMULATION AND MODELLING OF PARTICULATE SYSTEMS, DEPARTMENT OF CHEMICAL ENGINEERING, MONASH UNIVERSITY, CLAYTON, VIC 3800, AUSTRALIA

August 2018

Contents

Abstract

Fast fluidized bed (FFB) is widely used in coal combustion and gasification, fluid catalytic cracking and Fischer-Tropsch synthesis due to its high efficiency in gas-solid reaction, heat and mass transfer. There have been extensive investigations regarding the fundamentals of gas-solid flow characteristics on fast fluidized bed. However, the lack of understanding on meso-scale structure, e.g. cluster behaviour in fast fluidized bed, especially for handling Geldart B particles, causes difficulties in design and optimization of fast fluidized bed systems. It is of paramount importance to understand the dynamics of the fast fluidized bed at a meso-scale and the repercussions of their behaviour for the overall system efficiency.

This study focuses on the investigation of cluster behaviour in fast fluidized bed through both experimental and numerical simulation approaches. A physical model of fast fluidized bed with the riser height of 3 meters and diameter of 100 mm was setup and a corresponding three dimensional numerical model was also developed within this study. The influences of operating conditions, including static bed height and superficial gas velocity on flow structure in fast fluidized bed were comprehensively studied. Five flow patterns in fast fluidized bed were distinguished, and the criterion and typical flow structures were proposed for categorising these flow patterns. The influences of superficial velocity and solid mass flux on solid volume fraction and gas-solid slip characteristics were also studied, revealing the relationship between the flow characteristics and the corresponding operating conditions. Moreover, based on the image and pressure analysis, typical flow patterns in high speed fluidization were characterised, and the fitting transition velocities for these patterns were developed.

The cluster measurement system which consists of cluster visualization system and fast fluidized bed system was established, and a software algorithm underpinned by MATLAB platform was developed to identify and measure particle clusters. Consequently, four types of particle cluster in the riser were observed; their characteristics, formation and evolution process were also investigated individually as well as the effects of operating conditions and particle characteristics on particle clusters properties.

A three-dimensional Eulerian-Lagrangian numerical model was established within this study by applying the multi-phase particle-in-cell (MP-PIC) methodology, the boundary conditions and simulation method were applied for fast fluidized bed handling Geldart B particles. The sensitivity of some crucial modelling parameters, such as grid resolution, the number of particles per parcel, the drag force model and the particle close pack volume fraction have been systematically analysed, and optimized. The full-loop numerical simulation of three-dimensional fast fluidized bed, including the riser, two-level cyclones, downer and J-type back-feeder was achieved.

The gas-solid flow characteristics of fast fluidized bed under different operating conditions were obtained by numerical simulation method. Three typical patterns of particle cluster in three-dimensional fast fluidized bed riser were captured by simulation method, and the cluster properties, i.e. solid volume fraction and velocity of particle cluster in the riser were characterised, which clearly illustrated the evolution process of particle cluster in the fast fluidized bed.

Acknowledgement

My thesis was completed under the joint support of Monash University and Southeast University in China. At this moment when l am approaching the end of the journey, there are many people to be acknowledged.

First and foremost, I would like to express my gratitude to my supervisor, Professor Aibing Yu at Monash University, for his continual guidance, invaluable support, remarkable patience, helpful feedback, and encouragement.

I would like to express my sincere thanks to my supervisor Professor Wenqi Zhong Southeast University in China for the support and guidance to establish this research project, for his patience, his encouragement and his help during my PhD study. I would also like to express my thanks to my co supervisor Professor Baosheng Jin.

My special gratitude goes to Dr. Ruiping Zou. I am very grateful for her patience in revising my work, continues support and encouragement during my study in Melbourne.

I would also like to thank my friends in SIMPAS and China, Xuejiao Liu, Ziwen Sun, Yingjuan Shao, Xi Chen, Guanwen Zhou, Jun Xie, Shangyi Yin, Li Ji, Yongli Wu, Shibo Kuang, Jieqing Gan, for their advice, help and friendship during my PhD study.

This work was supported by the National Key R&D Program of China (grant number 2016YFB0600802) and the National Natural Science Foundation of China [grant number 51390492, 51325601], ARC Hub for Computational Particle Science and Technology (Australian Research council, IHIH140100035)

Finally, I would like to thank my family, for their spiritual support and confidence in me, which has made me who I am. To my parents, my grandparents, my aunties and uncles and my boyfriend, thank you for your understanding and patience. It is you who support me throughout these years. Thank you for your unwavering belief in me which made it possible to finish this project.

COPYRIGHT NOTICE

I certify that I have made all reasonable efforts to secure copyright permissions for third-party content included in this thesis and have not knowingly added copyright content to my work without the owner's permission.

DECLARATION

This thesis contains no material which has been accepted for the award of any other degree or diploma at any university or equivalent institution and that, to the best of my knowledge and belief, this thesis contains no material previously published or written by another person, except where due reference is made in the text of the thesis.

Signature:

Print Name:

Date:

List of Figures

cluster:(c)H =1.5 m, u_g =5.28 m/s,G_s=57.5 kg/(m^{2}s),d_p=0.25 mm;(d)H =3.0 m, u_g =5.28 m/s,G_s=57.5 kg/(m^{2}s),d_p=0.25 mm.

Fig.6-23 Influence of average cross-sectional solid volume fraction on solid volume fraction of particle cluster: (a)H =1.5 m, u_g =5.28 m/s,G_s=57.5 kg/(m^{2}s),d_p=0.25 mm; (b)H =3.0 m, u_g =5.28 m/s,G_s=57.5 kg/(m^{2}s),d_p=0.25 mm.

List of Tables

Nomenclature

A_D area of downer, m^2

A_R area of riser, m^2

Ar Archimedes number

C negligible distance

C_D drag coefficient

D diameter of riser, m

D_p drag function

d_{cl} diameter of particle cluster, m

d_p diameter of particle, m

e particle-particle collision restitution coefficient

e_w particle-wall restitution coefficient

F rate of momentum exchange per volume between the gas and particle phases, (N/m^3s)

F_c cluster time fraction

G_s solid mass flux, $kg/(m^2s)$

h height, m

H height of riser, m

H_0 static bed height, m

I_{ave} average grayscale

I_c threshold grayscale

k turbulent kinetic energy, (m^2/s^2)

k_{cl} cluster identification factor

M_0 bed inventory, kg

p pressure drop, Pa

p_r total pressure drop in the riser, pa

Q gas flow rate, m^3/h

r radial position in the riser, m

R radius of the riser, m

t time, s

u_{ca} type A chocking velocity, m/s

u_g superficial gas velocity, m/s

u_{mp} the velocity corresponding to the minimum pressure drop, m/s

u_p superficial particle velocity, m/s

u_{tr} transition velocity in circulating fluidized bed, m/s

$u_{tr,f}$ the equivalent transition velocity of fluidized bed, m/s

V_g average superficial gas velocity, m/s

V_p average superficial particle velocity, m/s

V_{slip} apparent slip velocity, m/s

Greek symbols

β momentum exchange coefficient

ε volume fraction

ε_g gas volume fraction

ε_p particle volume fraction

ε_{cp} random close pack

ε_{tr} volume fraction at transition velocity

ε_p superficial solid volume fraction

μ_g viscosity of gas phase

μ_s viscosity of solid phase

μ_t viscosity of turbulent flow

λ_s bulk viscosity of solid phase

Φ average superficial slip factor

Θ granular temperature

ρ_g gas density, kg/m^{-3}

ρ_p particle density, kg/m^{-3}

τ_D collision damping time

τ_g gas stress tensor, N/m^2

τ_p particle normal stress, N/m^2

CHAPTER 1 Introduction

1.1 Introduction

Fast fluidized bed (FFB) is high efficient equipment widely used for gas-solid contact and mass and heat transfer. The study of fast fluidization starts from 1940s at the beginning of fluidization technology, which is used in industry for Sasol Fischer-Tropsch synthesis reactor from late 1950s[1]. As the fast fluidized bed offers a variety of economic and environmental advantages over conventional fluidized beds due to its strong gas-solid contacts, efficient mass and heat transfer and flexible operations, it has been widely used in many industries, e.g. petroleum, chemical, mineral, environmental and energy industries[2].

In the industrial application of fast fluidized bed, many problems are raised by the inhomogeneous of gas-solid flow caused by particle clusters, e.g. it is difficult to achieve uniform and ultrashort time contact between the oil gas and catalysts due to the severe inhomogeneous particle distribution and back-mixing in the catalytic cracking process[1]. In coal gasification industrial application, the core-annular structure in circulating fluidized bed leads to intensively momentum transfer between particles, which promotes the efficiency of the reactor [1]. Therefore, the understanding of gas-solid flow behaviour in fast fluidized bed is of significant importance.

Particle cluster was first proposed to study the high slip velocity in the gas-solid fluidized bed[4], refers to the aggregation of particles, which exists in many fluidization processes. Particle clusters can be observed in many fluidizing processes, including bubbling bed, riser and jets[5]. Particle clusters have significant influence on the gas-solid flow characteristics in fast fluidized bed, e.g. the particle mixing, entrainment and heat and mass transfer [6], which directly affects the gas-solid diffusion, axial and radial particle distribution, flow direction of particles. Thus the operating conditions of

fast fluidized bed are directly influenced by particle clusters. Therefore, an effective identification and enhanced understanding of evolutionary processes of particle cluster are crucial to the design, optimization, and operation of fast fluidized bed system[7]. Because of complexity in forming mechanism and difficulty in measure of particle clusters in the fast fluidized bed, it is still a very challenging issue in multiphase flow. so far, there is no unified definition and understanding of the structures and classification of particle clusters, and the profound study of the characteristics and evolutionary processes of particle clusters is still underdeveloped. Moreover, most of the models of particle clusters adopted in numerical simulation are empirical formulas, the understanding of the mechanism of particle cluster formation is still not clear.

1.2 Industrial application of fast fluidized bed

1.2.1 Coal combustion

Since the first industrial application of circulating fluidized (CFB) bed boiler in 1979, the CFB boiler has been widely used. Despite the advantages of the excellent adaptability to various fuel (e.g. different coals, biomass and wood), flexible operation and high efficiency in heat and mass transfer, the use of CFB boiler can ensure the sufficient combustion of fuel with low heat value and reduction of NO_x emissions and desulfurization cost, which is environmental friendly. Fig.1-1 is the schematic diagram of coal combustion of Foster Wheeler CFB boiler. The two stage air supply system is usually used in CFB boilers, the 40%-80% of the total air volume is provide by the primary air, while the secondary air provide about 20%-60% of the air, and the superficial gas velocity is approximately 5-10 m/s. The solid volume fraction under secondary air inlet is very high, and gas-solid flow is turbulent even bubbling

flow, while the gas-solid flows above that inlet usually are the fast fluidization or dilute phase flow.

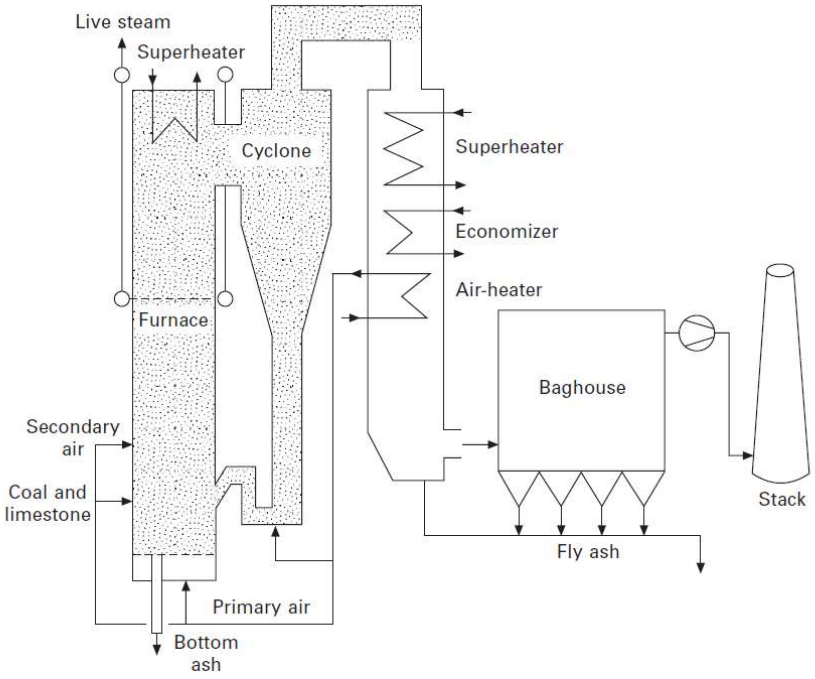

Fig.1-1Schematic of coal combustion of Foster Wheeler CFB boiler[2]

1.2.2Coal gasification

Coal gasification is an important way for efficient and clean utilization of coal, which converts the primary energy into clean secondary energy. The productions of coal gasification can provide (coal) gas, hydrogen and carbon monoxide. Due to the relative low efficiency of carbon conversion in conventional bubbling gasification reactor, the fast fluidized bed is increasing used in coal gasification. Higher efficiency of carbon conversion and better adaptability to various fuels can be achieved in fast fluidized bed. In recent years, the Integrated Gasification Combined Cycle (IGCC) is increasing popular because of its cost-effective and environmentFriendly characterises, Fig.1-2 is the flow chart of IGCC system.

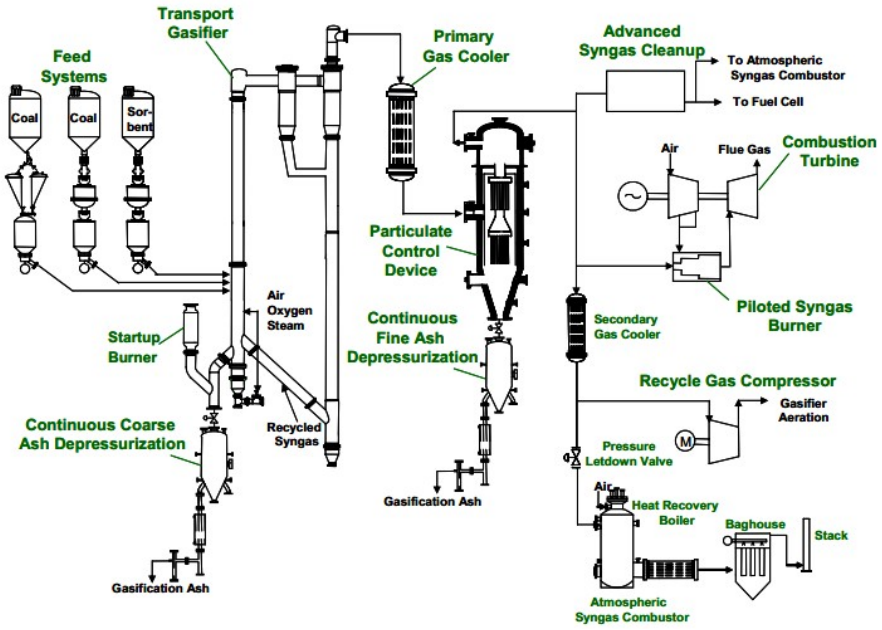

Fig.1-2Flow chart of IGCC system[2]

1.3 Objective of the research

1.2.1 Experimental work

The main object of the experiment work is to investigate flow structures and transition patterns in the fast fluidized bed handling Geldart B particle, and proposes the flow regime map of the fast fluidized bed. Moreover, characterize the influence of operating conditions and particle properties on the flow characteristics.

Meanwhile, the thesis is aim at establishing an accurate approach to identify and characterize the particle clusters in fast fluidized bed, and indicate the cluster structures and behaviours under different operating conditions.

1.2.2 Simulation work

The simulation work is aim at revealing the flow characteristics and cluster structure of a three-dimensional full-loop fast fluidized bed by MP-PIC method, and to investigate the evolutionary processes of the cluster behavior by simulation method.

1.4 Outline of the thesis

Based on the above analysis, the thesis has 7 chapters and the outline of each chapter is listed as follow:

Chapter 1 introduces the background of industrial application of fast fluidized bed, and the importance of this study on the flow behavior of fast fluidized bed, and the purpose of the present research.

Chapter 2 provides an in-depth literature review of the experimental study and numerical simulation on the flow structure and transitions in the fast fluidized bed and the cluster behavior within it, and summarized the research gaps of previous studies. The work has been published in J***ournal of Engineering Thermophysics***, 2015, 36(11): 2403-2406. (**catalogued by EI).**

Chapter 3conducted experiments in the flow patterns and transitions of a three-dimensional fast fluidized bed, and depicted a flow regime map in fast fluidized bed handling Geldart B particles. The influence of operating conditions on solid volume fraction and the gas-slip characteristics were discussed. The achievement has been published in *Chinese Journal of Chemical Engineering,* 2017, 25(9): 1153-1162.**(catalogued by SCI&EI, IF = 1.174)**

Chapter 4 established a visualization system and developed a binary image processing methodology to analyze identified particle clusters in the fast fluidized bed riser. Cluster characteristics including cluster structure, size and distribution feature were

discussed. Related work has been published in ***Canadian Journal of Chemical Engineering***, 2014, 92(6): 1150-1159. **(catalogued by SCI&EI, IF = 1.356)**.

Chapter 5 applied the Eulerian-Lagrangian approach based on MP-PIC method to simulate a fast fluidized bed with seal loop. The modelling parameters, including grid resolution, the number of particles per parcel, the drag model and the particle close pack volume fraction have been systematically analysed and optimized. The work has been published in ***10th World Congress of Chemical Engineering International Symposium on Spouted Beds***, Barcelona, Spain, 2017 and ***3rd International Symposium of Fluids and Thermal Engineering***,Ningbo, China, 2017.

Chapter 6 simulated the flow characteristics and cluster structure of a three-dimensional full-loop fast fluidized bed by MP-PIC method. The influence of operating conditionsincludingsuperficial gas velocity, seal loop aeration rate and their influences on the flow behavior was discussed. Moreover, the distribution of solid volume fraction and velocity of particle cluster were investigated. The work has been published in ***Journal of Chemical Industry and Engineering (China)***, 2018, 69(8):3443-3451. (**catalogued by EI).**

Chapter 7 concluded the whole work and discussed the strengths and limitation of the current research program, and recommendations for further study in the related area were provided.

CHAPTER 2Literature Review

As the application of fast fluidized bed is increasing popular in recent years, the research of its flow characteristics, especially for the meso-scale structure also increases. However, most of previous studies were conducted by Geldart A particles for chemical engineering, while the research on flow characteristics handling Geldart B particles is limited. Moreover, the understanding of structures and behavior of particle clusters in fast fluidized bed is still lacking. The research progress will consist with the experimental and modelling study on particle cluster behaviour in the fast fluidized bed.

2.1 Experimental study

The flow patterns and transition in fast fluidized bed is crucial to the industrial design of fast fluidized bed system. The flow characteristics of fast fluidized bed changes with operating condition, resulting in different residence and mixing time of the particles in the reactor and determines the efficiency and productivity of the reactor. A series studies on the flow characteristics have been carried out in recent years.

Bi et al.[8] study the flow regime transition and proposed a flow regime map with decreasing superficial gas velocity and constant solid mass flux, including homogeneous dilute-phase flow, core-annular dilute-phase flow and fast fluidization. Moreover, a flow regime maps are proposed with G_s/ρ_p and u_g. The homogeneous dilute-phase flow is the gas-solid flow with little axial particle gradient and no particle streamers in the wall region. The core-annular dilute flow is the gas-solid flow with low axial particle gradient and high radial voidage gradient. The fast fluidized regime is characterized by a concentration profile consisting of a dense bottom zone and dilute upper zone. The minimum pressure-drop point u_{mp} denotes the transition from

homogenous dilute flow to core-annular dilute flow, and the Type A choking velocity u_{ca} is used to define the transition from core-annular flow to fast fluidization.

$$u_{mp} = 10.1(gd_p)^{0.347}(G_s/\rho_g)^{0.310}(\frac{d_p}{D})^{-0.139}Ar^{-0.021} \quad (2\text{-}1)$$

$$\frac{u_{ca}}{\sqrt{gd_p}} = 21.6\,Ar^{0.105}(G_s/\rho_g u_{ca})^{0.542} \quad (2\text{-}2)$$

where ρ_g is the gas density (1.2kg/m^3), d_p is the average particle diameter and Ar is the Archimedes number.

Grace *et al.*[9] proposed the dense suspension upflow (DSU) as a new label for the flow regime of high-density circulating fluidized bed (HDCFB), using the dimensionally consistent equation for the onset of DSU:

$$u_{DSU} = 0.0113G_s^{1.192}\rho_g^{-1.064}(\mu_g g(\rho_p - \rho_g))^{-0.064} \quad (2\text{-}3)$$

where μ_g is gas viscosity.

Similarly, Gupta (1998)[10]proposed:

$$u_{fd} = 12.55\frac{\mu_g}{\rho_g d_p}(\frac{G_s}{u_t\rho_P})^{0.55}Ar^{0.36} \quad (2\text{-}4)$$

where u_t is particle terminal velocity.

Kim *et al.*[11]divided the fast fluidization regime into the fast transition region and fully developed fast fluidization region, and proposed a demarcation line between them. Kim et al.[12]considered the influence of height, and use u_p/u_t and $(u_g/\varepsilon)u_t$ to provide a demarcation between the flow regimes, where $(u_g/\varepsilon)u_t$is the ratio of average absolute gas velocity to the terminal particle velocity of particles. Fast fluidization is defined by net downflow at wall, dense suspension upflow is net upflow at wall and $\varepsilon_p \geq 0.07$ and the dilute pneumatic conveying is net upflow at wall and$\varepsilon_p < 0.07$.

As in Fig.2-4, boundary between the fast fluidization and the pneumatic transport regimes is:

$$\left(\frac{u_{PT}/\varepsilon}{u_t}\right) = 1160\left(\frac{G_s}{\rho_p \varepsilon_p u_t}\right)^{-0.9} Ar^{-0.20} \quad (2\text{-}5)$$

Boundary between DSU and the fast fluidization is:

$$\left(\frac{u_{DSU}/\varepsilon}{u_t}\right) = 22.8\left(\frac{G_s}{\rho_p \varepsilon_g u_t}\right)^{0.59} Ar^{-0.20} (2\text{-}6)$$

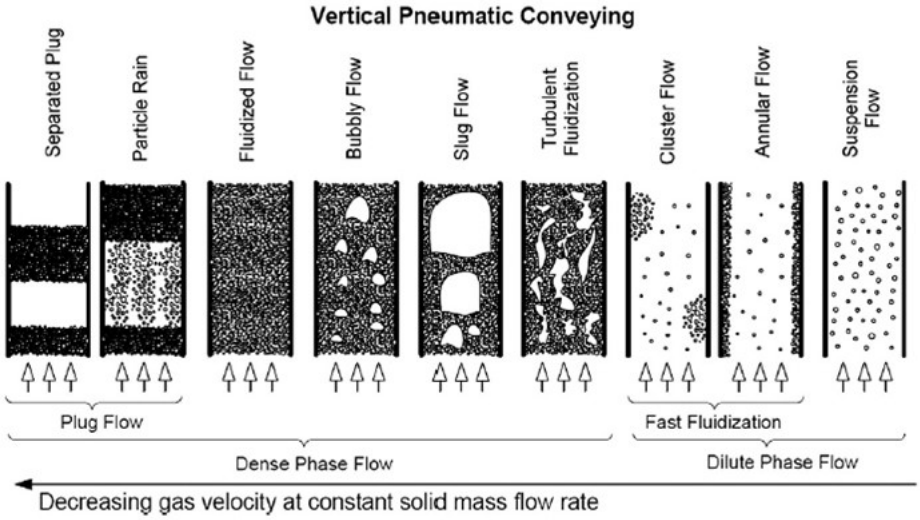

Fig.2-1 Flow regimes for vertical pneumatic conveying and fluidized bed systems.[13]

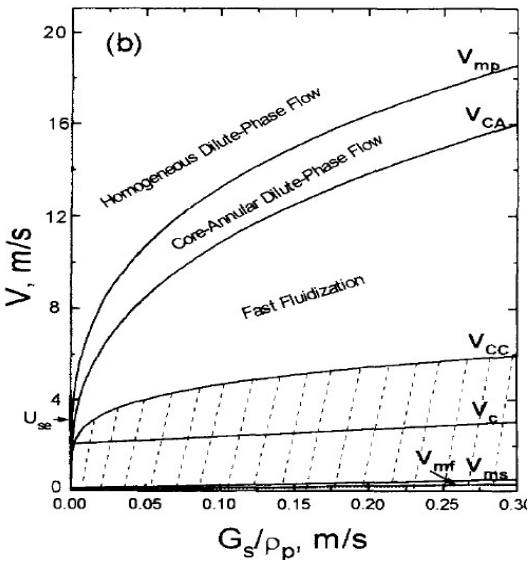

Fig.2-2 Flow regime map for Geldart A particles(Bi, 1995)[17].

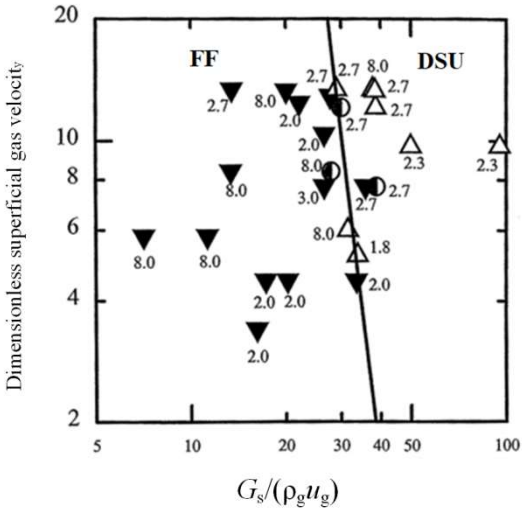

Fig.2-3 Dimensionless gas velocity vs. loading ratio for catalyst and sand particles(Grace, 1999)[9].

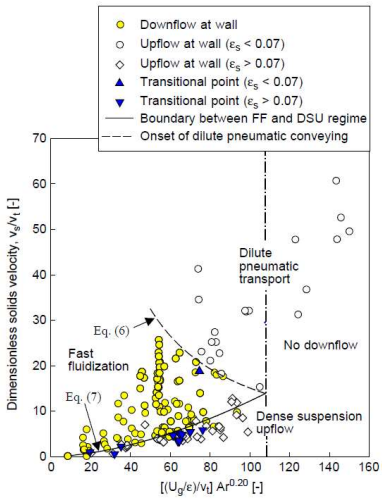

Fig.2-4 Flow regime map(Kim, 2004)[12].

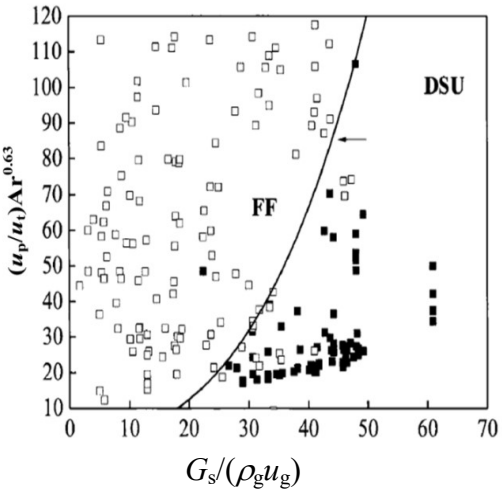

Fig.2-5 Flow regime map for circulating fluidized bed (Wang, 2013)[15].

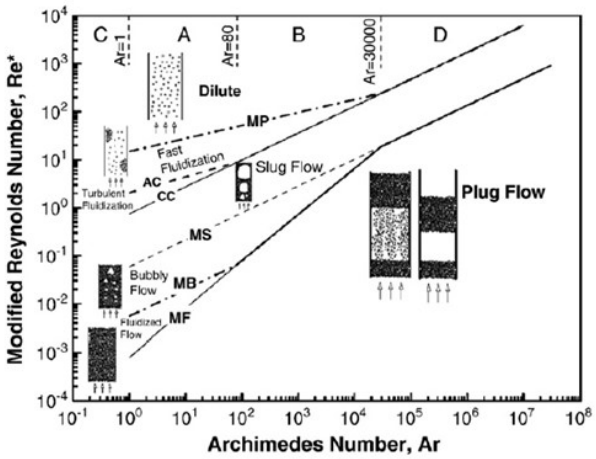

Fig.2-6 General flow regime diagram for vertical pneumatic conveying and fluidized bed system (Rabinovich, 2011)[13].

Rabinovich et al.[13]summarized the flow regimes for vertical pneumatic conveying and fluidized bed systems with various gas velocity, as in Fig.2-1, and divided the fast fluidization into cluster flow and annular flow.

Mahmoudi et al.[14]used Positron emission particle tracking (PEPT) to measure the velocity, residence time distribution, solid volume fraction and the flow pattern of particles. Four distinct flow regimes are defined for Geldart B particle in a circulating fluidized bed, i.e. Dilute riser flow (DRF), core-annulus flow (CAF), core-annulus flow

with turbulent fluidized bed at the bottom (CAF with TFBB) and dense riser upflow (DRU), and the flow regime map is depicted by u_g-u_{tr} and solid mass flux. Wang [15]adopted dimensionless velocity u_p/u_t, solid-gas ratio to divide the fast fluidization and DSU, as shown in Fig.2-5.

Anantharaman et al.[16] studied the effects of particle properties and operating conditions on the solid flow direction near the wall of the CFB riser with Geldart B particles, and the results have been compared with the regime maps proposed by Bi et al.[17], Grace et al.[9], Gupta et al.[10] and Kim et al.[12]. It is found that most regime classifications were proposed from the experimental results from Geldart A particles, so the discrepancies between prediction of previous regime map and experimental result for the Geldart B particles exist.

In the industrial application of fast fluidized bed, many problems are rised by the inhomogeneous of gas-solid flow caused by particle clusters, e.g. it is difficult to achieve uniform and ultrashort time contact between the oil gas and catalysts due to the severe inhomogeneous particle distribution and back-mixing in the catalytic cracking process [1]. Particle cluster is the aggregation of many particles, which has significant influence on the gas-solid flow characteristics in fast fluidized bed, e.g. the particle mixing, entrainment and heat and mass transfer [6]. The high slip velocity of particle cluster lower the carrying capacity of gas[18], decreasing the drag force in the circulating fluidized bed, which promotes the occurrence of core-annular flow in the riser[19, 20]. Therefore, the operating conditions of fast fluidized bed are directly influenced by particle clusters, and a comprehensive study of the particle cluster is crucial to the design, optimization, and operation of fast fluidized bed system[7].

The efficient identification and accurate characterization of particle clusters are the foundation of the study of cluster behaviour. In recent years, two methods have been used in measuring particle cluster properties are intrusive and non-intrusive method.

An intrusive method is use equipment such as capacitance probe, fiber optic probe to obtain simultaneous signals, and analyse characteristics of particle clusters, i.e. the size, velocity, solid volume fraction, frequency of the particle clusters by those signals[21-24].Soong et al.[22] proposed three characteristics to identify a cluster: (1) the solid volume fraction of particle cluster must be significantly above the average solid volume fraction at the same operating condition at the local position; (2) the fluctuation in solid volume fraction caused by particle cluster should be higher than the random fluctuation in background solid volume fraction; (3) the length of particle cluster should be larger than 100 particle diameters. The method utilizing the probe to obtain the simultaneous solid volume fraction and identify particle cluster is widely used[21][25, 26]. According to the first criterion, the simultaneous solid volume fraction of particle must be much higher than the average solid volume fraction, which can be expressed as n-times the standard deviation of the sampled signal over the local average solids volume fraction, i.e.$\varepsilon_c=\varepsilon_{ave}+ n\sigma$. Manyeleet al.[25]suggested that the optimal n value should between 1.0-1.4, while Xu et al.[26]used n=2.0. It is notable that the definition of particle cluster is crucial to the study of particle clustering behaviour. Therefore, Rudnick et al.[27] tried to discriminate the influence of definition of particle cluster. Yang et al.[28] distinguished the dense cluster from the gas void phase by the method of multiresolution analysis (MRA) of wavelet transform.

Non-intrusive method is to visualize the internal flow outside the system, and obtain the characteristics of particle clusters through image processing [19, 29-31]. The definition of particle cluster adopted in this method is also derived from the criterion proposed by

Soong *et al.*[22]. As the solid concentration in the cluster is higher than the average local solid holdup, the grayscale value of the cluster in the images is accordingly higher than the average local grayscale value. Lackermeier et al.[23]applied a high-speed video combined with the laser sheet to calculate the shape and velocity of particle cluster, similar identification method is adopted by Xu et al.[32]， Mondal et al.[30]to measure the size and velocity of particle cluster. Yang et al.[33] further proposed a relationship between solid volume fraction and the according image grayscale value, and separating the dense and dilute phase by a proper solid volume fraction thresholds to obtain the cluster size and volume fraction.

Based on different identification and characterization of particle clusters, many researches on structure and behaviour of particle cluster (e.g. size, time fraction and solid volume fraction of cluster) have been carried out. Various definitions of cluster structure have been proposed, according to the shape, size and appearance position of particle clusters. Bi et al.[34]group the particle aggregations into four categories: (1) particle cluster is refer to a group of particles aggregated in form of string, triangle and other shapes in the riser to reduce the effective drag force exerted on them; (2) particle streams refer to large clusters with dense cloud in stripe shape; (3) particle sheets are dense particle group falling near the wall region; (4) particle swarms are the particle aggregation at the dilute condition on the wall region. Shi et al.[7]classified the clusters into four kinds by the distance between particles and the shape and appearance position, i.e. micro-cluster , sparse cluster, core-annular cluster and compact cluster.

In the study on the particle cluster size, O'Brien et al.[35]suggested that the particle cluster is ten times large as a single particle. Guentheret al.[36] further confirmed that particle cluster is the aggregation of 10 to 20 particles. Cocco et al.[37] believed that particle clusters can exist on two scales: micro-clusters consisting of a few to 20 or

more particles, and macro-clusters made of hundreds of particles in the shape of sphere, strands or streamers. Mondal et al.[30] proposed that when particle diameter is 0.255mm, a large fraction of particles travel in cluster with width ranging around 5mm.

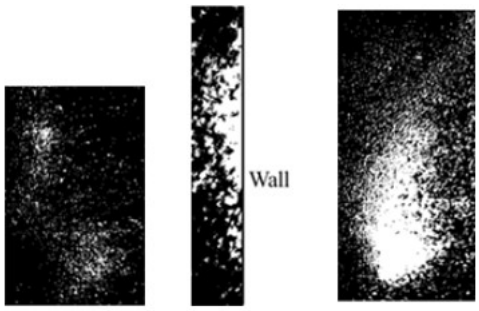

(a) (b) (c)

Fig.2-7 Classification of particle clusters (Shi, 2007)[7]:(a)sparse cluster; (b) core-annular cluster; (c) compact cluster.

Zou et al.[38] developed a simple particle cluster size distribution model with only one parameter, and introduce a novel roundness factor to describe the shape of the cluster.

Li et al.[39] studied the size distribution and behaviour of particle clusters in the fast fluidized by using optical fibre probes. The results showed that cluster velocity is in direct proportion to the superficial gas velocity and the averaged cluster velocity is larger at the centre than the near wall, moreover, the cluster velocity is larger in the lower dense zone than in the upper dilute zone. It is notable that most of the clusters in the wall region move downward. Li et al.[40] discussed the multi-scale characteristics of clusters in fast fluidized bed, proposing that cluster consists of many sub-clusters with different size and discrete particles. The particle clusters in a circulating fluidized bed with high gas velocity is much smaller than that in the conventional fluidized bed because of the strong collision between particle clusters.

Liu et al.[41] investigated the particle cluster properties including solid volume fraction, occurrence frequency, time fraction and velocity of particle clusters in a fluidizedbed with square cross-section of 0.1m×0.1m andheight of 2.4 mby phase Doppler particle

analyzer (PDPA). The axial and radial profiles of solid volume fraction and velocity of particle clusters are similar to those of discrete particle, respectively. The result showed that particle cluster properties are closely related to average solid volume fraction and turbulent fluctuation ofparticles. Liu et al.[20] proposed the capture mechanism of discrete particles into clusters and the shedding mechanism of particles from cluster.

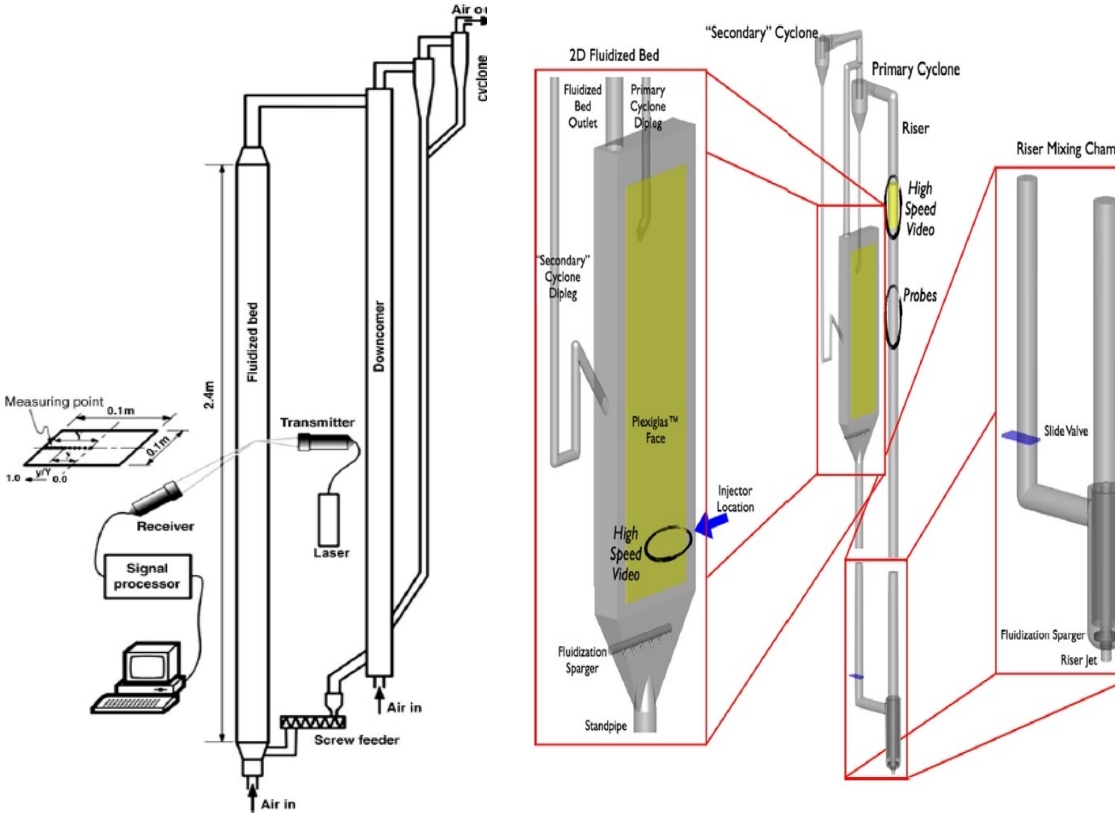

(a) (b)

Fig.2-8 (a) Schematic diagram of experimental equipment and measuring pointdistribution by Liu et al. [41]. (b)Schematic diagram of experimental equipment by McMillan et al.[5]

Particulate Solid Research, incorporated (PSRI), National Energy Technology Laboratory (NETL) carried out a series study on the formation mechanism and characteristics of particle clusters. Cocco et al.[37] studied the formation mechanism of particles by using a high-speed camera with a modified rigid boroscope. The results suggested that hydrodynamics may not be the only responsible for cluster formation,

while cohesive forces including electrostatics, capillary and van der Waalsforces, may play an important role in formation of particle clusters. Chew et al.[44, 45] studied the characteristics of particle clusters in a circulating fluidized bed with Geldart B particles, revealing the influence of riser position, operating condition and solid properties on the appearance probability, duration, and frequency of particle clusters. McMillan et al.[5]provided an insight to the nature of particle clustering, proposing that particle clustering in a fluidized bed may due to van der Waals or coulombic forces, likely assisted by the lack of momentum transfer to particlerotation. Moreover, the fluctuations and gradients in the hydrodynamic forces may be responsible for the particle clustering in the riser. Kiani et al.[24, 46]suggested that the size of particle cluster increases and their distributions becomes wider with increasing superficial gas velocity. Moreover, the larger particles tend to form large particle clusters, and the particle clusters in the centre are larger than those in the wall region.

2.2 Simulation study

The clusters in the core region of riser could not be observed directly by non-intrusive method due to the dense annulus particle layer at the wall, the understanding of clusters hydrodynamics properties is still lacking. The numerical simulation method is an important way to study the gas-solid flow behaviour in a complex dense gas-solid flow, which can effectively overcome the shortage of the existing experimental conditions and measurement, and simulate the flow structure and the details of the gas-solid flow. There are two primary modelling approaches for the typical fluidization system, consisting of Eulerian-Eulerian method and Eulerian-Lagrangian method. In two-fluid models (TFM), the gas and solid phase are both considered as continuous mediums, described in terms of separate sets of conservation equations and coupling by the

interaction terms between the gas and solid phase. It provides a convenient and simple method to calculate the gas-solid behaviour. However, the traditional TFM cannot provide detailed information of particle movement, the discrete character of solid phase at microscopic level lose due to its continuum assumptions.

The Eulerian-Lagrangian (EL) method treats particles as separate, solid objects and their behaviors are modeled by theNewtonian equations of motion. The traditional Eulerian-Lagrangian approach, CFD-DEM (computational fluid dynamics-discrete element method), can track each discrete particle and compute particle-particle collision. However, the high computational cost limits the application of this method in large dense solid gas flow system

Recently, another Eulerian-Lagrangian approach, MP-PIC method, has attracted much attention because of its specific advantages at the extremely efficient calculation. In MP-PIC scheme, the particle-particle collision is not calculated directly as CFD-DEM, but through the particle stress gradient based on the Eulerian grid. Meanwhile, the real particles are grouped into computational particles (parcel) each including one or a certain amount of particles with uniform size, density, velocity, etc. On the basis the computational particles, the dense gas-solid fluidization system at large scale can be analysed through a reasonable amount of particles.

Due to the limitation of computational resources and the complexities of flow characteristics in simulation of full loop circulating fluidized bed, most the early simulations of fast fluidized bed are conducted by the riser part or separate structure. However, as the downer maintain the pressure balance and realize a self-equilibrium of the loop[47], thus the simulation result from separated part of the circulating fluidized bed may be quite different from the experimental results. The simulation of full-loop fast fluidized bed could capture the flow behaviour of the whole circulation

system efficiently and obtain detail information of gas-solid flow[48], which has got widely attention recently. Moreover, with the development of computing capability and the improvement of simulation method, more and more studies have been proposed on flow behaviour of fast fluidized bed by full-loop simulation method.

Zhang et al.[48] simulated the three-dimensional (3D) full-loop CFB by Eulerian granular multiphase model with a drag coefficient correction based on the energy-minimization multi-scale (EMMS) model, deriving the flow regime diagram for air-FCC system. Nikolopoulos et al.[49] and Lu et al.[52] simulated the small scale CFB carbonator and industrial scale circulating fluidized bed, indicating that the drag model can well predict the pressure distribution and solid mass flux of circulating fluidized bed.The axial and radial distribution of solid volume fraction and velocity of particle cluster can be achieved, and capture the particle clustering and evolutionary processes. However, Lu et al.[52] suggested that the EMMS model was proposed in limited operating conditions, which may underestimate the drag force in industrial-scale circulating fluidized bed.

Guan et al.[53] simulated a 3D full loop interconnected fluidized bedconsists of a riser, a bubbling bed, a cyclone and a loop-seal. The effects of operating gas velocity, particle sizeand bed inventory on the solids mass flux are investigated.

Wang[47, 54] studied the gas solid flow characteristics in a CFB with a loop seal, and the influence of operating conditions, i.e. loop seal aeration rate, superficial gas velocity and bed inventory on the solid circulation characteristics (e.g. solid mass flux and packing height).Ma et al.[55] predicted the main features of gas –solid flow in the riser in the 3D full loop HDCFB is qualitatively using MP-PIC method. Tu et al.[56]applied the CPFD method to investigate the flow characteristics of a complex CFB with six cyclones, and characterize different fluidization regimes. The results obtained from

EMMS drag model are compared with those obtained from Wen-Yu model. Wu et al.[57]applied the CPFD approach based on the MP-PICmethod to investigate the flow hydrodynamics and chemical reaction characteristicsin CFB riser reactors with Geldart A particles.

Luo et al.[61] investigated the pressure signals and solid back-mixing behaviour in a 3D full-loop CFB operating in fast fluidization (FF) anddilute phase transport (DPT) regimeby using the CFD-DEM coupling approach. Wang et al.[62]investigatedthe influence of cyclone arrangements on the gas-solid flow characteristics in the 3D full-loop CFB.Lu et al.[63] simulated a pilot scale CFB to demonstrate the accuracy, capability and efficiency of different simulation method.

Particle cluster is the most important characteristic in fast fluidization, significantly influences the gas-solid flow characteristics in fast fluidized bed, e.g. the particle mixing, entrainment and heat and mass transfer. Moreover, the formation of particle cluster decreases the drag force exert on the particles compared with that exerts on the single particle. Therefore, the influence of particle cluster on the drag coefficient should be considered.

Tsuo et al.[64] simulated the influence of superficial gas velocity, solid mass flux, particle size and the diameter of riser on the formation of particle cluster in the CFB by TFM. However, the effect of particle cluster on drag force is neglected. Gomez et al.[65, 66] characterized the particle cluster using MICEFLOW code based on the identification criterion proposed by Sharma et al.[21]. The simulated result underestimated the number of particle clusters, which suggest the operating conditions and the bed structures should be considered in the identification of particle clusters.

Lu et al.[67]develop a two-fluid model with cluster-based approach (CBA) which assumes that particles move as clusters in the riser to predict the hydrodynamics of

cluster flow in the circulating fluidized bed, and well predict the core-annular flow structure in the riser. Wang et al.[68]further developed the CBA with particle rotation and friction stress models. Lu et al.[69] introduced the closure equation for the dispersed particles in the dilute phase and clusters in the dense phase. The difference between the simulated and experimental flow behaviour were noticed, which may be explained by the deficiencies of mass transfer model for the particles in the dilute phase and the clusters in the dense phase and the interaction between the clusters and gas in the dilute phase. Chalermsinsuwan et al.[70] predicted the cluster size and solid volume fraction in the riser and downer. Agrawal et al.[71] suggested that coarse-grid simulation of gas-solid flow must include sub-grid models, accounting for the influences of the unresolved meso-scale structures.

Tsuji et al.[72] compared the simulation results of gas-solid flow in the riser based on DSMC (direct simulation Monte Carlo) method and two-fluid model, and found that the cluster number is larger in the DSMC method than in the two-fluid model. Moreover, the clusters size may increases with the riser size in DSMC method while disappear in the riser in two-fluid model. However, due to the limitation of computational sources, most of the previous studies were conducted in two dimensional riser. Ouyang et al.[73] adopted the particle-motion-resolved discrete model which can simulate bubbles and cluster formation to study the influence of operating conditions on cluster structure. Helland et al.[74, 75]studied the influences of different clusters on the gas–particle flow behaviour, i.e. dilute cluster(less than 3%–5% solids volume fraction) and dense cluster (more than 10% solids volume fraction),and proposed two possible combined drag laws which take both of these influence into consideration. The combined drag laws improve the discrepancies generally reported for CFD simulations of circulating fluidized beds concerning the correct estimation of

solid circulation rates. Zhang et al.[76] simulated the particle clustering behaviour in a riser/downer, demonstrating that the formation of clusters is influenced by many factors including operating conditions, particle properties and bed geometry. Zhao et al.[77] simulated the fully developed hydrodynamics of a riser and a downer in a 2D channel of 10cm in width. The results showed that particles are densely aggregated in the cluster in riser, while the clusters consist of loose packed particles in the downer. Lu et al.[52]well predicted the onset of the fluidization and the stable flow in CFB risers used in the experiment conducted by Horio et al.[78] using EMMS-based discrete particle method. Varas et al.[79]simulated the gas-solid flow in a pseudo-2D riser, well predicted the core-annular flow and other hydrodynamics parameters including frequency, solid volume fraction of particle clusters. However, the simulations overestimated the number of large clusters, and a better insight about the influence of drag force on cluster behaviour is needed.

Despite the DEM method, the direct simulation Monte Carlo (DSMC) method is also widely used to study the cluster behaviour in the fast fluidized bed. Tanaka et al.[80] investigated the unstable flow and the formation of cluster by DSMC method, a V-shaped cluster was observed. Wang et al.[81] suggested that the particles in the dilute phase exist individually, while the particles in the cluster phase are enmeshed to give various shapes and different sizes. Liu et al.[82] also simulated the hydrodynamics of gas-solid flow in the CFB by using Eulerian-Lagrangian approach, investigating the distributions of solid volume fraction and velocity of particle clusters. Simulated results showed that the upward clusters exhibits a horseshoe shape with a dense head and both dilute tails, while the downward cluster exhibits an inversed-V shape. Moreover, a low-pressure zone can be found between their tails. Liu et al.[83]investigated the influence of superficial gas velocity on the particle clusters characteristics (e.g. solid

volume fraction, velocity and frequency of particle clusters) in the wall region and in the centre of the riser. Berrouk et al.[84] discussed the severe disadvantage of the phase coupling scheme used in the context of a two-dimensional DPM. The two-phase coupling scheme presented by Liu et al.[82] underestimated the pressure drop and result in erroneous prediction of the minimum fluidization velocity. Capecelatro et al.[85]found that the simulation of two dimensional riser may lead to unphysical accumulation of particles due to the restriction of particle motion in a plane, which may lead to over predict in volume fraction and velocity fluctuations. The radial motion of particles to avoid falling clusters is increased in the riser.

2.3 Summary and research gaps

Increasing researches are being focus on the flow characteristics, especially for the particle clusters since 1990s. However, the understanding of flow characteristics in fast fluidized bed is insufficient, especially for the meso-scale structure, e.g. cluster behaviour in fast fluidized bed with Geldart B particles. As particle cluster in the most important characteristic in fast fluidization, the study of particle cluster covers various particle properties and numerous different operating conditions by intrusive or non-intrusive method. Nevertheless, the research the identification, structure and behaviour of particle cluster are still insufficient to provide the comprehensive basis for the design, operating and optimization of fast fluidized bed system. Basedon the literature review, several gaps have been identified as follows:

(1) The definitions of flow patterns in the fast fluidized bed are ambiguous, different definition are proposed based on various method, while the same flow pattern may be defined by different names. Nevertheless, most of the studies on the flow patterns and transitions are conducted by Geldart B particles, which are unable to predict the

gas-solid flow by Geldart B particles. Therefore, it is worthwhile to investigate the flow patterns and transitions in fast fluidized bed handling Geldart B particles.

(2) The measurement of particle clusters in fast fluidized bed is mainly conducted by intrusive method, which may introduce disturbance into the gas-solid flow. The accurate identification and characterization of particle clusters by non-intrusive method is in great request.

(3) The classification of particle cluster is ambiguous, various definitions of cluster structure have been proposed, according to the shape, size and appearance position of particle clusters. Moreover, the study of the evolutionary processes of particle cluster is still lacking and comprehensive and accurate understanding of formation mechanism of particle clusters is needed.

(4) Contradictory results have been obtained in the study on particle clustering behavior. Guenther *et al.* [36] found that cluster size increases with increasing solid mass flux, while Horio *et al*. [78] proposed that cluster sized decreases with higher solid mass flux. Moreover, the studies on the influence of riser position on the particle cluster also come to inverse conclusions [86, 87].

(5) Very few simulation studies on flow characteristics of fast fluidized bed are presented in three dimensional full loop fast fluidized bed systems, and most of the researches are for the Geldart B particles. Moreover, the influences of operating conditions on the flow characteristics need to be further revealed.

(6) The studies of particle clusters by Eulerian-Lagrangian method are mainly presented in two dimensional riser, and most of the result are qualitative prediction.

2.4 Reference

[1] Jin Y., Zhu J. Wang Z. W., et al.. Fluidization Engineering Principles [M]. Tsinghua University Press, 2001.

[2] Li X. X.,Shi Y. F.,Huang W.S. et al. Nonlinear Analysis of Gas-solid Flow behavior in fast fluidized bed riser [J]. *Journal of Chemical Industry and Engineering*.*China* **2004**, 55(2): 182-188.

[3] Duan F., Jin B. S., Huang Y. J. et al. Effect of Gasifying Agent Preheating Temperature on Pressurized Turbulent CFB Coal Gasification. *CIESC Journal***2009**, 60(12): 3112-3116.

[4] WilhelmRH, Kwauk M. Fluidization of solid particles[J].*ChemicalEngineering Progress***1948**, 44(3): 201-218.

[5] Mcmillan J, Shaffer F, Gopalan B, et al. Particle cluster dynamics during fluidization[J]. *Chemical Engineering Science***2013**, 100: 39-51.

[6] Chew J W, Hays R, Findlay J G, et al. Cluster characteristics of Geldart group B particles in a pilot-scale CFB riser. II. Polydisperse systems[J]. *Chemical Engineering Science***2012**, 68(1): 82-93.

[7] Shi H. Experimental research of flow structure in agas-solid circulating fluidized bed riser by PIV[J]. *Journal of Hydrodynamics, Ser. B***2007**, 19(6): 712-719.

[8] Bi H T, Grace J R. Flow regime diagrams for gas-solid fluidization and upward transport [J].*International journal of multiphase flow***1995**, 21(6): 1229-1236.

[9] Grace J R, Issangya A S, Bai D R, et al. Situating the high-density circulating fluidized bed[J]. *AIChE Journal***1999**, 45(10): 2108-2116.

[10] Gupta S K, Berruti F. Modeling considerations for large scale high density risers[M]. Fan L S, Knowlton T M, **1998**, 205-212.

[11] Kim S W, Namkung W, Kim S D. Solids flow characteristics in loop-seal of a circulating fluidized bed[J]. *Korean Journal of Chemical Engineering***1999**, 16(1): 82-88.

[12] Kim S W, Kirbas G, Bi H, et al. Flow behavior and regime transition in a high-density circulating fluidized bed riser[J]. *Chemical Engineering Science***2004**, 59(18): 3955-3963.

[13] Rabinovich E, Kalman H. Flow regime diagram for vertical pneumatic conveying and fluidized bed systems[J]. *Powder Technology***2011**, 207(1-3): 119-133.

[14] Mahmoudi S, Chan C W, Brems A, et al. Solids flow diagram of a CFB riser using Geldart B-type powders[J]. *Particuology***2012**, 10(1): 51-61.

[15] Wang S.D. Hydrodynamic Characteristics in Dense Transport Bed. [D].Beijing: Institute of Engineering Thermophysics, Chinese Academy of Sciences,**2012**.

[16] Anantharaman A, Issangya A, Karri S B R, et al. Annulus flow behavior of Geldart Group B particles in a pilot-scale CFB riser[J].*Powder Technology* **2017**, 305: 816-828.

[17] Bi H T, Grace J R. Flow regime diagrams for gas-solid fluidization and upward transport[J]. *International Journal of Multiphase Flow***1995**, 21(6): 1229-1236.

[18] Harris A T, Davidson J F, Thorpe R B. The prediction of particle cluster properties in the near wall region of a vertical riser [J]. *Powder Technology***2002**, 127(2): 128-143.

[19] Yang J, Zhu J. Cluster identification using image processing[J]. *Particuology***2015**, 23: 16-24.

[20] Liu X, Gao S, Song W, et al. Effect of particle acceleration/deceleration on particle clustering behavior in dilute gas-solid flow[J]. *Chemical Engineering Science***2006**, 61(21): 7087-7095.

[21] Sharma A K, Tuzla K, Matsen J, et al. Parametric effects of particle size and gas velocity on cluster characteristics in fast fluidized beds[J]. *Powder Technology***2000**, 111(1): 114-122.

[22] Soong C H, Tuzla K, Chen J C. Experimental determination of cluster size and velocity in circulating fluidized bed[M]. Fluidization Ⅷ, Large, JF, Laguerie, Ced; New York:Engineering Foundation, **1995**, 219-227.

[23] Lackermeier U, Rudnick C, Werther J, et al. Visualization of flow structures inside a circulating fluidized bed by means of laser sheet and image processing[J]. P*Powder Technology***2001,** 114(1-3): 71-83.

[24] Firuzian N, Sotudeh-Gharebagh R, Mostoufi N. Experimental investigation of cluster properties in dense gas-solid fluidized beds of different diameters[J]. *Particuology***2014**, 16: 69-74.

[25] Manyele S V, P Rssinen J H, Zhu J X. Characterizing particle aggregates in a high-density and high-flux CFB riser[J]. *Chemical Engineering Journal***2002**, 88(1): 151-161.

[26] Xu J, Zhu J. Visualization of particle aggregation and effects of particle properties on cluster characteristics in a CFB riser[J]. *Chemical Engineering Journal***2011**, 168(1): 376-389.

[27] Rudnick C, Werther J. The discrimination of cluster characteristics from fiber-optical probe signals in circulating fluidized beds[M]. Fan L S, Knowlton T M, **1998**, 573-580.

[28] Yang T, Leu L. Multiresolution Analysis on Identification and Dynamics of Clusters in a Circulating Fluidized Bed[J]. *AIChE Journal***2009**, 55(3): 612-629.

[29] Casleton D K, Shadle L J, Ross A A. Measuring the voidage of a CFB through image analysis[J]. *Powder Technology***2010**, 203(1): 12-22.

[30] Mondal D N, Kallio S, Saxen H. Length scales of solid clusters in a two-dimensional circulating fluidized bed of Geldart B particles[J]. *Powder Technology***2015**, 269: 207-218.

[31] Yang J, Zhu J. A novel method based on image processing to visualize clusters in a rectangular circulating fluidized bed riser[J]. *Powder Technology***2014**, 254: 407-415.

[32] Xu J, Zhu J. A New Method for the Determination of Cluster Velocity and Size in a Circulating Fluidized Bed[J]. *Industrial & Engineering Chemistry Research***2012**, 51(4): 2143-2151.

[33] Yang J, Zhu J. Cluster identification using image processing[J]. *Particuology***2015**, 23: 16-24.

[34] Bi X. T., Zhu J., Jin Y. et al., Forms of Particle Aggregation in CFB[C]. **1993**.

[35] O'Brien T J, Syamlal M. Particle cluster effects in the numerical simulation of a circulating fluidized bed[M]. Preprint Volume for Circulating Fluidized Beds Ⅳ, 1993.

[36] Guenther C, Breault R. Wavelet analysis to characterize cluster dynamics in a circulating fluidized bed[J]. *Powder Technology* **2007**, 173(3): 163-173.

[37] Cocco R, Shaffer F, Hays R, et al. Particle clusters in and above fluidized beds[J]. *Powder Technology***2010**, 203(1): 3-11.

[38] Zou B, Li H Z, Xia Y S, et al. Cluster structure in a circulating fluidized bed [J]. *Powder Technology***1994**, 78(2): 173-178.

[39] Li H, Zhu Q, Liu H, et al. The cluster size distribution and motion behavior in a fast fluidized bed[J]. *Powder Technology***1995**, 84(3): 241-246.

[40] Li H. Multi-scale aggregation of particles in gas-solids fluid beds[J]. China *Particuology***2004**, 21(3): 101-106.

[41] Liu X, Gao S, Li J. Characterizing particle clustering behavior by PDPA measurement for dilute gas−solid flow[J]. *Chemical Engineering Journal***2005**, 108(3): 193-202.

[42] Cocco R, Shaffer F, Karri S B R. Particle clusters in fluidized beds: The 13th International Conference on Fluidization[Z]. 2010.

[43] Jia W C, Hays R, Findlay J G, et al. Species segregation of binary mixtures and a continuous size distribution of Group B particles in riser flow[J]. **2011**, 178: 348-358.

[44] Chew J W, Hays R, Findlay J G, et al. Cluster characteristics of Geldart Group B particles in a pilot-scale CFB riser. I. Monodisperse systems[J]. C*hemical Engineering Science***2012**, 68(1): 72-81.

[45] Chew J W, Hays R, Findlay J G, et al. Cluster characteristics of Geldart group B particles in a pilot-scale CFB riser. II. Polydisperse systems[J]. *Chemical Engineering Science* **2012**, 68(1): 82-93.

[46] Kiani A, Sotudeh-Gharebagh R, Mostoufi N. Cluster size distribution in the freeboard of a gas‐solid fluidized bed[J]. *Powder Technology***2013**, 246(Supplement C): 1-6.

[47] Wang Q, Yang H, Wang P, et al. Application of CPFD method in the simulation of a circulating fluidized bed with a loop seal, part I-Determination of modeling parameters[J]. *Powder Technology***2014**, 253: 814-821.

[48] Zhang N, Lu B, Wang W, et al. Virtual experimentation through 3D full-loop simulation of a circulating fluidized bed[J]. *Particuology***2008**, 6(6): 529-539.

[49] Nikolopoulos A, Nikolopoulos N, Charitos A, et al. High-resolution 3-D full-loop simulation of a CFB carbonator cold model[J]. *Chemical Engineering Science***2013**, 90: 137-150.

[50] Wang Q, Yang H, Wang P, et al. Application of CPFD method in the simulation of a circulating fluidized bed with a loop seal Part II-Investigation of solids circulation[J]. *Powder Technology***2014**, 253: 822-828.

[51] Wang Q, Yang H, Wang P, et al. Application of CPFD method in the simulation of a circulating fluidized bed with a loop seal, part I-Determination of modeling parameters[J]. *Powder Technology***2014**, 253: 814-821.

[52] Lu L, Xu J, Ge W, et al. EMMS-based discrete particle method (EMMS-DPM) for simulation of gas–solid flows[J]. *Chemical Engineering Science***2014**, 120: 67-87.

[53] Guan Y, Chang J, Zhang K, et al. Three-dimensional full loop simulation of solids circulation in an interconnected fluidized bed[J]. *Powder Technology***2016**, 289: 118-125.

[54] Wang Q, Yang H, Wang P, et al. Application of CPFD method in the simulation of a circulating fluidized bed with a loop seal Part II-Investigation of solids circulation[J]. *Powder Technology***2014**, 253: 822-828.

[55] Ma Q, Lei F, Xu X, et al. Three-dimensional full-loop simulation of a high-density CFB with standpipe aeration experiments[J]. *Powder Technology***2017**, 320: 574-585.

[56] Tu Q, Wang H. CPFD study of a full-loop three-dimensional pilot-scale circulating fluidized bed based on EMMS drag model[J]. *Powder Technology***2017**.

[57] Wu Y, Peng L, Qin L, et al. Validation and application of CPFD models in simulating hydrodynamics and reactions in riser reactor with Geldart A particles[J]. *Powder Technology***2018**, 323: 269-283.

[58] Alobaid F, Stroehle J, Epple B. Extended CFD/DEM model for the simulation of circulating fluidized bed[J]. *Advanced Powder Technology***2013**, 24(1): 403-415.

[59] Adamczyk W P, Kozolub P, Kruczek G, et al. Numerical approach for modeling particle transport phenomena in a closed loop of a circulating fluidized bed[J].*Particuology***2016**, 29: 69-79.

[60] Luo K, Wu F, Yang S, et al. High-fidelity simulation of the 3-D full-loop gas-solid flow characteristics in the circulating fluidized bed[J]. *Chemical Engineering Science* **2015**, 123: 22-38.

[61] Luo K, Wang S, Yang S, et al. Computational Fluid Dynamics-Discrete Element Method Investigation of Pressure Signals and Solid Back-Mixing in a Full-Loop Circulating Fluidized Bed[J]. *Industrial & Engineering Chemistry Research***2017**, 56(3): 799-813.

[62] Wang S, Luo K, Hu C, et al. CFD-DEM study of the effect of cyclone arrangements on the gas-solid flow dynamics in the full-loop circulating fluidized bed[J]. *Chemical Engineering Science***2017**, 172: 199-215.

[63] Lu L, Xu J, Ge W, et al. Computer virtual experiment on fluidized beds using a coarse-grained discrete particle method-EMMS-DPM[J]. *Chemical Engineering Science***2016**, 155: 314-337.

[64] Tsuo Y P, Gidaspow D. Computation of flow patterns in circulaitng fluidized beds [J]. *AIChE Journal***1990**, 36(6): 885-896.

[65] Cabezas-Gómez L, Da Silva R C, Navarro H A, et al. Cluster identification and characterization in the riser of a circulating fluidized bed from numerical simulation results[J]. *Applied Mathematical Modelling***2008**, 32(3): 327-340.

[66] Gomez L C, Milioli F E. A numerical simulation analysis of the effect of the interface drag function on cluster evolution in a CFB riser gas-solid flow[J]. *Brazilian Journal of Chemical Engineering* **2004**, 21(4): 569-583.

[67] Lu H L, Sun Q Q, He Y R, et al. Numerical study of particle cluster flow in risers with cluster-based approach[J]. *Chemical Engineering Science***2005**, 60(23): 6757-6767.

[68] Wang S Y, Shen Z H, Lu H L, et al. Numerical predictions of flow behavior and cluster size of particles in riser with particle rotation model and cluster-based approach[J]. *Chemical Engineering Science***2008**, 63(16): 4116-4125.

[69] Lu H L, Wang S Y, He Y R, et al. Numerical simulation of flow behavior of particles and clusters in riser using two granular temperatures[J]. *Powder Technology***2008**, 182(2): 282-293.

[70] Chalermsinsuwan B, Gidaspow D, Piumsomboon P. Comparisons of particle cluster diameter and concentration in circulating fluidized bed riser and downer using computational fluid dynamics simulation[J]. *Korean Journal of Chemical Engineering***2013**, 30(4): 963-975.

[71] Agrawal K, Loezos P N, Syamlal M, et al. The role of meso-scale structures in rapid gas-solid flows[J]. *Journal of Fluid Mechanics***2001**, 445: 151-185.

[72] Tsuiji Y, Tanaka T, Yonemura S. Cluster patterns in circulating fluidized beds predicted by numerical simualtion (discrete particle model versus two-fluid model)[J]. *Powder Technology***1998**, 95: 254-264.

[73] Jie O Y, Li J H. Discrete simulations of heterogeneous structure and dynamic behavior in gas-solid fluidization[J]. *Chemical Engineering Science***1999**, 54(22): 5427-5440.

[74] Helland E, Bournot H, Occelli R, et al. Drag reduction and cluster formation in a circulating fluidised bed[J]. *Chemical Engineering Science***2007**, 62(1-2): 148-158.

[75] Helland E, Occelli R, Tadrist L. Computational study of fluctuating motions and cluster structures in gas–particle flows[J]. *International Journal of Multiphase Flow***2002**, 28(2): 199-223.

[76] Zhang M H, Chu K W, Wei F, et al. A CFD–DEM study of the cluster behavior in riser and downer reactors[J]. *Powder Technolog.***2008**, 184(2): 151-165.

[77] Zhao Y, Cheng Y, Wu C, et al. Eulerian-Lagrangian simulation of distinct clustering phenomena and RTDs in riser and downer[J]. *Particuology*2010, 8(1SI): 44-50.

[78] Horio M, Ishii H, Nishimuro M. On the nature of turbulent and fast fluidized beds[J]. *Powder Technology***1992**, 70(3): 229-236.

[79] Carlos Varas A E, Peters E A J F, Kuipers J A M. CFD-DEM simulations and experimental validation of clustering phenomena and riser hydrodynamics[J]. *Chemical Engineering Science***2017**, 169(Supplement C): 246-258.

[80] Tanaka T, Yonemura S, Kiribayashi K, et al. Cluster formation and particle-induced instability in gas-solid flow predicted by DSMC method[J]. *JSME International Journal***1996**, 39(2): 239-245.

[81] Wang S, Liu H, Lu H, et al. Flow behavior of clusters in a riser simulated by direct simulation Monte Carlo method[J]. *Chemical Engineering Journal* **2005**, 106: 197-211.

[82] Liu H, Lu H. Numerical study on the cluster flow behavior in the riser of circulating fluidized beds[J]. *Chemical Engineering Journal***2009**, 150(2): 374-384.

[83] Liu H P, Liu D Y, Liu H. Study of cluster behavior in the riser of CFB by the DSMC method[M]. AIP Conference Proceedings, Guo L J, Joseph D D, Matsumoto Y, et al, 2010: 1207, 951-956.

[84] Berrouk A S, Wu C L. Two-dimensional discrete particle model: Comment on the numerical simulation of cluster flow behavior in the riser of circulating fluidized beds by Liu and Lu[J]. *Chemical Engineering Journal***2010**, 160(2): 810-811.

[85] Capecelatro J, Pepiot P, Desjardins O. Numerical characterization and modeling of particle clustering in wall-bounded vertical risers[J]. *Chemical Engineering Journal* **2014**, 245(Supplement C): 295-310.

[86] Lu H, Wang S, He Y, et al. Numerical simulation of flow behavior of particles and clusters in riser using two granular temperatures[J]. *Powder Technology***2008**, 182(2): 282-293.

[87] Wang S Y, Shen Z H, Lu H L, et al. Numerical predictions of flow behavior and cluster size of particles in riser with particle rotation model and cluster-based approach[J]. *Chemical Engineering Science***2008**, 63(16): 4116-4125.

CHAPTER 3 Experimental study on gas-solid flow pattern and transition in fast fluidized bed

3.1 Introduction

Different operating conditions result in various gas-solid flow characteristics in fast fluidized bed, e.g. different particle residence time and mixing time, affecting the reacting efficiency in fast fluidized bed. Thus study on gas-solid flow characteristics is crucial to industrial design, amplification and optimization of fast fluidized bed. A series of research on gas-solid flow characteristics have been conducted by many scientists. Bi et al. [1] observed the particle flow in fast fluidized bed and defined three flow regimes, including homogeneous dilute transport, core-annular dilute transport and fast fluidization. Grace et al.[2] defined the dense suspension upflow (DSU) in high-density circulating fluidized bed. Kim et al.[3] divided the fast fluidization regime into the fast transition region and the fully develop fast fluidization region. Mahmoudi et al. [4] measured the particle velocities, residence time distribution, population densities of the particles in the cross-sectional area of the riser and solids flow pattern at the bottom of the riser, identifying four regimes in a CFB riser: dilute riser flow (DRF), core-annuls flow(CAF), core-annulus flow with turbulent fluidized bottom bed (CAF with TFBB) and dense riser upflow (DRU). Researchers identified and defined flow structures in various methods, while one flow structure may has different names.

Most studies on flow structure in fast fluidized bed are conducted by Geldart A particles, while research conducted by Geldart B particles are limited. The fluidizations of Geldart A and Geldart B particles are very different, especially for the particle viscosity[5]. As are widely used of Geldart B particles in coal gasification and combustion, the study on flow structure of Geldart B particles are become increasingly important. Chew et al. [7]revealed the presence of a reverse core-annulus profile (i.e., a dense core with a dilute annulus) under certain conditions. Anantharaman et al. [8] studied the influence of particle properties and operating

conditions on annulus flow behaviour in a pilot scale CFB riser. Moreover, the experiment result have been compared with prediction of flow regime map of Bi et al.[1], Grace et al. [2], Gupta et al.[9] and Kim et al.[10], and found that discrepancies between the predictions of regime map and experimental data exist, which may be due to the fact that the regime classifications were developed from experimental data obtained mostly from Geldart Group A particles. Therefore, the comprehensive experimental studies of flow structure in fast fluidized bed handling Geldart B particles were need.

In chapter 3, a three-dimensional visual fast fluidized bed with riser height H=3m and diameter D=0.1m was established, and the pressure signal and high-speed image acquisition system were adopted. The superficial gas velocities were set from 0 to 5.28m/s, while the solid mass flux varies from 0 to 120kg/(m^{2}s). The flow pattern and transition were studied by Geldart B particles with different diameter, and the influence (e.g., superficial gas velocity, solid mass flux) on solid volume fraction and gas-solid slip velocity were discussed. Moreover, typical flow pattern map was plotted and the fitting transition velocities for these patterns were developed.

3.2 Experimental study

3.2.1 Experimental apparatus and procedure

A three-dimensional visual fast fluidized bed system consists of fast fluidized bed, air supply system and differential pressure signal sampling and processing system, is shown in Fig.3-1. The fast fluidized bed is consists of Plexiglas riser, downer and two stage cyclone, and riser is made of Plexiglas with 3.0 m in height and 0.1 in inner diameter. The primary air at ambient temperature and pressure was supplied to the riser bottom through a perforated distributor plate with free area of 11% in 2.0 mm of orifice diameter. At the top of riser, the gas and solids passed through a smooth elbow and then

first separated in the primary cyclone, then further gas-solid separated and collected by secondary cyclone and bag filter. The downer kept sufficient solid inventory and gave pressure head to provide a wide range of solid flow rate in the riser.

Moreover, the gas flow rate was measured by rotameters. The solid mass flux was calculated by multiplying the bulk density of solid material known by the solid volumetric flow rate, which was estimated by measuring the velocity of a tracer particle travelling in downcomer. Thirteen pressure taps were set at heights of 0.050, 0.100, 0.150, 0.300, 0.510, 0.720, 1.005, 1.290, 1.575, 1.860, 2.145, 2.430 and 2.715m above the gas distributor and each two adjacent taps were connected to a pressure sensor. The pressure difference from two adjacent taps was collected by the pressure sensors and then converted into digital values by the A/D convertor, as seen in Fig.3-1.

Meanwhile, a high-speed camera was set to investigate the flow structure of fast fluidized riser, the snapshots flow pattern and transition of the riser under various operating condition were captured by high-speed camera and further analysed.

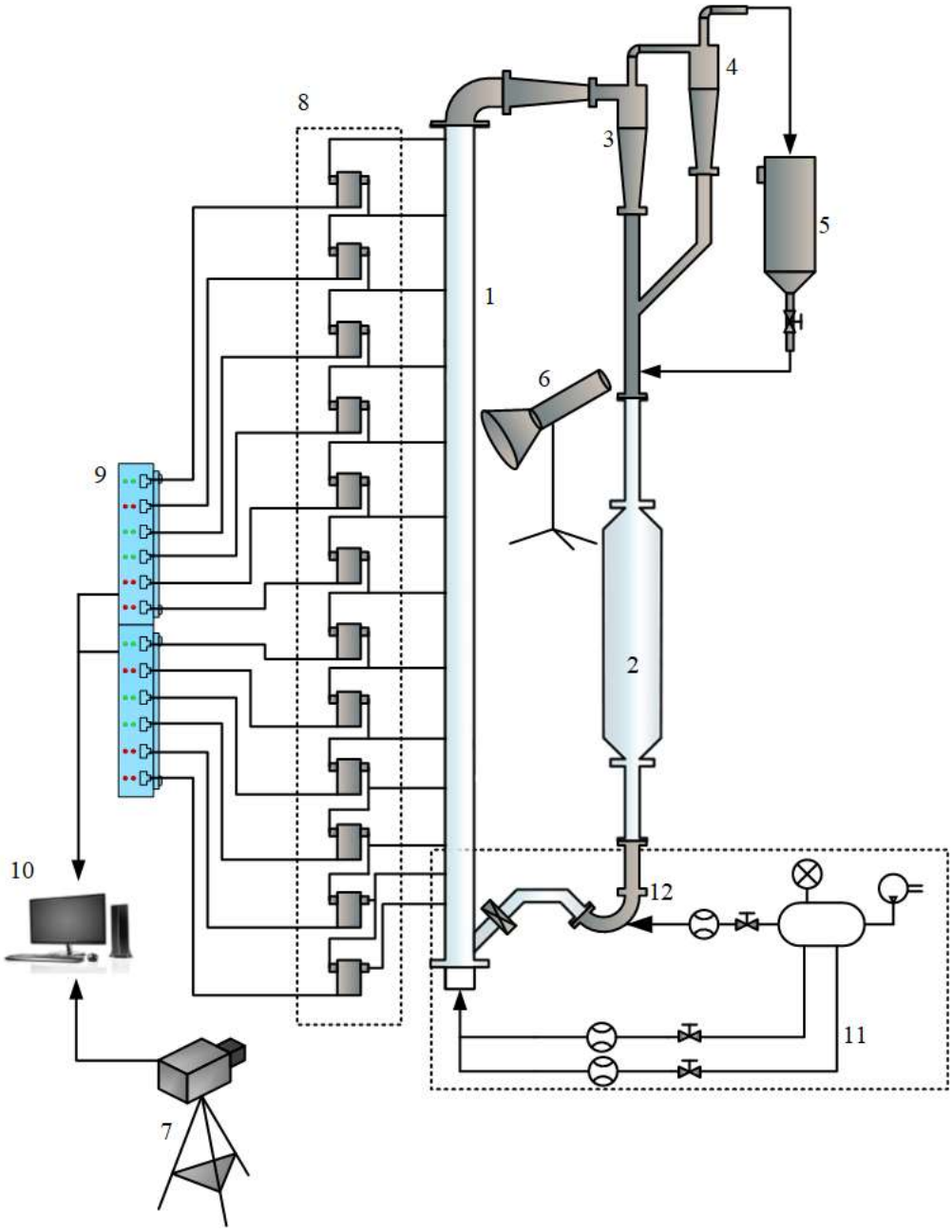

Fig.3-1 Schematic of the experimental set-up:1-Riser, 2-Downer with storage tank, 3-First stage cyclone separator, 4-Secondary stage cyclone separator, 5-Duster, 6-LED, 7-CCD camera, 8-Differential pressure transmitter, 9-Data acquisition card, 10-computer, 11-Air supply system, 12-Loop seal.

3.2.2Materials

The quartz sand particles with various diameters were used in experiment, as seen in Table 3-1.

Table 3-1 Materials

Materials	Quartz sand particles
Particle mean diameter d_p（μm）	100
	139
	177
	215
	250
	350
	370
Particle density（kg/m^3）	2650

3.2.3 Parameters measurement

(1) Superficial gas velocity (u_g)

Superficial gas velocity is gas volume flow rate divided by riser area, and the gas flow rate is measured by rotameter considering the pressure effect.

(2) Solid mass flux (G_s)

Solid mass flux is the average solid mass flow rate per unit cross-sectional area in the riser. Solid mass flux could be calculated by multiplying the bulk density of solid material known by the solid volumetric flow rate which was estimated by measuring the velocity of a tracer particle travelling in downcomer. The velocity of the tracer particle is the movement distance S_d divided by movement time t. The measurements are repeated 10 times for each parameter.

$$G_s = \frac{A_D \rho_P}{A_R} \frac{S_d}{t} \quad (3\text{-}1)$$

A_R、A_D are the cross-sectional area of riser and downer.

(3) Apparent solid volume fraction ε_p

Apparent solid volume fraction is calculated from the pressure drop in the riser. According to previous studies, the pressure loss caused by the particle acceleration, friction between the particle-wall and gas-particle can be neglected [11, 12]. The apparent solid volume fraction can be calculated at a certain position from the pressure drop, and the deviation would be within 10% [13].

$$\varepsilon_p = \frac{\frac{\Delta P}{g \Delta z} - \rho_g}{\rho_p - \rho_g} \quad (3\text{-}2)$$

(4) Apparent slip velocityV_{slip}

The apparent slip velocity can be used to study the interaction between gas and solid, revealing the mechanism of high efficient gas-solid contact[14]. The apparent slip velocity V_{slip} in the riser can be calculated by:

$$V_{slip} = V_g - V_p = \frac{u_g}{1-\varepsilon_p} - \frac{G_s}{\rho_p \varepsilon_p} \quad (3\text{-}3)$$

where V_g is the average apparent superficial gas velocity, V_p is the average apparent superficial particle velocity.

(5) Apparent slip factor Φ

The apparent slip factor $\Phi$is the ratio of average apparent superficial gas velocity to the average apparent superficial particle velocity.

$$\Phi = \frac{V_g}{V_p} = \frac{u_g}{1-\varepsilon_p} \frac{\rho_p \varepsilon_p}{G_s} \quad (3\text{-}4)$$

3.3 Results and discussion

3.3.1 Flow patterns and characteristics in fast fluidized bed

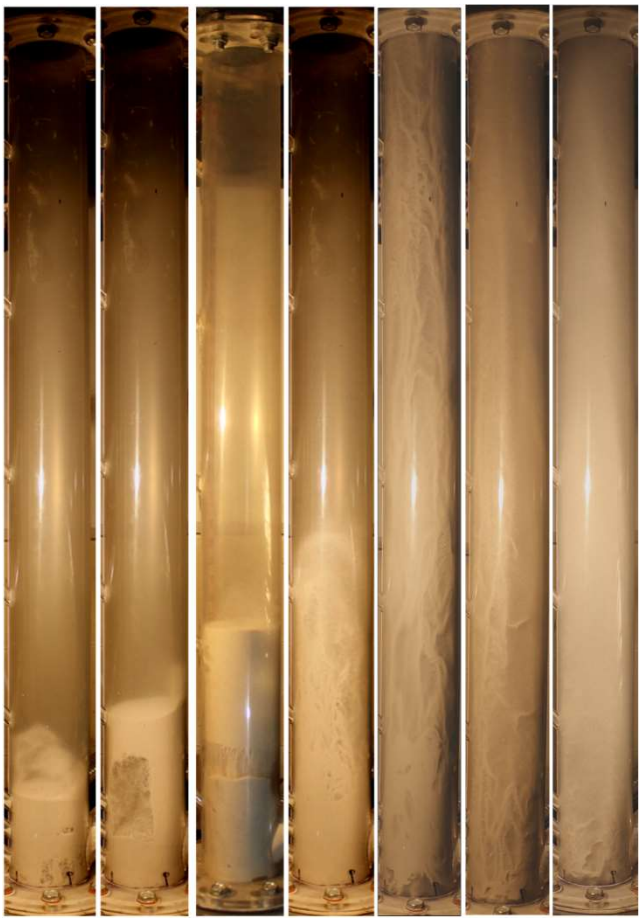

(a) (b) (c) (d) (e) (f) (g)

Fig. 3-2 Typical flow pattern images of a fast fluidized bed

(a)H_0/D=1.5, u_g =0.10 m/s, G_s=0; (b)H_0/D=1.5, u_g=0.29 m/s, G_s=0;

(c)H_0/D=1.5, u_g =0.52 m/s, G_s=0; (d)H_0/D=3.0,u_g=0.46 m/s, G_s=0;

(e) u_g=2.91 m/s,G_s=34.0 kg/(m^2·s); (f) u_g =2.91m/s,G_s=28.8 kg/(m^2·s);

(g) u_g =2.91 m/s, G_s=23.4 kg/(m^2·s).

Fig.3-2 illustrates typical flow pattern images of a fast fluidized bed with increasing superficial gas velocity under various static bed heights. As shown in Fig.3-2 (a)(b)(c), the flow pattern of riser went through bubbling flow (BF), slug flow (SF) and turbulent flow (TF) with increasing superficial gas velocity when the ratio of static bed height to

the riser diameter H_0/D was kept at 1.5. As H_0/D was increased to 3, the particle fluidization in the riser was not achieved, and the "particle rain" occurs[15]。

Moreover, when the superficial gas velocity came over the transition velocity u_{tr}, the particles should be collected by cyclone and feed back to the riser through J valve to keep a stable circulation in fast fluidized bed. As solid mass flux decreased, the flow patterns transited from fast fluidization (FF) to dilute phase flow (DPF) at u_g=2.91 m/s as seen in Fig.3-2 (e)(f)(g).

At lower u_g, the flow patterns transited from fix bed (FB), bubbling flow (BF) to turbulent flow (TF) with increasing superficial gas velocity, while the ratio of static bed height to the riser diameter H_0/D was lower than 1. At $1 \le H_0/D \le 2$， the rise of gas flow causes to form big bubble about the size of bed diameter, instead of increasing the distance between particles. It is notable that slug forms between bubbling flow and turbulent flow, and the transition velocity of turbulent flow increase with static bed height. Moreover, when H_0/D is higher than 2 and the gas velocity is lower than minimum fluidization velocity, the space between particles increases with the increase in gas velocity. Meanwhile, the big bubble still exists with similar character of turbulent flow. The pressure fluctuation caused by slug leads to the uneven of heat and mass transfer, and the unstable fluidization, which should be avoid in industrial application.

The turbulent flow begins to show similar character as fast fluidization with increasing gas velocity. With higher carrying capacity of the gas flow, more particles were blew out the riser, and once the gas velocity is higher than u_{tr}, the particles need to be separated by the cyclone and fed back into the riser to keep the stable fluidization. At lower G_s, the particle suspension along the riser was well-distributed, known as dilute phase flow (DPF). As increasing solid mass flux at a constant gas velocity or lowering the gas velocity while maintaining the solid mass flux, the solid volume fraction in the

riser would rise and the particle clusters came into shape, forming a dense zone in the bottom. Yerushalmi et al.[16]proposed that the formation of particle clusters indicated the begin of fast fluidization. In the previous studies on the flow structure of riser, some research[17, 18]found the existence of S-shaped axial solid volume fraction, i.e. a dense turbulent flow in the bottom with a dilute core-annular flow in the top of riser, while some [1, 19]observed an acceleration zone without dense turbulent flow in the bottom.

A series of experiments were conducted on the fast fluidized bed system to study the flow structure of the riser, the superficial gas velocity varied from 0 m/s to 5.28 m/s, and the solid mass flux, G_s, ranged from 0 to 100kg/(m^{2}s), as shown in Table 3-2.

Table 3-2 Operating conditions of experiments

Cases	u_g (m/s)	H_0/D	G_s (kg/m^{2}s)	d_p (μm)
case 1	0.09	1/1.5/2/3/4.5	0	215
case 2	0.12	1/1.5/2/3/4.5	0	215
case 3	0.17	1/1.5/2/3/4.5	0	215
case 4	0.23	1/1.5/2/3/4.5	0	215
case 5	0.29	1/1.5/2/3/4.5	0	215
case 6	0.35	1/1.5/2/3/4.5	0	215
case 7	0.40	1/1.5/2/3/4.5	0	215
case 8	0.46	1/1.5/2/3/4.5	0	215
case 9	0.52	1/1.5/2/3/4.5	0	215
case 10	0.58	1/1.5/2/3/4.5	0	215
case 11	0.69	1/1.5/2/3/4.5	0	215
case 12	0.81	1/1.5/2/3/4.5	0	215
case 13	0.92	1/1.5/2/3/4.5	0	215
case 14	1.04	1/1.5/2/3/4.5	0	215

case 15	1.15	1/1.5/2/3/4.5	0	215
case 16	1.27	1/1.5/2/3/4.5	0	215
case 17	1.38	1/1.5/2/3/4.5	0	215
case 18	1.50	1/1.5/2/3/4.5	0	215
case 19	1.61	1/1.5/2/3/4.5	0	215
case 20	1.73	1/1.5/2/3/4.5	0	215
case 21	2.04	3	7.37/7.2	215
case 22	2.33	3	12.3/13.3	215
case 23	2.62	3	23.5/26.1	215
case 24	2.91	3	36.4/41.9	215
case 25	3.24	3	46.1/53.6	215
case 26	3.53	3	56.4/69.1/72.8	215
case 27	3.83	3	69.1/79/85	215
case 28	4.12	3	76.8/95.3/86.4	215
case 29	4.41	3	86.4/110.6	215
case 30	4.71	3	95.3/110.6	215
case 31	5.01	3	110.6	215

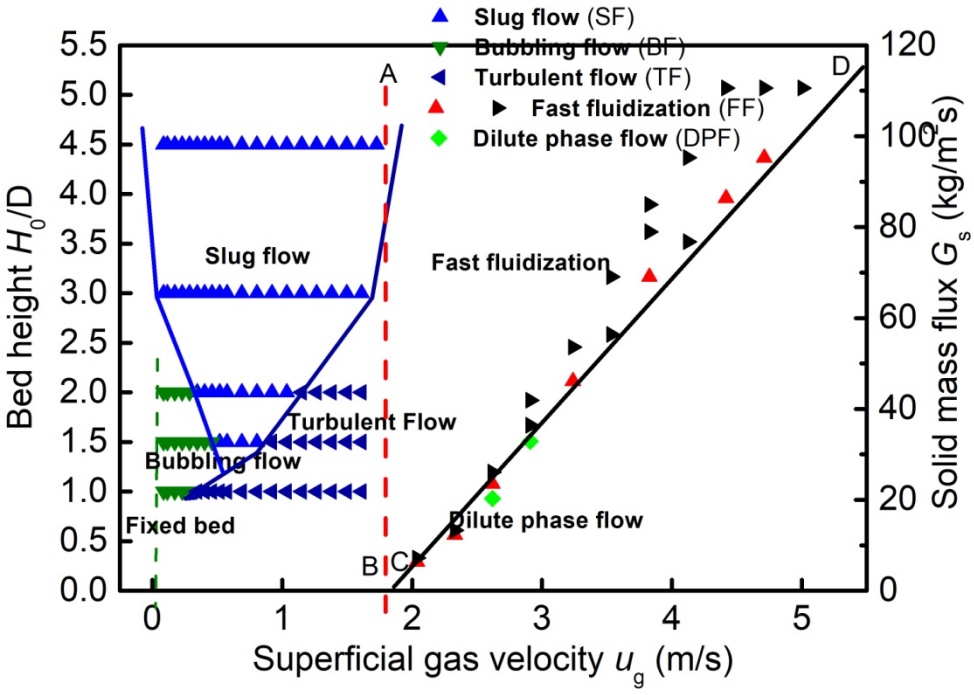

Fig.3-3 Typical flow pattern map under various superficial gas velocities

The typical flow pattern map was sketched under various superficial gas velocities, static bed height and solid mass flux based on visual system and pressure system, as in Fig.3-3. As seen in Fig.3-3, with increasing superficial gas velocity, the flow patterns change with static bed height and solid mass flux. The line AB shows the transition velocity from turbulent flow to fast fluidization flow according to the experiments, while the line CD indicates the transition from fast fluidization to dilute phase flow. The definition of transport velocity from turbulent flow to fast fluidization proposed by Perales[20]was adopted in this chapter, and particles with different diameters (i.e. 0.100 mm, 0.139 mm, 0.177mm, 0.250 mm and 0.375 mm) were used in the experiments. Results were plotted using minimum transport Reynolds number (Re_{tr}) and Archimedes (Ar_{tr}) as coordinates. Previous correlations listed in Table 3-3 were compared with our results seen in Fig.3-4. The correlation proposed by Bi *et al.*[1,26] corresponds well with

the experimental results, and the correlation could be further revised by the experimental findings as follow:

$$Re_{tr} = 2.5Ar^{0.45} \quad (3\text{-}5)$$

Table 3-3Correlations for the transport velocity

Reference	Correlations
Mori et al. (1986)[21]	$Re_{tr} = 1.46Ar^{0.56}$
Lee et al. (1990)[23]	$Re_{tr} = 2.916Ar^{0.345}$
Perales et al.(1991)[20]	$Re_{tr} = 1.45Ar^{0.484}$
Bi et al. (1992)[24]	$Re_{tr} = 2.28Ar^{0.419}$
Adanez et al.(1993)[25]	$Re_{tr} = 2.078Ar^{0.463}$
Bi et al. (1995)[1,26]	$Re_{tr} = 1.53Ar^{0.50}$

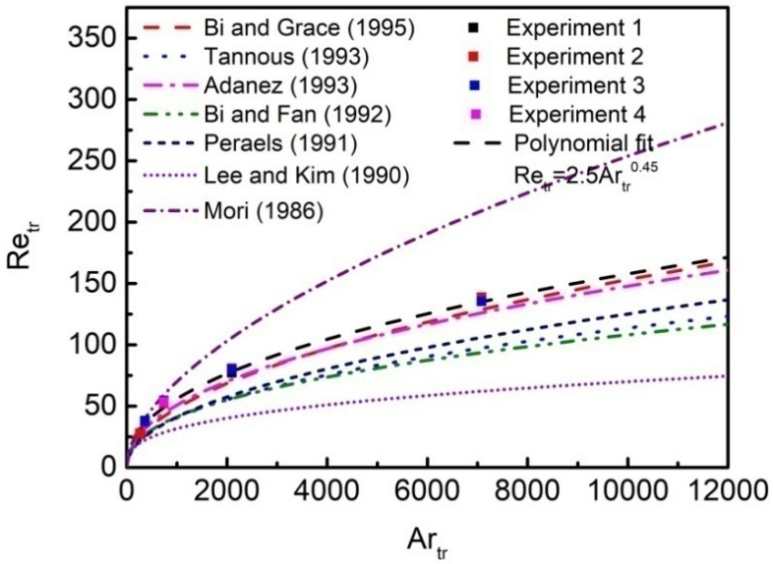

Fig. 3-4 Comparison of experimental results and predicted values of u_{tr}

3.3.2 Apparent solid volume fraction

3.3.2.1 Influence of superficial gas velocity

The solid volume fraction is one of the most important characteristics when considering flow structure in fast fluidized bed. Fig.3-5 shows the axial distribution of solids volume fraction in the riser with increasing superficial gas velocity. The solid volume fraction under all operation conditions declined with riser height. For the larger particles, e.g. d_p=250 μm and d_p=375 μm, a dense turbulent zone in the bottom and a dilute zone (ε_p< 0.05) in the riser can be observed, the profile of axial solid volume fraction was approximately S-shaped. It can be seen that solid volume fraction in the bottom decreased dramatically at first and then reduced gradually with increasing superficial gas velocity. However, when the solid volume fraction was reduced to a certain value, further increase of superficial gas velocity leads very little change in solid volume fraction.

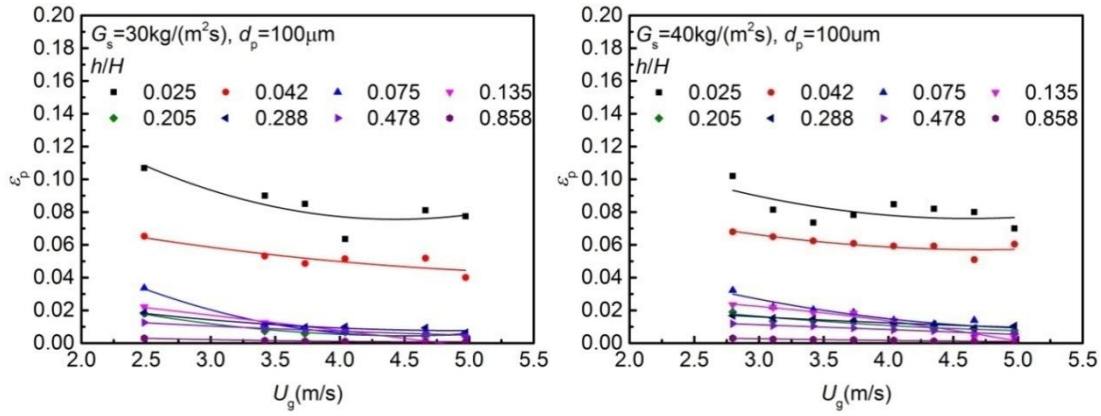

(a) (b)

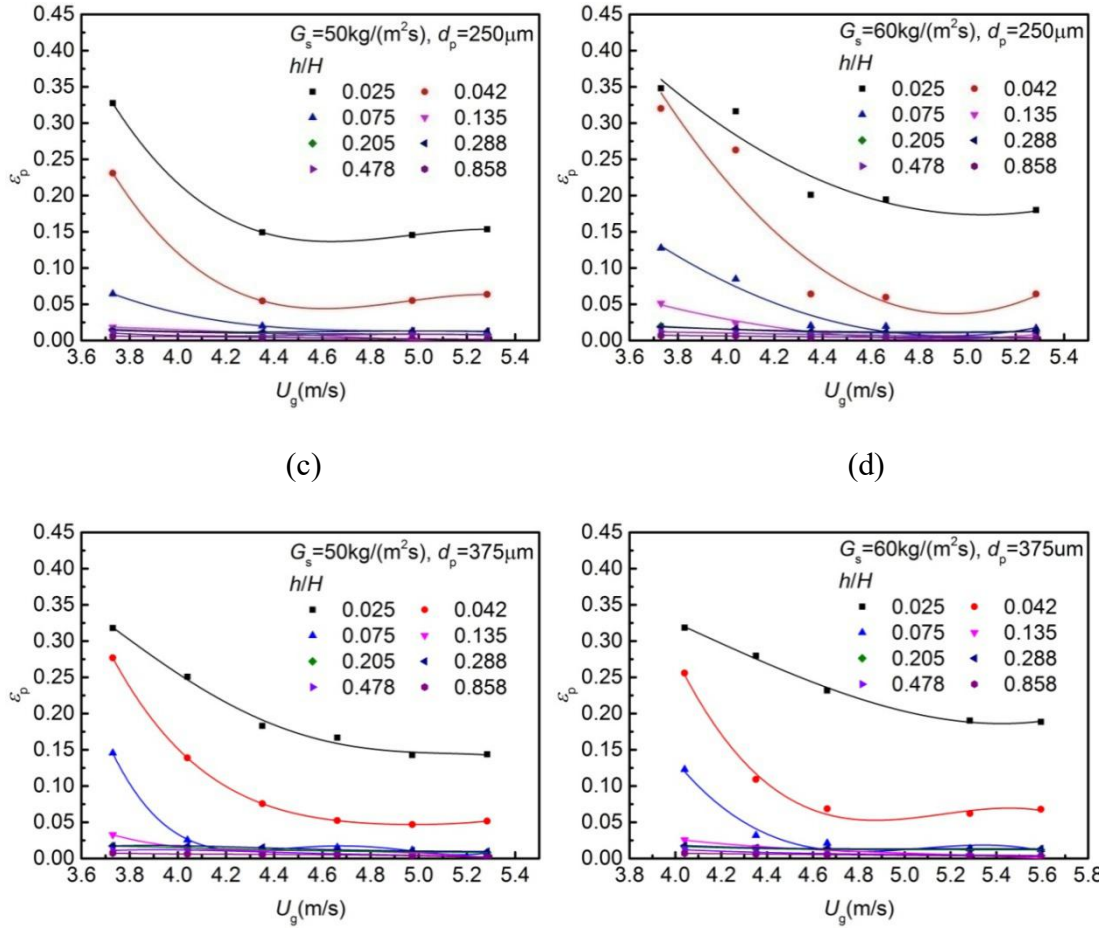

Fig.3-5 Effect of superficial gas velocity on axial distribution of solid volume fraction

(a) d_p=100 μm, G_s=30kg/(m^{2}s); (b) d_p=100 μm, G_s=40kg/(m^{2}s);

(c)d_p=250μm, G_s=50kg/(m^{2}s); (d)d_p=250μm, G_s=60kg/(m^{2}s);

(e)d_p=375μm, G_s=50kg/(m^{2}s); (f)d_p=375μm, G_s=60kg/(m^{2}s).

Due to the formation of dense zone in the bottom, increasing energy owing to the elevation of gas flow was mainly used in enhancing the velocity of particles in the dense bottom. However, for the particle of d_p=0.100 mm under similar operating condition, exponential distribution of solid volume fraction was observed without a dense bottom, and the solid volume fraction changed very little with superficial gas velocity.

3.3.2.2Influence of solid mass flux

Fig.3-6 gives the axial distribution of solid volume fraction in the riser as a function of solid mass flux. The solid volume fraction rose with increasing solid mass flux at the given superficial gas velocity. The effect of solid mass flux shows similar trend with superficial gas velocity, e.g. have little influence on solid volume fraction of small particles (d_p=100μm). As for the larger particles, a higher solid mass flux leads to a denser bottom, but has less impact for the top of the riser. It can be explained by that the elevation of solid mass flux results in a larger amount of particles fed back through the feeder. Therefore, the gas-solid turbulence and particle impact which decelerate the particles become more intensive, and particles aggregate more seriously in the bottom.

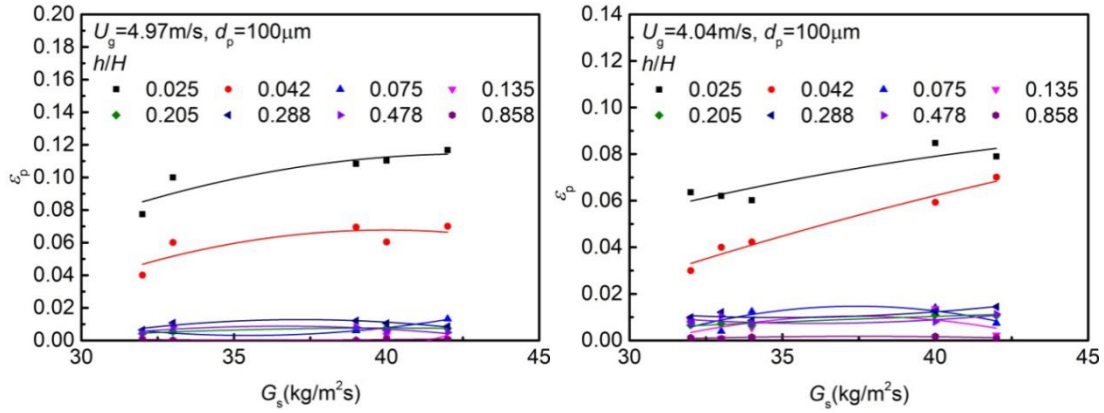

(a)

(b)

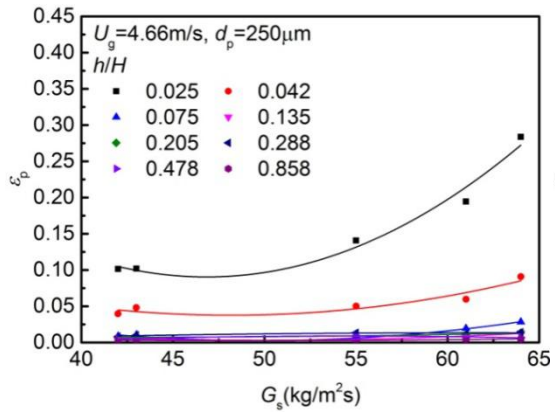

(c)

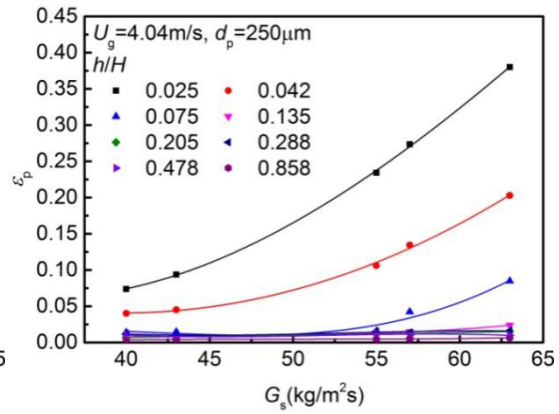

(d)

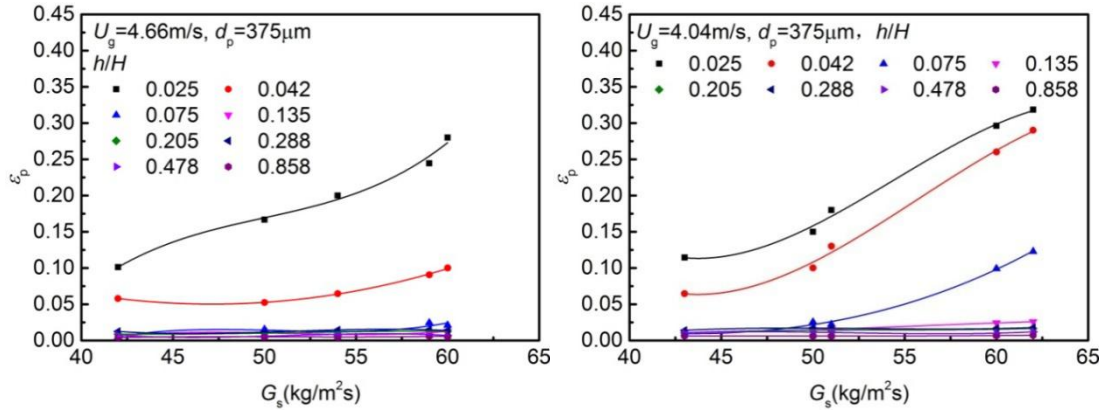

(e) (f)

Fig.3-6 Effect of solid mass flux on axial distribution of solid volume fraction

(a) d_p=100 μm, u_g=4.97 m/s; (b) d_p=100 μm, u_g=4.04 m/s;

(c)d_p=250μm, u_g=4.66 m/s; (d)d_p=250μm, u_g=4.04 m/s;

(e)d_p=375μm, u_g=4.66 m/s; (f)d_p=375μm, u_g=4.04 m/s.

The solid volume fraction of the riser increases significantly with higher solid mass flux at lower gas velocity, e.g.u_g=4.04 m/s, and the influence of solid mass flux on the solid volume fraction reduces with superficial gas velocity. This might be because that when the gas velocity is low, the saturation carrying capacity of gas is relatively low. When the solid mass flux exceeds the saturation carrying capacity of gas, particles start to assemble in the riser. With the increase of superficial gas velocity, the saturation carrying capacity of gas is improved, and the higher solid mass flux leads to higher solid volume fraction in the riser. Therefore, particles are more likely to be blow out of the riser at a higher gas velocity, results in less increment in solid volume fraction than that at the lower gas velocity.

3.3.3Gas-solid slip characteristics

3.3.3.1 Influence of solid mass flux

Fig. 3-7 shows the effect of solid mass flux on slip velocity and slip factor of different axial locations in the riser at u_g=4.66m/s. As shown in Fig. 3-7(a), slip velocity increase smoothly with increasing solid mass flux in the top of the riser, while it shows a reverse trend in the lower part of the riser. It is obvious that the slip factor declines sharply and then decreases slowly with increasing solid mass flux, as seen in Fig.3-7(b). This is because the acceleration of gas on particles slowly losing in the higher riser, so the V_p decreases gradually with the change of solid mass flux. It is notable that slip factor increases with increasing solid mass flux at the bottom of the riser, while it changes much less in the top of the riser. It can be explained by that particles are much less in dilute phase flow in the top, which leads to a lower energy consumption in transporting particles. Thus, the average gas velocity is quite similar with u_g. The increase of solid mass flux exerts great impact on solid volume fraction in the bottom, leading to a greater growth of slip factor in the lower part of the riser than that in the upper part.

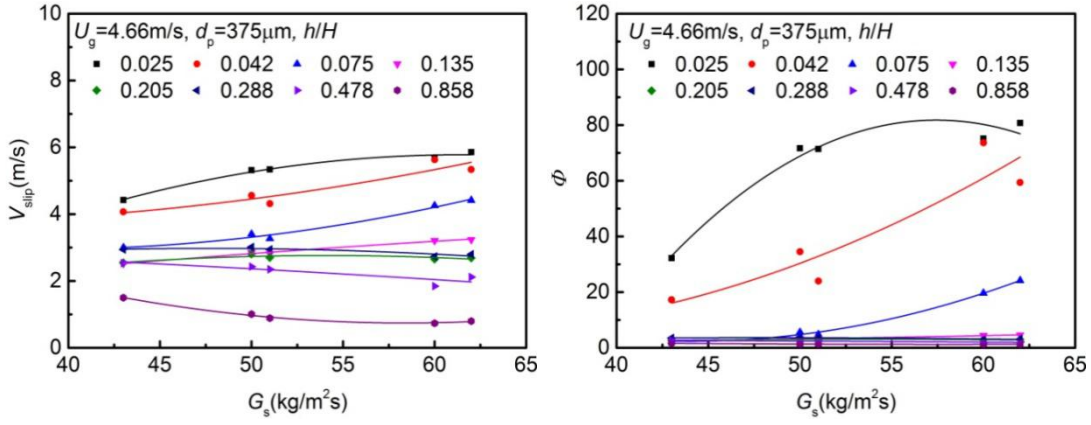

(a) (b)

Fig.3-7 Effect of solid mass flux on: (a) slip velocity and (b) slip factor.

3.3.3.2Influence of solid volume fraction

Fig.3-8 shows the variation of slip velocity with solid volume fraction while superficial gas velocity ranges from 4.04 m/s to 5.28 m/s. It is obvious that slip velocity is much higher than terminal velocity of single particle, which caused by inhomogeneous distribution of particles [27], e.g. particle clusters in the riser. The slip velocity first increases sharply and then slower with increasing solid volume fraction. It is because the higher solid volume fraction results in greater particle aggregation in the riser, which weakens the drag force on the particles [28]. It is notable that the slip velocity changes rapidly with solid volume fraction when solid volume fraction is lower than 0.05, which is consistent with previous studies [29]. However, when solid volume fraction is higher than 0.05, the slip velocity slowly increases with higher solid volume fraction. Moreover, the slip velocity also increases with increasing superficial gas velocity when solid volume fraction is kept constant. It is notable that slip velocity increases with increasing solid volume fraction at the same superficial gas velocity, which is unlikely influenced by the particle size.

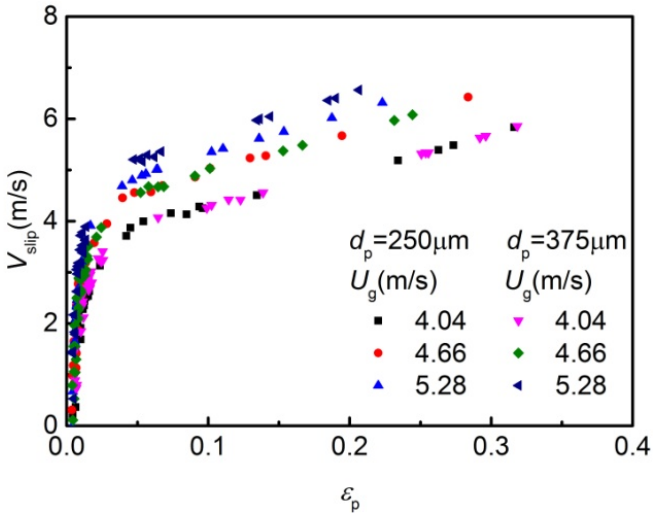

Fig.3-8 Effect of solid volume fraction on slip velocity.

3.3.3.3 Relationship between gas-solid slip characteristics and operating conditions

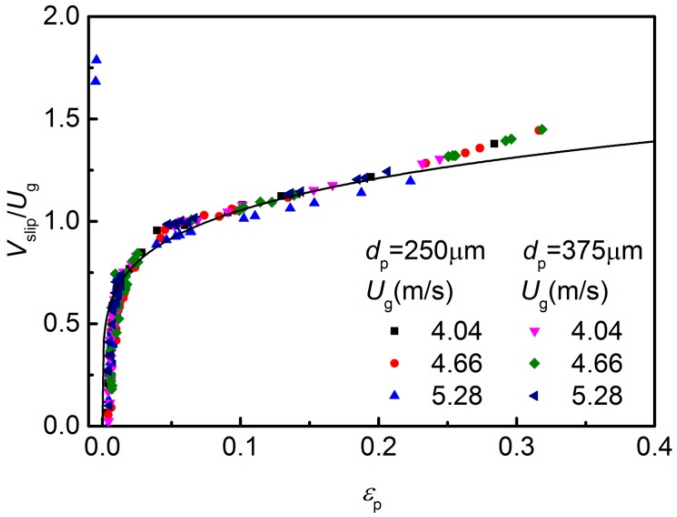

Fig.3-9 Effect of solid volume fraction on dimensionless slip velocity.

The slip velocity is closely related to the superficial gas velocity and solid volume fraction. Fig.3-9 shows the effect of solid volume fraction on dimensionless slip velocity, with u_g ranges from 4.04m/s to 5.28m/s and the particles size d_p=250 μm and 375 μm. To further illustrate gas-solid slip characteristics, Issangya et al. [30]proposed a correlation of dimensional slip velocity and solid volume fraction based on experiments conducted with Geldart A particles as follow:

$$V_{slip}/u_g = 1.67\varepsilon_p^{0.25} \quad (3\text{-}6)$$

Wang et al.[29]proposed an equation for Geldart B particles, and the Yin et al.[13] further conducted a series of research on pressurized high-flux circulating fluidized bed

$$V_{slip}/u_g = 1.83\varepsilon_p^{0.27} \quad \text{(Wang et al. 2008)} \quad (3\text{-}7)$$

$$V_{slip}/u_g = 2.09\varepsilon_p^{0.42} \quad \text{(Yin et al. 2014)} \quad (3\text{-}8)$$

The data in Fig.2-9 can be well represented by the following equation:

$$V_{slip}/u_g = 1.62\varepsilon_p^{0.2} \quad (3\text{-}9)$$

It is obvious that Geldart B particles have similar trend with Geldart A particles, which is the dimensionless slip velocity changes greater under higher operating pressure[13] and solid mass flux[29].

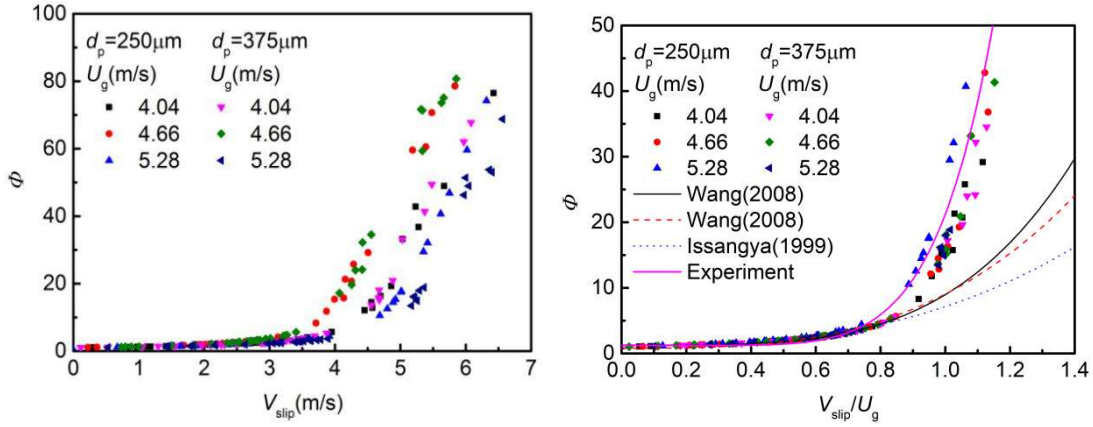

(a) (b)

Fig. 3-10 (a) Effect of slip velocity on slip factor;

(b) Effect of dimensionless slip velocity on slip factor.

Fig.3-10 gives the variation of slip factor with slip velocity and dimensionless slip velocity at superficial gas velocities of 4.04, 4.66 and 5.28 m/s for particles of d_p=250 μm and 375 μm. Some correlations have been presented by previous studies under different operating conditions, e.g.

Geldart B particles:

$$\Phi = 1.262 + 7.7(V_{\text{slip}}/u_g)^{3.884}$$ [29](3-10)

$$\Phi = 0.809 + 8.228(V_{\text{slip}}/u_g)^{3.086}$$ [29](3-11)

Geldart A particles:

$$\Phi = 1.21 + 5.92864(V_{\text{slip}}/u_g)^{2.76602}$$ [31](3-12)

As shown in Fig.3-10 (b), the relation between slip factor and dimensionless slip velocity for Geldart B particles can be well represented by the following equation:

$$\Phi = 1.21 + 20(V_{\text{slip}}/u_g)^6 \quad (3\text{-}13)$$

For Geldart B particles, similar trend with Geldart A particles [31] can be found considering relation between gas-solid characteristics and operation conditions, but slip factor of Geldart B particles changes much faster.

3.3.4 Flow regime map

When the superficial gas velocity is higher than u_{tr}, the high velocity fluidization is achieved. Therefore, particles should be separated by the cyclone and feed back into the riser to ensure stable fluidization in the riser. Therefore, the transport velocity can be calculated by equivalent transition velocity of fluidized bed coupled with slip velocity caused by solid mass flux [15], i.e.:

$$u_{tr} = u_{tr,f} + \frac{\varepsilon_{tr}}{(1-\varepsilon_{tr}} \frac{G_s}{\rho_p} \quad (3\text{-}14)$$

where u_{tr} is transition velocity for circulating fluidized bed, $u_{tr,f}$ is the equivalent transition velocity of fluidized bed, ε_{tr} is void fraction. According to Bi et al.[32] , the void fraction at the accumulated choking point is around 0.99 for Geldart B particles.

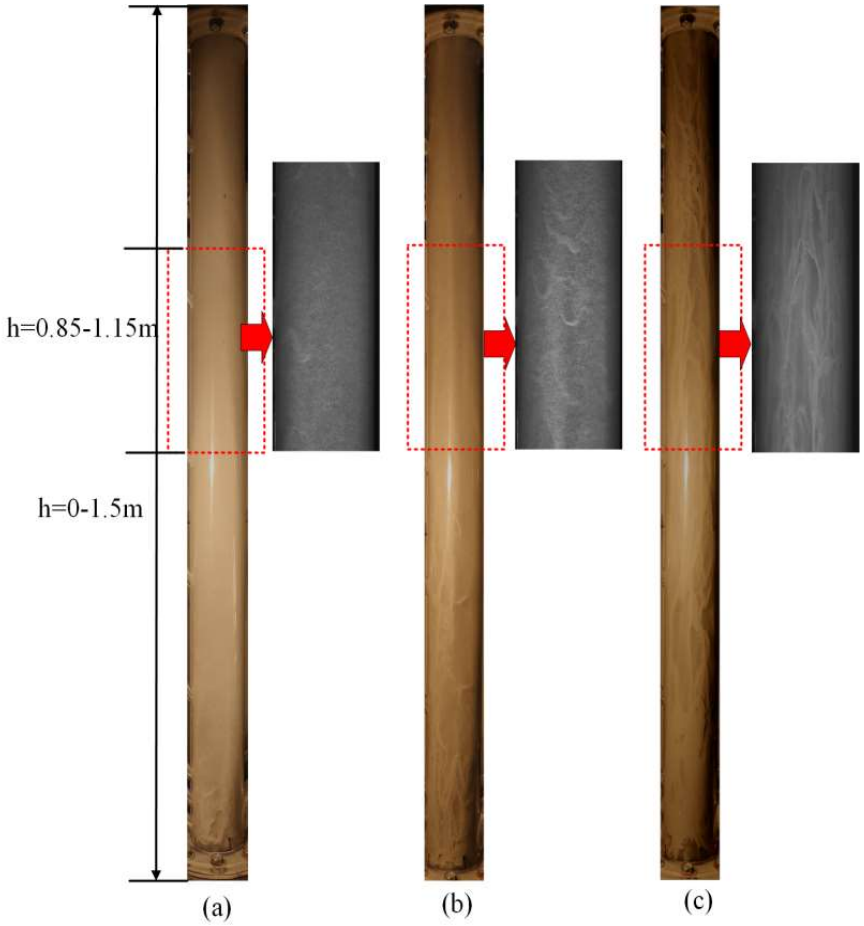

Fig.3-11 Typical flow pattern images of a fast fluidized bed:

(a)Dilute phase flow,u_g=2.91m/s,G_s=23.4kg/(m^2·s);

(b) Fast fluidization 1, u_g=2.91 m/s, G_s=28.8 kg/(m^2·s);

(c) Fast fluidization 2, u_g=2.91 m/s, G_s=34 kg/(m^2·s).

The changes in pressure difference and images recorded by a high resolution digital CCD camera were used to analyse the flow patterns. Two flow patterns in high velocity fluidization are identified, i.e. dilute phase flow and fast fluidization, and a schematic representation of flow patterns is seen in Fig.3-11. The flow pattern images of bed riser of h=0.85-1.15m are further magnified by high speed camera on the right in Fig.3-11.

Dilute phase flow (DPF): In this flow pattern, the solid volume fraction is usually lower than 0.1 in the riser and the particles are homogeneous distributed, and most of the particles flow dispersedly as shown in Fig.3-11(a).

Fast fluidization (FF): (1) a dense bottom with solid volume fraction at 0.1-0.4 and a dilute upper zone in the riser can be observed, and the profile of solid volume fraction is S-shaped. Meanwhile, some dispersed clusters can be observed in the wall of the riser, as seen in Fig.3-11(b). Moreover, when further increase superficial gas velocity or decrease solid mass flux, the flow may transit to dilute phase flow; (2) when particle diameter is smaller than 100 μm, the axial distribution of solid volume fraction in the riser change much slower with different superficial gas velocity and solid mass flux, and are exponential distributed. In this flow pattern, many particle clusters are emerging, and the distance between particles in the cluster are very short due to particle viscosity as in Fig.3-11(c).

The equation of transition velocity can be converted to be expressed by the Reynolds number according to Eq.3-14 as follow:

$$Re^* = \frac{\rho d}{\mu}\left[u_{\mathrm{tr}} - \frac{\varepsilon_{\mathrm{tr}}}{(1-\varepsilon_{\mathrm{tr}}}\frac{G_{\mathrm{S}}}{\rho_{\mathrm{p}}}\right] \quad (3\text{-}15)$$

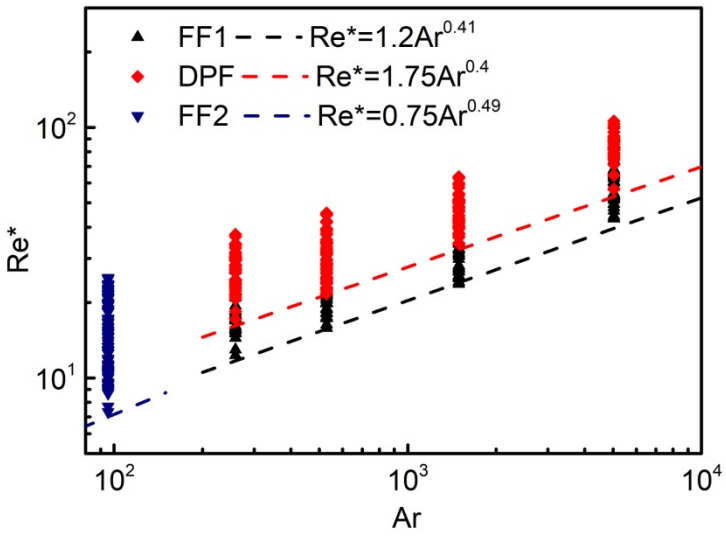

Fig.3-12 Typical flow pattern map of fast fluidized bed.

According to Fig.3-12, the transition velocity can be described by theArchimedes number. The transition velocity for fast fluidized 1 can be expressed by:

$$Re^* = 1.2Ar^{0.41} \qquad 300<Ar<104 \qquad (3\text{-}16)$$

The transition velocity for dilute phase flow can be expressed by:

$$Re^* = 1.75Ar^{0.4} \qquad 300<Ar<104 \tag{3-17}$$

The transition velocity for fast fluidized 2 can be expressed by:

$$Re^* = 0.75Ar^{0.49} \qquad 80<Ar<300 \tag{3-18}$$

3.4 Conclusions

The flow patterns and transitions in a fast fluidized bed were investigated in this chapter. Experiments were carried out to study the effects of operating conditions on flow structure, e.g. solid volume fraction, gas-solid slip characteristics. The finding can be summarized as follows:

(1) The flow structures from low velocity fluidization to high velocity fluidization in a fast fluidized bed have been investigated, and five distinct flow patterns can be identified. With increasing superficial gas velocity at various static bed heights, the flow patterns transit from bubbling flow (BF), slug flow (SF) and turbulent flow (TF). When the superficial gas velocity exceeds transition velocity u_{tr} , with increasing solid mass flux, the flow patterns transit from dilute phase flow (DPF) to fast fluidization (FF).

(2) The solid volume fractions in the bottom of the riser first drop rapidly and then slightly with increasing superficial gas velocity. It is notable that when particle size d_p=100μm, the solid volume fraction changes very little with increasing superficial gas velocity. Moreover, the solid volume fraction increases with increasing solid mass flux gradually with constant superficial gas velocity. Likely, the increase of solid mass flux exerts less influence on the solid volume fraction of small particle, e.g. d_p=100μm.

(3) The gas-solid slip characteristics is closely related to the superficial gas velocity and solid volume fraction. With increasing superficial gas velocity at constant solid volume

fraction, the slip velocity increases. Moreover, the particle size shows no effect on the impact of solid volume fraction on slip velocity, and the solid volume ration shows exponential relationship with dimensionless slip velocity. The variation of slip characteristics of Geldart B particles and Geldart A particles have similar tendency and the relations between slip characteristics and operating conditions are represented by equations.

(4) The changes in pressure difference and images recorded by a high resolution digital CCD camera were used to identify and analyse the flow patterns of high velocity fluidization in a fast fluidized bed. Two flow patterns in high velocity fluidization are identified, i.e. dilute phase flow and fast fluidization, and the flow characteristics are further investigated. Moreover, a typical flow pattern map of a fast fluidized bed is plotted, and the equation for transition velocity is proposed to further illustrate the flow structures in high velocity fluidization.

3.5 Reference

[1] Bi H T, Grace J R. Flow regime diagrams for gas-solid fluidization and upward transport [J]. *International Journal of Multiphase Flow***1995**, 21(6): 1229-1236.

[2] Grace J R, Issangya A S, Bai D R, et al. Situating the high-density circulating fluidized bed[J]. *AICHE Journal***1999**, 45(10): 2108-2116.

[3] Kim S W, Namkung W, Kim S D. Solids flow characteristics in loop-seal of a circulating fluidized bed[J]. *Korean Journal of Chemical Engineering***1999**, 16(1): 82-88.

[4] Mahmoudi S, Chan C W, Brems A, et al. Solids flow diagram of a CFB riser using Geldart B-type powders[J]. *Particuology***2012**, 10(1): 51-61.

[5] Geldart D. Types of gas fluidization [J]. *Powder Technology***1973**, 7(5): 285-292.

[6] Paudel B, Feng Z. Prediction of minimum fluidization velocity for binary mixtures of biomass and inert particles[J]. *Powder Technology* **2013**, 237: 134-140.

[7] Chew J W, Hays R, Findlay J G, et al. Reverse core-annular flow of Geldart Group B particles in risers[J]. *Powder Technology***2012**, 221: 1-12.

[8] Anantharaman A, Issangya A, Karri S B R, et al. Annulus flow behavior of Geldart Group B particles in a pilot-scale CFB riser[J]. *Powder Technology***2017**, 305: 816-828.

[9] Gupta S K, Berruti F. Modeling considerations for large scale high density risers[M]. Fan L S, Knowlton T M, 1998, 205-212.

[10] Kim S W, Kirbas G, Bi H, et al. Flow behavior and regime transition in a high-density circulating fluidized bed riser[J]. *Chemical Engineering Science***2004**, 59(18): 3955-3963.

[11] Issangya A S, Bai D, Bi H T, et al. Suspension densities in a high-density circulating fluidized bed riser[J]. *Chemical Engineering Science***1999**, 54(22): 5451-5460.

[12] Kim J, Tachino R, Tsutsumi A. Effects of solids feeder and riser exit configuration on establishing high density circulating fluidized beds[J]. *Powder Technology***2008**, 187(1): 37-45.

[13] Yin S.Y. Experimental and Modeling Study on a Pressurized High-Density Circulating Fluidized Bed [D]. Nanjing: Southeast University, 2014.

[14] Contractor R, Dry R J, White C, et al. Circulating fluidized beds:diameter, solids hold-up, axial gas-mixing, and contact efficiency[J]. *Powder Technology***2000**, 111(1-2): 132-144.

[15] Rabinovich E, Kalman H. Flow regime diagram for vertical pneumatic conveying and fluidized bed systems[J]. *Powder Technology* **2011**, 207(1-3): 119-133.

[16] Yerushalmi J, Cankurt N T. Further studies of the regimes of fluidization[J]. *Powder Technology*.**1979**, 24(2): 187-205.

[17] Adanez J, Gayan P, Garcialabiano F, et al. Axial voidage profiles in fast fiuidized beds[J]. **1994**, 81: 259-268.

[18] Van de Velden M, Baeyens J, Seville J P K, et al. The solids flow in the riser of a Circulating Fluidised Bed (CFB) viewed by Positron Emission Particle Tracking (PEPT)[J]. *Powder Technology***2008**, 183(2): 290-296.

[19] Bai D R, Jin Y, Yu Z Q, et al. The axial distribution of the cross-sectionally averaged voidage in fast fluidized beds[J]. *Powder Technology* **1992**, 71(1): 51-58.

[20] Perales J F, Coll T, Llop M F, et al. On the transition from bubbling to fast fluidization regimes[M]. Circulating Fluidized Bed Technology Ⅲ, Basu P, Horio M, Hasatani M, Oxford, UK:Pergamon Press, 1991.

[21] Van de Velden M, Baeyens J, Seville J P K, et al. The solids flow in the riser of a Circulating Fluidised Bed (CFB) viewed by Positron Emission Particle Tracking (PEPT)[J]. *Powder Technology***2008**, 183(2): 290-296.

[22] Mori S, Hashimoto O, Haruta T, et al. Turbulent fluidization phenomena[M]. Pergamon Press, 1986: 115-122.

[23] Lee G S, Kim S D. Bed expasion characteristics and transition velocity in turbulent fluidized beds [J]. Powder Technology**1990**, 62(3): 207-215.

[24] Bi H T, Fan L S. Existence of turbulent regime in gas-solid fluidization[J]. *AIChE Journal***1992**, 38(2): 297-301.

[25] Adanez J, Dediego L F, Gayan P. Transport velocities of coal and sand particles[J]. *Powder Technology***1993**, 77(1): 61-68.

[26] Bi H T, Grace J R. Flow regime diagrams for gas-solid fluidization and upward transport[J]. *International Jounral of Multiphase Flow***1995**, 21: 1229-1236.

[27] Yerushalmi J, Cankurt N T. Further studies of the regimes of fluidization[J]. *Powder Technology***1979**, 24(2): 187-205.

[28] Patience G S, Chaouki J, Berruti F, et al. Scaling considerations for circulating fluidized bed risers[J]. *Powder Technology***1992**, 72(1): 31-37.

[29] Wang X. F.Experimental and Simulation Study on Flow Behaviors in aHigh-Flux Circulating Fluidized Bed. [D].Nanjing: Southeast University, 2010.

[30] Issangya A S, Bai D, Bi H T, et al. Suspension densities in a high-density circulating fluidized bed riser[J]. *Chemical Engineering Science***1999**, 54(22): 5451-5460.

[31] Issangya A S. Hydrodynamics of a high-density circulating fluidized bed[D]. Vancouver, Canada: The University of British Columbia, 1998.

[32] Bi H T, Grace J R. Flow regime diagrams for gas-solid fluidization and upward transport[J]. *International Journal of Multiphase Flow***1995**, 21(6): 1229-1236.

CHAPTER 4 Experimental study on particle clustering behaviours in a fast fluidized bed

4.1 Introduction

Fast fluidized bed (FFB), usually working at a high operating gas velocity offers a variety of economic and environmental advantages over conventional fluidized beds due to its strong gas-solid contact, efficient mass and heat transfer and flexible operations[1-3], and has been widely used in many industries, e.g. petroleum, chemical, mineral, environmental and energy industries [4-7]. However, similar to many other gas-solid fluidized systems, the fast fluid bed has been reported to suffer from the clustering behaviours of particles [8-10]. Clusters, on the order of ten particle diameters in size, are considered to significantly affect the performance of the fast fluidized bed in terms of solid flow, mixing, and heat and mass transfer[11-13]. For example, the particle clusters with higher slip velocities tend to weaken the entrainment of gas [14], and facilitate the formation of core-annulus flow structures[15, 16]. Particle clusters existing in the riser are also responsible for the reduction of drag forces observed in the circulating fluidized bed experiments[17].

Given such significant influences of cluster, increasing researches are being focused on its behaviour and characteristics. Numerous research has been carried out on cluster structures in circulating fluidized bed. Bi et al. [18]presented four forms of particle clusters, including particle cluster, particle streamer, particle sheets and particles swarms based on experiment conducted in two-dimensional (2D) circulating fluidized bed. Horio et al. [10]studied the cluster behaviour and observed the horseshoe shape cluster in adilute phase flow by laser sheet technique. Shi et al. [19]classified four kinds of clusters, namely, micro clusters, core-annulus cluster, compact cluster and sparse clusters, and studied the effect of clusters on the flow field by particle imaging velocimetry (PIV) method. Xu et al. [20] concluded that four cluster forms were mainly observed in the centre region, i.e., upward-facing U-shape cluster,

downward-facing U-shape cluster, strand cluster and particle cluster. But the cluster structures presented in these studies are mostly qualitatively described, and most of the experiments were conducted in limited operating conditions in a 2D riser.

McMillan et al. [21]illustrated the particle dynamics in riser by high-speed video. Yang et al. [22]and Mondal et al.[23]developed a systematic cluster identification process by image processing. The characteristic of clusters，mainly including the cluster structure and size, cluster duration time, appearance probability and solid concentration and their possible affecting factors (e.g., reactor structure, particle property and operating condition) had also been investigated in numerous previous studies[24-26].

However, unanimous conclusions have not yet been achieved up to now. Some research results available even appear to give contradictory trends about the influences of the key parameters such as particle properties and operating conditions. For example, Guenther et al. [27] found that cluster size increases with solid mass flux (G_s) monotonically, while Horio et al. [10] believed that cluster size decreased with G_s. Moreover, some researchers believed that cluster sizes increase with riser height[28], while other works indicated a reverse trend[29, 30].Additionally, most of previous studies were conducted under limited operating conditions in 2D circulating fluidized bed, but few studies of particle clusters have been carried out in 3D fast fluidized bed，which is more common in practice. Therefore in-depth understanding of the flow hydrodynamics, especially the cluster behaviours, is essentially important and urgently required.

In the current study, a 3D fast fluidized bed with the riser of 3.0 m in height and 0.1 m inner diameter was established to study the cluster behaviours of Geldart B particles. A series of experiments were conducted for quartz sand particles with various sizes under different conditions. A visualization system which captures cluster snapshots

and the binary image processing proposed by Mondal et al. [23]was further developed to analyse cluster characteristics. Cluster characteristics including the cluster structure, size and distribution feature were discussed, and the effects of particle properties and operating conditions were also investigated.

4.2 Experimental system

4.2.1 Fast fluidized bed apparatus

Experiments were conducted in a fast fluidized bed which was illustrated schematically in Fig.3-1. The riser is made of Plexiglas with 3.0 m in height and 0.1 min inner diameter. The primary air at ambient temperature and pressure was supplied to the riser bottom through a perforated distributor plate with free area of 11% in 2.0 mm of orifice diameter. The humidity of the gas fed into the riser was 70~80%to avoid the misleading effects of electrostatic forces between particles [17]. At the riser top, the gas and solids passed through a smooth elbow and then first separated in the primary cyclone. Further gas-solid separation would be finished in the secondary cyclone and bag filter.

The gas flow rate was measured by rotameters. The solid circulation rate could be calculated by multiplying the bulk density of solid material known by the solid volumetric flow rate which was estimated by measuring the velocity of a tracer particle travelling in downcomer. Thirteen pressure taps were set at heights of 0.050, 0.100, 0.150, 0.300, 0.510, 0.720, 1.005, 1.290, 1.575, 1.860, 2.145, 2.43 and 2.715 m above the gas distributor and each two adjacent taps were connected to a pressure sensor. The pressure difference from two adjacent taps were collected by the pressure sensors and then converted into digital values by the A/D convertor, as seen in Fig.3-1.

The snapshots of gas-solid flow in the riser were captured by the high-speed camera. Five kinds of quartz sand particles with the density of 2480 kg/m^{3}were used as bed

materials in this study and their average diameters, d_p, are 0.100, 0.139, 0.177, 0.250 and 0.375 mm, respectively. In each experimental case, the total mass of the bed material was kept as 10kg. Superficial gas velocity, U_g, used in this paper varied from 2.486 m/s to 5.594 m/s, and the solid mass flux, G_s, ranged from 10 to 70 kg/(m^2s), which covered the most common flow regimes in fast fluidized bed.

4.2.2 Cluster measurement

The cluster visualization system consists of a high-speed camera, light resource and image processing program, shown in Fig.4-1. The frame rate of the high-speed camera is allowed up to 250 Hz, and the maximum resolution of images is 1280×1024 pixel. In experiments, the flow behaviors in three regions of the riser were respectively recorded by the high-speed camera as shown in Fig.4-2 with the observation time for each case being10s at the frame rate of 250 fps. Each video captured by high-speed camera then isconverted to 2500 sequential images in computer by a self-developed MATLAB program.

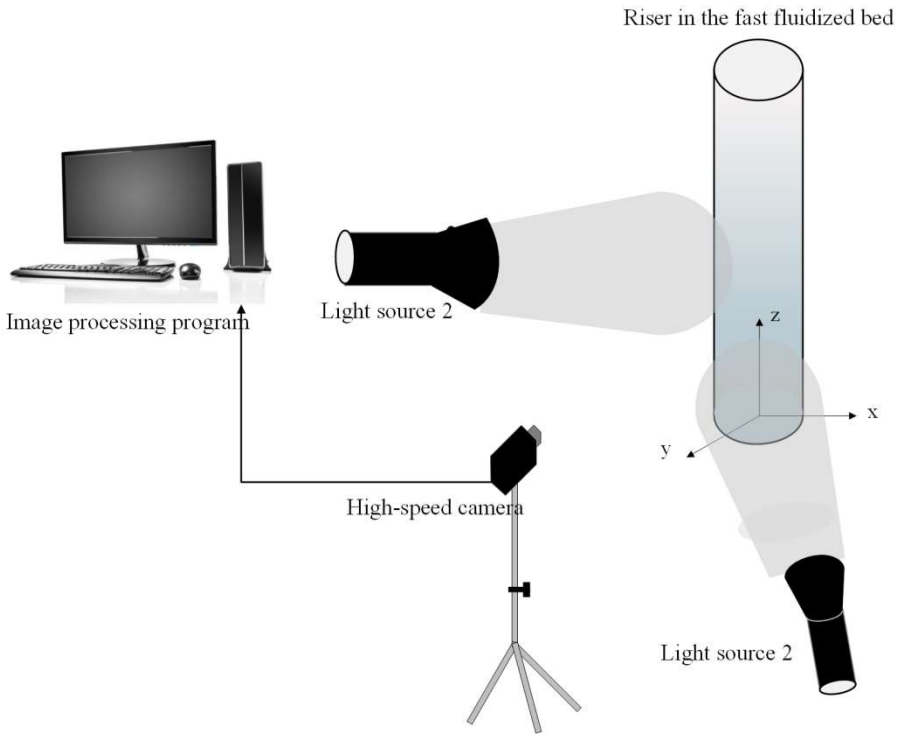

Fig.4-1 Schematic of cluster visualization system.

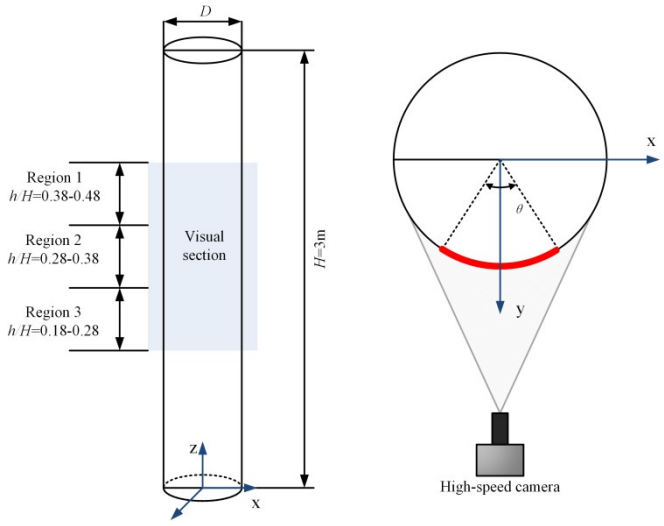

Fig.4-2 Schematic of visual section in the cluster visualization system.

The images captured by the high-speed camera were processed with self-developed binary image program. The image corresponds to an area in riser which is 30cm in height and 10cm in width. As the solid concentration in the cluster is higher than the average local solid holdup, the grayscale value of the cluster in the images is accordingly higher than the average local grayscale value [29]. Thus, a threshold grayscale I_c could be used to identify the cluster region. The pixel with grayscale value higher than I_c would be recognized as cluster pixel and converted to white color, while the rest were set to black by program. I_c is determined by the follow equation:

$$I_c = I_{ave} + k \cdot \sigma \quad (4\text{-}1)$$

For each pixel, I_{ave} was the average grayscale value calculated from the pixels at the same positions of 2500 frames images for 10s recording time; σ was the standard deviation of grayscale value for the pixel at this position during the recording time and k was cluster identification factor which would be discussed in detail in the next section. The grayscale values of every pixel in the image were evaluated respectively.

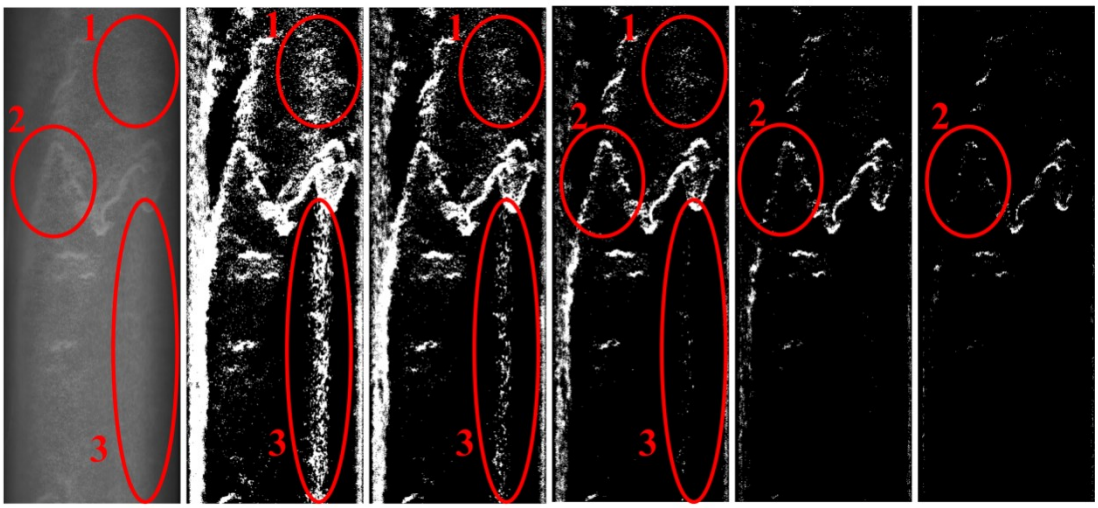

Fig.4-3 Images processing of clusters with various k:

(a) original image, (b)k=0.5,(c)k=1.0,(d)k=1.5,(e)k=2.0,(f)k=2.5

(U_g=4.35 m/s, G_s=66.9 kg/(m^{2}s), d_p= 0.250 mm).

In Equation (4-1), the factor k was used to differentiate the cluster from background noise [36]. Fig.4-3 shows the results of separating the clusters from background when k varied from 0.5 to 3.0. As shown in regions 1 and 3 marked in red, when k was 0.5 or 1, dispersed particles in original image were identified as cluster, and the detected cluster areas were larger than the actual ones. If k was increased to 2.0 or 2.5, the cluster shown in region 2 of original image would be disappeared. In current experiments, k =1.5 is considered suitable.

For a 3D fast fluidized bed, to reduce the difference of light illumination caused by the riser positions and curve surface, the visual region was carefully selected. The surface was marked in red line (from y direction) in Fig.4-2 was used in this study, and the central angle θ of visual region was $\pi/3$ in which the influence of curve surface could on the grayscale value be neglected.

The cluster size used in this study is referring to the cluster width at a specified height. Thus the cluster size at a specified height was calculated by adding up the consecutive

cluster pixels at that height. To reduce errors caused by small gap inside a large cluster, a negligible distance C was proposed in this paper. If the distance between two separated cluster pixels was less than C, the two cluster pixels would be identified as the same cluster, otherwise two cluster pixels would be defined as two separated clusters. The total number of the cluster sand the cluster size are crucial parameters to evaluate the cluster behaviors, and obviously, the value of C would significantly affect the detected size and number of clusters.

Fig.4-4 shows the different detected results of cluster size and number with varying C. When C=5 or C=10, the small branches of cluster would be recognized as two or three separated clusters, while C>15, different clusters were well distinguished. Thus, C=15 is selected in this experiment.

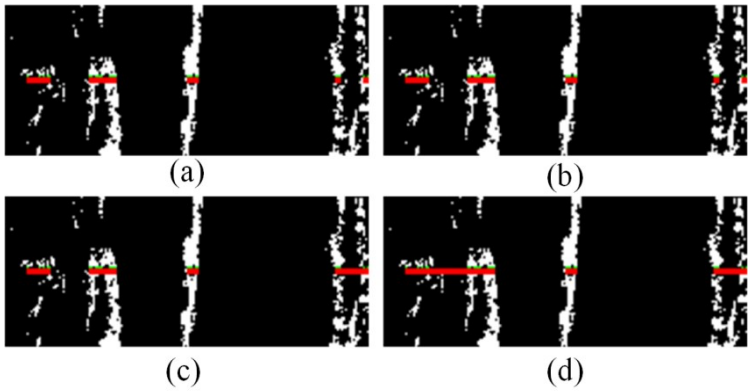

Fig.4-4 Image processing of cluster with various C: (a) C=5, (b)C=10, (c)C=15, (d)C=20 (U_g=2.80 m/s,G_s=37.1 kg/(m^{2}s),d_p= 100 mm).

4.3Results and discussion

4.3.1 Cluster structures and evolutionary processes

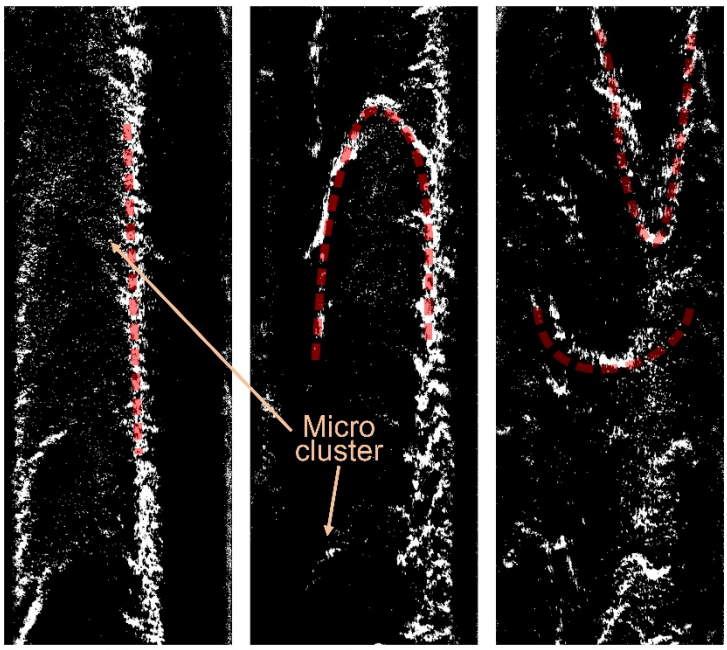

Fig.4-5Typical cluster structures observed in the riser wall of the fast circulating bed: (a) Stripe-shaped cluster, (b) Saddle-shaped cluster and (c) U-shaped cluster, with micro clusters accompanying them (U_g=4.04 m/s,Gs=54.9 kg/(m^{2}s),d_p= 0.375 mm).

In current experiments with Geldart B particles, clusters are found to always appear at the interface between particle streams that have obvious velocity difference. According to the different cluster shapes and evolutionary processes, four typical cluster structures, namely stripe-shaped cluster, saddle-shaped cluster, U-shaped cluster and micro cluster were found in the wall region as seen in Fig.4-5.

- **Stripe-shaped cluster**:

The stripe-shaped cluster with the length usually ranging from about 300 mm to 1000 mm is the most common cluster observed when the riser presents the core-annulus flow structure in the current study. In literature, it was also known as “strand cluster” with

length varying from 100 mm to 500 mm [20].In the core-annulus flow regime exists the rapid upward dilute particle stream in the centre of riser with a relatively dense annulus near the wall, where particle streams may move downwards or upwards with a significant slower velocity. Because such significant differences in velocity magnitudes or even the opposite velocity directions exist between the particle streams, the particles will obviously decelerate and accumulate at the interfaces where they encounter each other.

At the radial direction, particles at the interface region tend to be further compressed to form stripe-shaped clusters moving to the wall, as shown in Fig.4-6(a). This is because the accumulated particles in the interfaces build up the resistance to the gas-solid flows, the flows must re-distribute their paths with the least resistance by compacting accumulated particles to be dense stripes and pushing them from the riser centre aside to the wall according to the theory of energy minimization.

The above evolutions of the stripe-shaped clusters are closely related to the flow conditions and the particle properties. For larger particles, the stripe-shaped clusters are possible to move upwards when the upward flowing dilute particle stream has the relatively stronger momentum due to its higher speed; otherwise, the clusters may travel downwards when the momentum of downward particle stream is stronger due to its denser solid concentration shown in Fig.4-6(b). Due to instable gas-solid flows, the state of these stripe-shaped clusters including their length, width, position may constantly change until they finally vanish. At the same time new strip-shaped clusters appear continuously at other positions in the riser, as shown in Fig.4-6(c)-(j). Additionally, Fig.4-6(c) shows that sometimes particles might aggregate much more seriously at some locations than others in the stripe-shaped clusters. As some branches of the cluster grow to a large size and overbalance the carrying capacity of the gas flow,

they will collapse from the stripe-shaped clusters and fall down much faster as shown in Fig.4-6(d). Such velocity difference between the collapsed clusters and their surrounding particles will bring numerous micro clusters whose size are usually smaller than 30 mm on the lateral sides, as seen in Fig.4-6(f).

Such collapsing phenomena of particle aggregations are more common for small particles, for example, d_s=100 μm. The smaller particles tend to aggregate more closely in the stripe-shaped clusters, making them harder to be blown over by the gas. Therefore, when the sizes of Geldart B particles are very small, the gas-solid flows in the riser tend to be more complicated with the continuously forming and collapsing macro stripe-clusters and the abundant micro clusters.

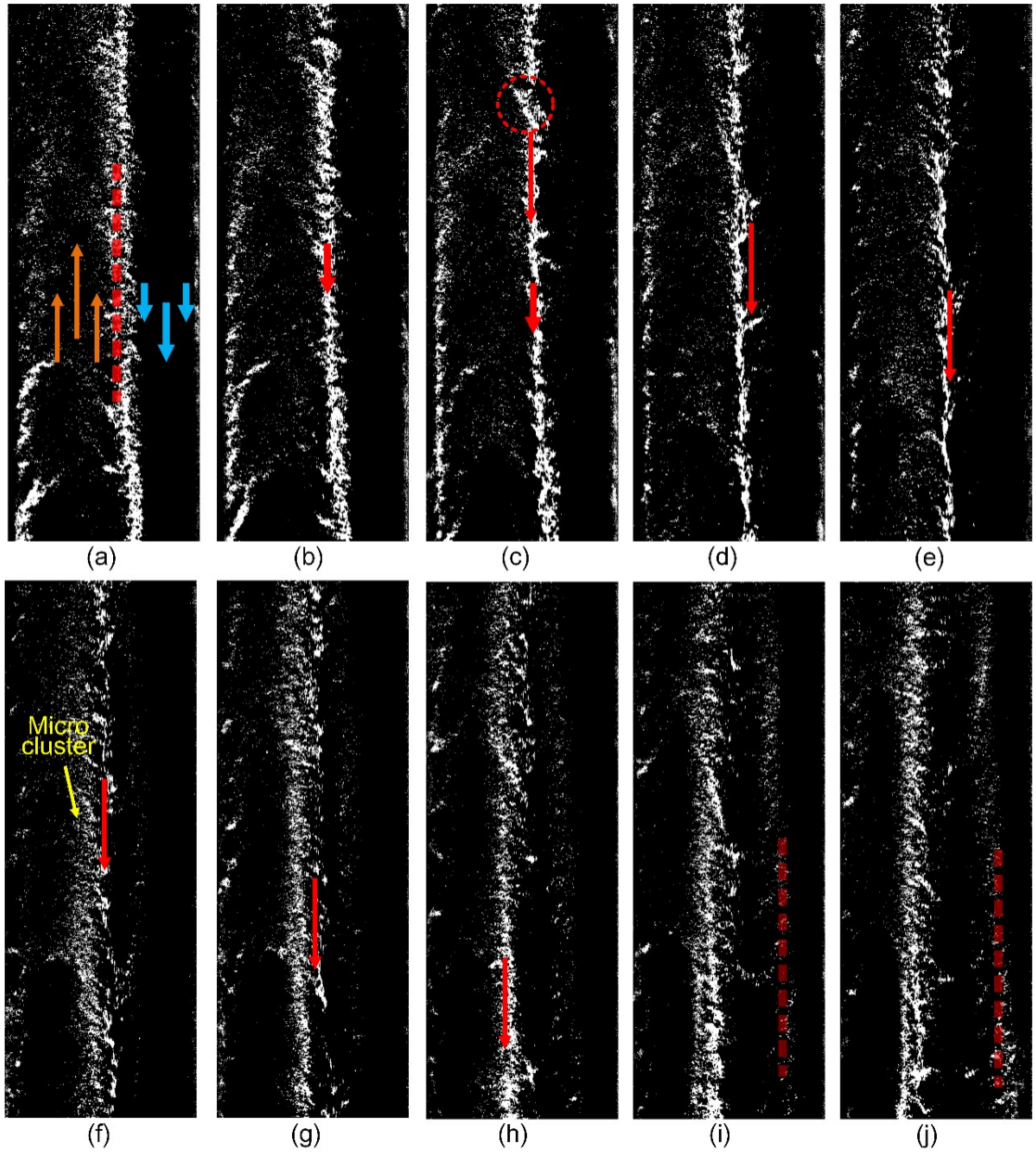

Fig.4-6Typical evolutionary processes of the stripe-shaped cluster

(Δt=0.04 s, U_g=4.04 m/s,G_s=54.9 kg/(m^{2}s),d_p= 0.375 mm).

- **Saddle-shaped cluster**

When the dilute gas-solid streams or jet flows upwards, both micro and macro clusters may appear at their fronts. In the central region of the riser with the low solid concentration, micro clusters often form when the rapid upward particle stream encounters the surrounding particles, and then are quickly blown off or swept away.

However, in the wall region, the instable upward dilute gas-solid stream or jet may encounter the dense downward particle streams, and the large saddle-shaped clusters, with its length usually ranging from 30mm to 200mm in the current study, will be observed at the fronts of gas-solid streams as seen in Fig.4-7(a).

The following motion and evolution of the saddle-shaped clusters are closely related to the dynamical states of particlessteams located in the different sides of the interface. If the momentum of ascending particle stream/jet with higher speed is larger than that of the descending particle stream with higher solid concentration, the saddle-shaped clusters at the front interface will move and expend upward. Finally, they may be broken up by the upward particle stream itself, or they may be impacted and destroyed by the other strong clusters. Otherwise, if the momentum of the downward particle stream is larger than that of the upward particle stream/jet, the saddle-shaped cluster at the interface of these two streams of particles will move downwards with a slow velocity (about 0.33m/s in Fig.4-7)and become denser by aggregating more particles, as seen in Fig.4-7(b)-(i). During they move downward, the saddle-shaped interface will keep narrowing because the front of upward flow is being compacted, until the cluster may finally lose its saddle shape, as shown in Fig.4-7(f)-(i). Another possibility is that the growing particle aggregation finally suddenly collapse and fall down rapidly as it overbalanced with the stream carrying capacity.

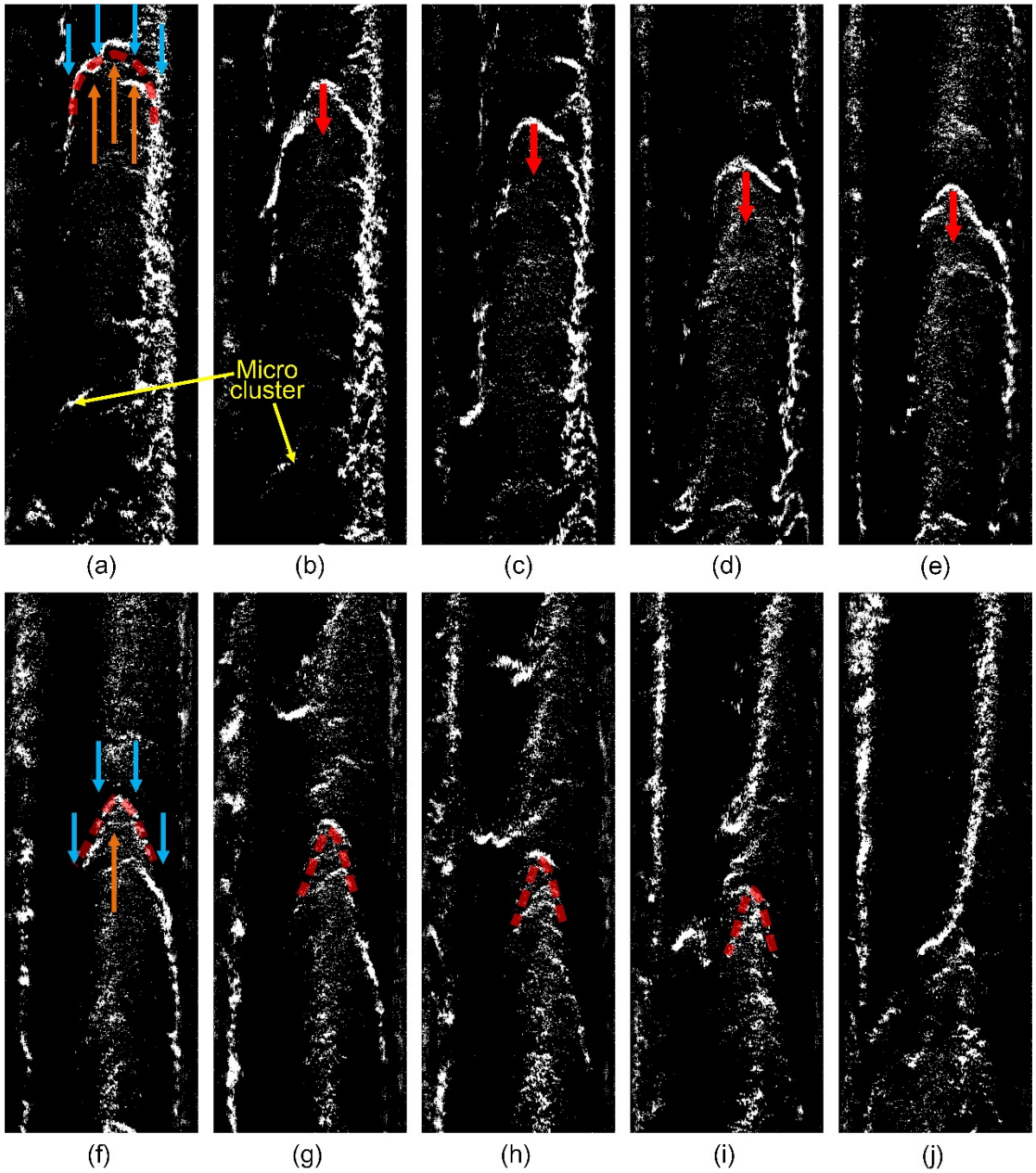

Fig.4-7 Typical evolutionary processes of the saddle-shaped cluster

(Δt=0.04 s, U_g=4.04 m/s,G_s=54.9 kg/(m^{2}s),d_p= 0.375 mm).

- **U-shaped cluster**:

As mentioned above, particle aggregations possibly collapse from the original interface and fall down rapidly. The falling particle aggregates with faster velocities than the surrounding particles will bring the U-shaped clusters along the boundaries, as shown in Fig.4-8(a) and (b).The U-shaped cluster consists of the downward dense cluster core,

namely the originally collapsed particle cluster, and two upward sparse tails, namely the new cluster formed along the boundary as the cluster core falling. The total length of U-shaped cluster usually vary from 50 mm to 300 mm and its falling velocity is about 0.9m/s in Fig.4-8, which is more than 2 times the velocity of the other kinds of clusters (in Fig.4-6 and Fig.4-7). The U-shaped clusters have also been observed in wall regions in previous studies [10][20].It is notable that the U-shaped clusters observed in the study of Horio *et al*. [10] are smaller than that in the current study, because the particles used in their experiments are smaller than quartz sand particles used in our study.

When the U-shaped clusters fall as shown in Fig.4-8(c)-(h),more particles possibly aggregate at the front and its cluster core becomes denser. At last, the growing cluster core might collapse again from the front of the U shaped cluster as shown in Fig.4-8(i)-(j)and falls down rapidly. The original U-shaped cluster will then deform or even disappear.

As discussed above, U-shaped cluster usually forms as the particle aggregations are very large or dense. Its serious particle aggregations and rapid falling speed will significantly disturb the gas-solid flow in the riser and are very unfavourable for the heat and mass transfer and reaction.

- **Micro cluster**:

Apart from often accompanying the fast-moving macro clusters or appearing in the dilute gas-solid streams in the central region of the riser, numerous micro clusters also have been observed in the riser. Micro cluster, which is also called as particle cluster [18], is usually smaller than 30mm. The gas-solid turbulence causes the velocities and directions of particles to change constantly and form low pressure region, which draw the surrounding particles toward them. As the turbulent particle streams keep crashing

with each other, a large number of micro clusters appear frequently and then quickly disappear.

The formation and evolution of clusters in the riser of the fast circulating bed are very complicated, as the above four typical clusters often appear simultaneously, influence mutually and sometimes interconvert into each other. For example, when a larger particle aggregation collapses from the stripe-shaped cluster or the saddle-shaped cluster, the original cluster probably disappears, while a new U-shaped cluster forms. When two U-shaped clusters fall abreast, a saddle-shaped cluster could be easily found between them. Besides, clusters with irregular shapes probably forms when the above typical clusters encounter each other.

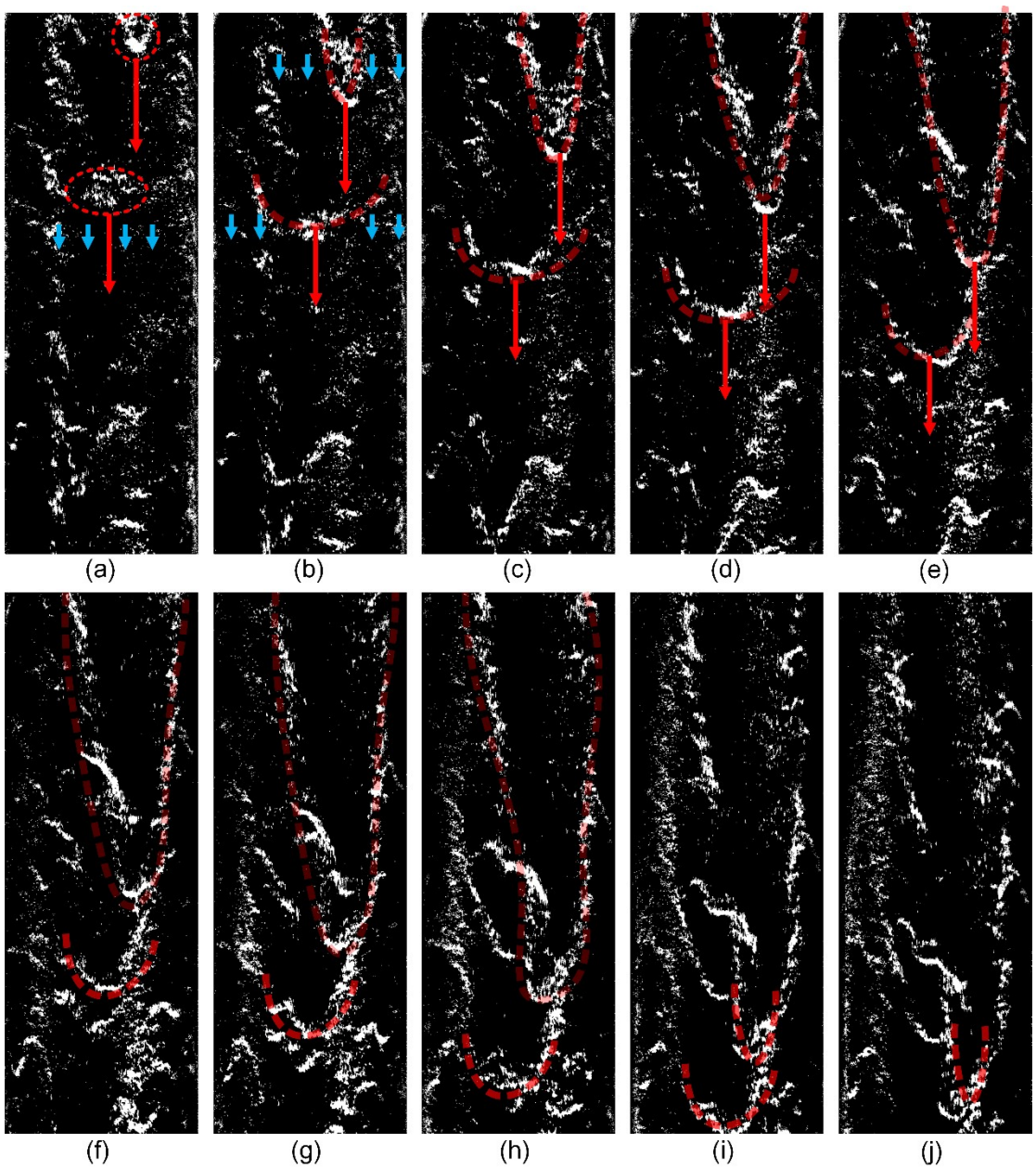

Fig.4-8 Typical evolutionary processes of the U-shaped cluster

(Δt=0.02 s, U_g=4.04 m/s,G_s=54.9kg/(m^{2}s),d_p= 0.375mm).

4.3.2 Cluster size

In this section, the effects of operating conditions and particle properties on the cluster size are studied in terms of horizontal width of the cluster. The average cluster sizes are calculated by analysing the processed images from 10s high speed camera at 250fps, with the U_g ranges from 2.486m/s to 5.594m/s and the solid mass flux is approximately

55kg/(m^{2}s). Fig.4-9 displays the average cluster size d_{cl} as functions of U_g at three heights, i.e. h/H=0.23, 0.33, 0.43. It can be seen from the figure that the average cluster size increases with increasing superficial gas velocity, which is inconsistent with previous study [23]. This may be because two studies are conducted in different flow regimes and riser structures. The experiments of Mondal *et al*. [23]are carried out in a much lower superficial gas velocity, where the U_g changes the solid holdup in the riser significantly and the solid holdup may affect the formation of cluster obviously. When U_g increases, the drag force exerted on the particles is getting greater[31], so as the gas carrying capacity. As the U_g increases from 2.486m/s to 5.594m/s, the flow regime changes from fast fluidization to dilute flow. The account of downward particles decreases with increasing U_g, and the interactions between upward and downward particle streams become less severe. Thus particle clusters are less likely to be shed or broken down by the particle flows from different directions and are easier to form wider clusters with most upward particles at higher U_g. Moreover, it can be seen from the figure that larger particles make wider clusters, which agrees with previous studies [31, 32], and the effect of U_g on the average cluster size appears to be greater for the larger particles. Especially, when d_p=0.10 mm, the average cluster size changes very little with increasing U_g at three heights. For small particles, the structures of clusters are narrower and more stable because of denser packing. Thus, increasing U_g is more likely to result in more disperse cluster distribution, rather than broking them or changing the shapes of the clusters. As for large particles, e.g. d_p= 0.250 mm or 0.375 mm, the structure of cluster is more loose, which is easier changed by the particle flows. It is notable that the increasing axial position results in larger average cluster size, which is consistent with result of Mondal *et al*. [23]. At the lower part of riser, due to the intensive gas-solid turbulence, the particles interact with each other severely, thus the

clusters are more likely to break into smaller ones. As riser height increases, particles experiencing more shear stresses tend to aggregate into larger clusters.

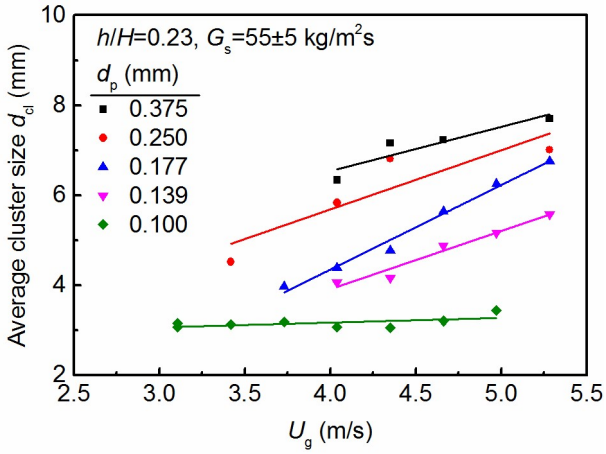

(a)

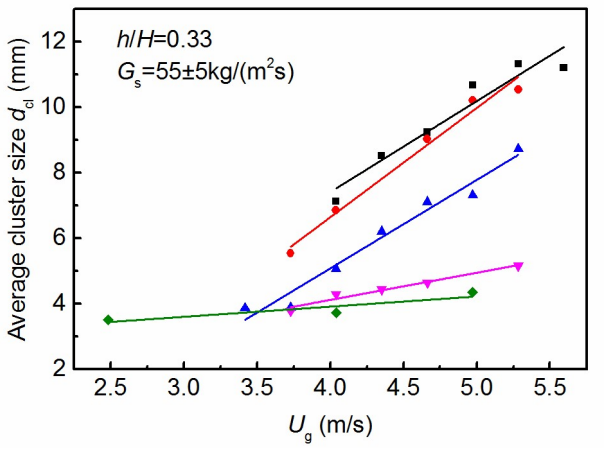

(b)

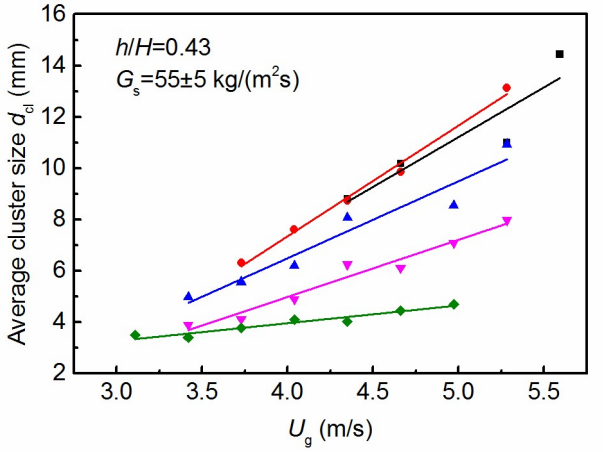

(c)

Fig.4-9 Effects of superficial gas velocity on average cluster size at three heights: (a) *h/H*=0.23; (b) *h/H*= 0.33; (c) *h/H*=0.43.

Fig.4-10 shows the effect of solid mass flux on the average cluster size at three heights, i.e. *h/H*=0.23, 0.33, 0.43. The overall trend shows that the increase in solid mass flux results in smaller cluster at each height, this is in accordance with the work of Horio *et al.* [10]. At the lower region of the riser (*h/H*=0.23), the cluster size changes slightly with increasing G_s, especially for d_p=0.100 mm, the cluster size of which shows little difference with various G_s.

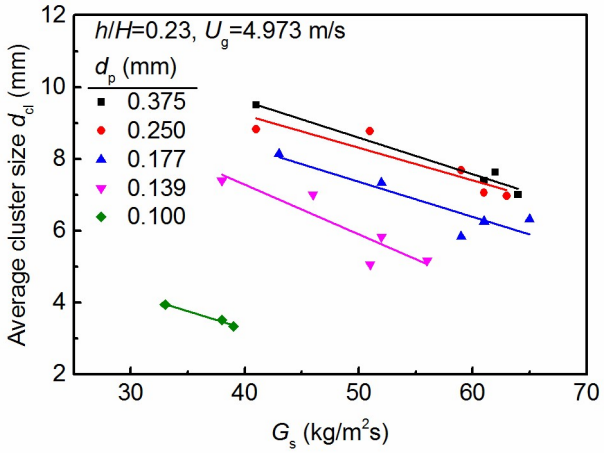

(a)

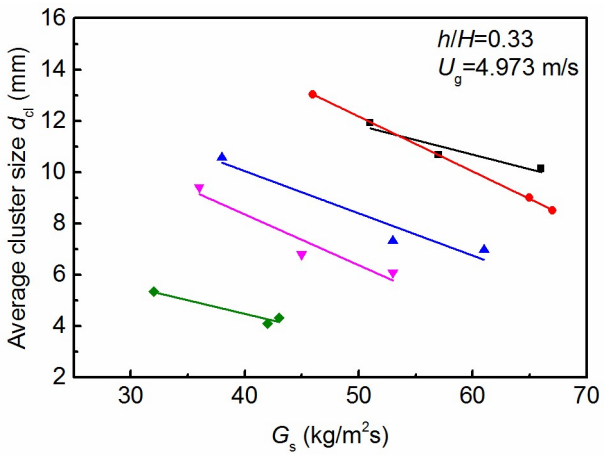

(b)

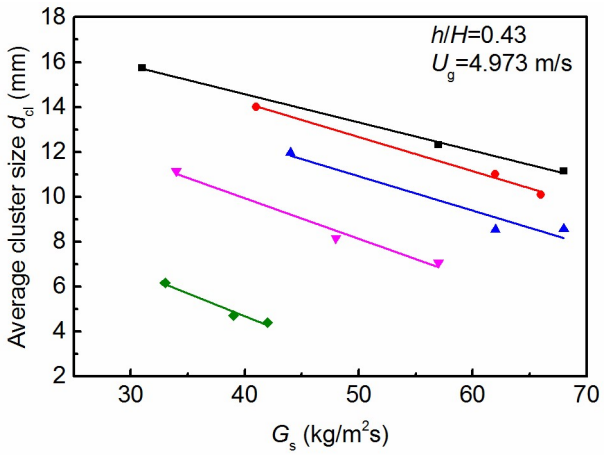

(c)

Fig.4-10 Effects of solid mass flux on average cluster size at three heights:

(a) h/H=0.23; (b) h/H= 0.33; (c) h/H=0.43.

At h/H =0.33, it is notable that small particles (d_p=0.100 mm, 0.139 mm, 0.177 mm) show similar trend as in Fig.4-10 (a), while the cluster size of large particles (d_p=0.250 mm, 0.375 mm) decreases dramatically with increasing G_s. It can be explained by that the increasing solid mass flux gives rise to solid volume fraction and increases gas-solid turbulence. Thus, it is more likely to break the large cluster in the higher bed into small ones, while the small clusters in the lower bed are less susceptible to increasing gas-solid turbulence. As shown in Fig.4-10 (c), the cluster size distribution shows the same trend as that of lower region, because the larger clusters are easier to be interfered by the solid mass flux.

4.4 Cluster time fraction

In this study, the cluster time fraction at a specified height, F_c, is defined as the ratio of the sum time of the clusters appears to the total sampling time at that height.Fig.4-11 presents the influence of superficial gas velocity on cluster time fraction at three heights. The cluster time fraction is several times higher than previous studies [9, 34],

because the detect area in this research is much wider compared with previous studies. In the lower part of the bed shown in Fig.4-11(a), the effect of increasing superficial gas velocity on the cluster time fraction is less significant compared with the higher bed. Due to the intensive gas-solid turbulence in the lower part, the cluster time fractions of particles with different sizes are kept at 0.6 to 0.9 and change slightly at h/H=0.23. High up in the riser, the cluster time fraction decreases with increasing superficial gas velocity, which may be explained by that higher superficial gas velocity at constant solid mass flux leads to lower solid volume fraction. Lower solid concentration results in less intensive gas-solid turbulence and less frequency of clusters. The effect of particle size on the cluster time fraction becomes more obvious in higher bed. It is notable that cluster time fraction of small particles, e.g. d_p=0.100 mm, change mildly with increasing superficial gas velocity, while that of larger particles reduces greatly with higher U_g. This is consistent with our previous result that clusters of smaller particles are more packed than those of larger particles, especially for the particles of d_p=0.100 mm. As shown in Fig.4-11(b) and (c), the effect of axial positions on the cluster time fractions is surprisingly insignificant, which can be explained by that the solid concentration in both heights are with small variations.

The effect of solid mass flux on cluster time fraction at three heights is illustrated in Fig.4-12. At lower part of riser (h/H=0.23), the cluster time fraction ranges between 0.6 to 0.8 and increases slightly with increasing solid mass flux, while decreases with increasing particle size. As shown in Fig.4-12(b) and (c) at h/H= 0.33 and 0.43, the cluster time fraction increases with increasing solid mass flux, this may be explained by that the intensive gas-solid turbulence in higher G_s encourages cluster formation and results in higher cluster frequency. The effects of G_s and d_p becomes more obviously at h/H= 0.33 and 0.43. With increasing particle size, the reduction of cluster time fraction

due to increasing G_s for large particles becomes greater. This can be explained by that the large particles form loose cluster while small particles make more packed clusters, which makes it more difficult to break the cluster of small particles with increasing G_s. Moreover, the increase of cluster time fraction becomes the most significant at h/H=0.43. The solid concentration at higher bed is relative low compared with lower bed, thus the gas-solid turbulence introduced by increasing G_s plays more significant role in increasing cluster frequency and cluster time fraction.

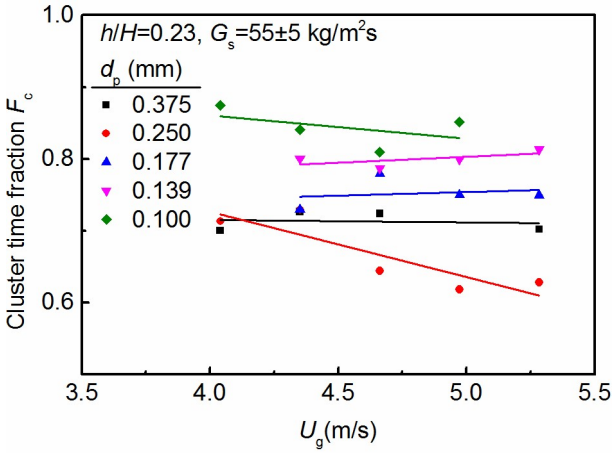

(a)

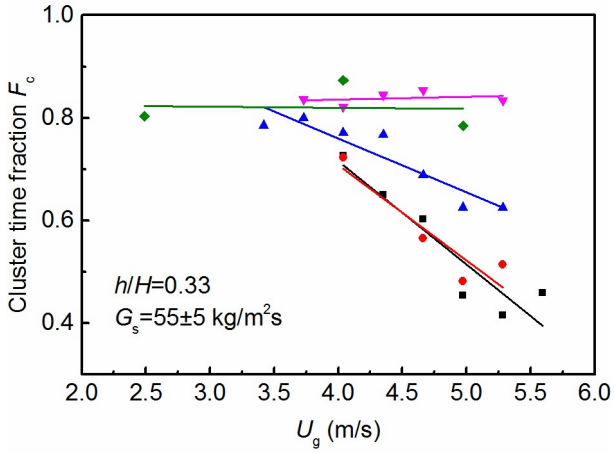

(b)

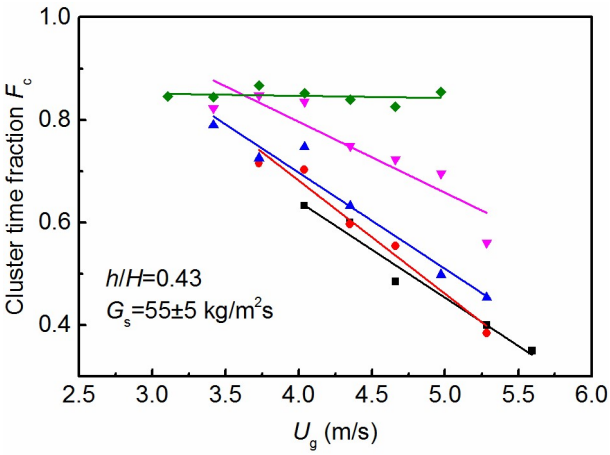

(c)

Fig.4-11 Effects of superficial gas velocity on cluster time fraction at three heights:

(a) h/H=0.23; (b) h/H= 0.33; (c) h/H=0.43.

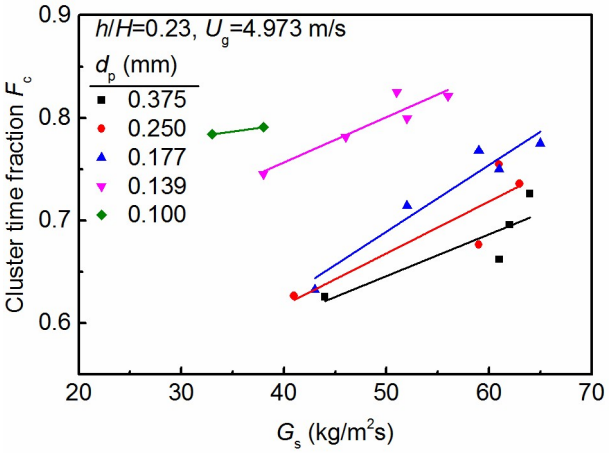

(a)

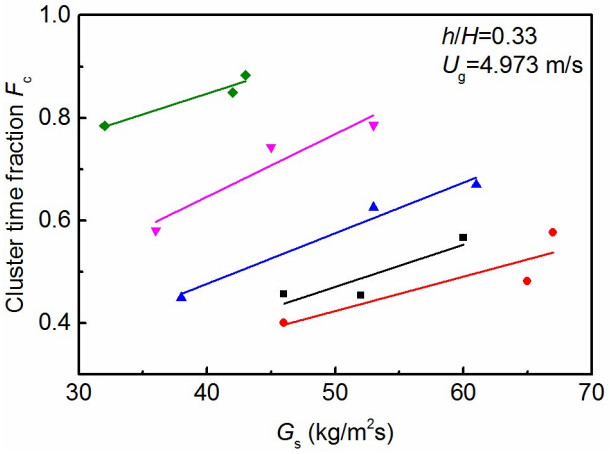

(b)

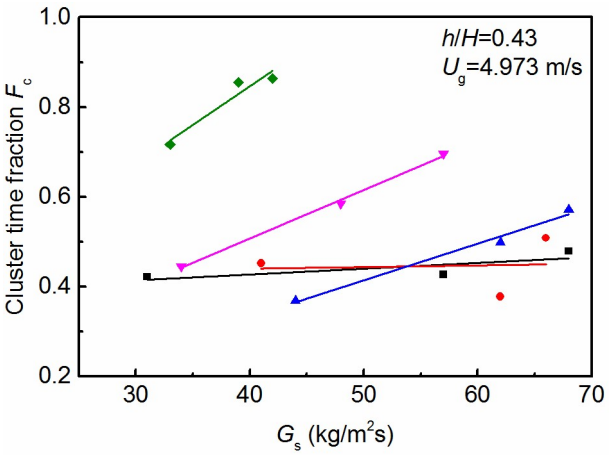

(c)

Fig.4-12 Effects of solid mass flux on cluster time fraction at three heights:

(a) h/H=0.23; (b) h/H= 0.33; (c) h/H=0.43.

4.5 Conclusions

A three-dimensional (3D) fast fluidized bed with the riser of 3.0 m in height and 0.1 m in inner diameter was established to experimentally study the particle clustering behaviours of Geldart B particles. Five kinds of quartz sand particles (d_p=0.100, 0.139, 0.177, 0.250 and 0.375 mm and ρ_p=2480 kg/m^3)were respectively investigated, with the total mass of the bed material kept as 10kg/(m^{2}s) and the superficial gas velocity ranging from 2.486 to 5.594 m/s. Particle cluster characteristics and evolutionary processes in the different positions of the riser were captured by the cluster visualization systems and analysed by the self-developed binary image processing method. Main results can be summarized as follows:

(1) In the riser of the fast fluidized bed with Geldart B particles, four typical cluster structures, namely the macro-scale stripe-shaped cluster, saddle-shaped cluster, U-shaped cluster and the micro cluster are commonly found in the core-annulus flow regime, while only stripe-shaped cluster and micro clusters mainly forms in the dilute

flow regime. Macro clusters with clear shapes start to appear in the region that higher than about1/4 riser height.

(2) The average cluster size increases with increasing superficial gas velocity and particle size, while decreases with growing solid mass flux in the riser. When particle size is small, the effect of superficial gas velocity on the average cluster size becomes less obvious, especially for particles less than 0.100 mm. The average cluster size usually presents a significant increase with the axial height varying from the 1/5 to 1/3 of riser height, and then changes slightly with height in the higher region.

(3) The cluster time fraction decreases with increasing superficial gas velocity and particle size, while it increases with rising solid mass flux. The effects of operating conditions on cluster time fraction also become less obvious for small particles. The cluster time fraction in the lower region is much higher than that of higher bed.

4.6 Reference

[1] Zhu X.L., Yang C.H., Li C.Y., Liu Y.B., Wang L., Li T., Geng Q., Comparative study of gas-solids flow patterns inside novel multi-regime riser and conventional riser, *Chemical Engineering Journal***2013**, 215-216:188-201.

[2] Chew J.W., Hays R., Findlay J.G., Knowlton T.M., Karri S.B.R., Cocco R.A., Hrenya C.M., Reserve core-annular flow of Geldart Group B particles in risers, *Powder Technology***2012**,221:1-12.

[3] Wang X.H., Gao S.Q., Xu Y.H., Zhang J.S., Gas-solids flow patterns in a novel dual-loop FCC riser, *Powder technology***2005**,152: 90-99.

[4] Kunii, O. Levenspiel, Fluidization Engineering, Butterworth-Heinemann, Massachusetts, 1991.

[5] Grace J.R., Avidan A.A., Knowlton T.M., Circulating Fluidized Beds, 1st ed.

Blackie Academic & Professional, London; New York, 1997.

[6] Fan L.S., Zhu C., Principles of Gas–Solid Flows, Cambridge University Press, New York, 1998.

[7] Yang W., Handbook of Fluidization and Fluid-Particle Systems, Marcel Dekker.

[8] Yerushalmi J., Turner D.H., Squires A.M., The Fast Fluidized Bed, *Industrial & Engineering Chemistry Process Design & Development***1976**, 15 (1) :47-53.

[9] Matsen J.M., Mechanisms of choking and Entrainment, *Powder Technology* **1982**, 32: 21-33.

[10] Horio M., Kuroki H., Three-dimensional flow visualization of dilutely dispersed solids in bubbling and circulating fluidized beds, *Chemical Engineering Science* **1994**, 9(15): 2413-2421.

[11] Manyele S.V., Parssinen J.H., Zhu J.X., Characterizing particle aggregates in a high-density and high-flux CFB riser, *Chemical Engineering Journal***2002**, 88: 151-161.

[12] Shaffer F., Gopalan B., Breault R.W., Cocco R., Karri S.B.R., Hays R., Knowlton T., High speed imaging of particle flow fields in CFB risers, *Powder Technology* **2013**,242: 86-89.

[13] Cocco R., Shaffer F., Hays R., Karri S.B.R., Knowlton T., Particle clusters in and above fluidized beds, *Powder Technology***2010**, 203: 3-11.

[14] Harris A.T., Davidson J.F., Thorpe R.B., The prediction of particle cluster properties in the near wall region of a vertical riser, *Powder Technology* **2002**, 127:128-143.

[15] Bai D., Shibuya E., Masuda Y., NishioK., Nakagawa N., Kato K.. Distinction

between upward and downward flows in circulating fluidized beds. *Powder Technology***1995**, 84:75-81.

[15] Liu X.H., Gao S.Q., Song W.L., Li, J.H. Effect of particle acceleration/deceleration on particle clustering behavior in dilute gas-solid flow, *Chemical Engineering Science* **2006**, 61:7087-7095.

[16] Brien T., Syamlal M.. Particle cluster effects in the numerical simulation of a circulating fluidized bed. Preprint volume for Circulating Fluidized Beds IV. 1993: 345-350.

[17] Bi X.T., Zhu J.X., Jin Y., Yu Z.Q., Forms of Particle Aggregation in CFB, in: Proceedings of the Sixth Chinese Conference on Fluidization, Wuhan, China, 1993.

[18] ShiH.X., Wang Q.H., Xu L.H., Luo Z.Y., Cen K.F., Visualization of clusters in a circulating fluidized bed by means of particle-imaging velocimetry (PIV) technique, in: Proceedings of the 9th International Conference on Circulating Fluidized Beds, Hamburg, Germany, 2008, pp.1013-1019.

[19] Xu J., Zhu J., Visualization of particle aggregation and effects of particle properties on cluster characteristics in a CFB riser, *Chemical Engineering Journal***2011**, 168:376-389.

[20] McMillan J., Shaffer F., Gopalan B., Chew J.W., Hrenya C., Hays R., KarriS.B.R., Cocco R., Particle cluster dynamics during fluidization, *Chemical Engineering Science***2013**,100:39-51.

[21] Yang J.S., Zhu J., Cluster identification using image processing, *China Part.***2015**, 23: 16-24.

[22] Mondal D.N., Kallio S., Saxen H., Length scales of solid clusters in a two-dimensional circulating fluidized bed of Geldart B particles, *Powder Technology*

2015, 269:207-218.

[23] Cahyadi A., Anantharaman A., Yang S.L., Karri S.B.R.,. Findlay J.G, Cocco R.A., Chew J.W., Review of cluster characteristics in circulating fluidized bed (CFB) risers, *Chemical Engineering Science***2017**, 158:70-95.

[24] Anantharaman A., Issangya A., Karri S.B.R., Findlay J., Hrenya C.M., Cocco R.A., Chew J.W., Annulus flow behavior of Geldart Group B particles in a pilot-scale, *Powder Technology* **2017**, 305:816-828.

[25] Chan C.W., Seville J.P.K., Parker D.J., Baeyens J., Particle velocities and their residence time distribution in the riser of a CFB, *Powder Technology***2010**, 203: 187-197.

[26] Guenther C., Breault R., Wavelet analysis to characterize cluster dynamics in a circulating fluidized bed, *Powder Technol*ogy **2007**, 73:163-173.

[27] Gomez L.C., Milioli F.E., Numerical study on the influence of various physical parameters over the gas-solid two-phase flow in the 2D riser of a circulating fluidized bed, *Powder Technology***2003**, 132 :216-225.

[28] Lu H.L., Wang, S.Y., He Y.R., et al. Numerical simulation of flow behavior of particles and clusters in riser using two granular temperatures, *Powder Technology* **2008**, 182: 282-293.

[29] WangS.Y. ,ShenZ.H., Lu H.L. et al., Numerical predictions of flow behavior and cluster size of particles in riser with particle rotation model and cluster-based approach, *Chemical Engeering Science* **2008**, 63:4116-4125.

[30] Kiani A., Sotudeh-Gharebagh R., Mostoufi N., Cluster size distribution in the freeboard of gas-solid fluidized bed, *Powder Technology* **2013***,* 246 :1-6.

[31] Xu J., Zhu J., A new method for the determination of cluster velocity and size in a circulating fluidized bed, *Industrial & Engineering Chemistry Research***2012**, 51:2143-2151.

[32] Sharma A.K., Tuzla K., Matsen J., et al. Parametric effects of particle sizeand gas velocity on cluster characteristics in fast fluidized beds[J]. *Powder Technology* **2000**, 111: 114-122.

[34] Chew J.W., Hays R., Findlay J.G., et al. Cluster characteristics of Geldart Group B particles in a pilot-scale CFB riser. I. Monodisperse systems[J]. *Chemical Engineering Science***2012**, 68: 72-81.

CHAPTER 5 Three dimensional Eulerian-Lagrangian Simulation of a Fast Fluidized Bed

5.1 Introduction

The clusters in the core region of riser could not be observed directly by non-intrusive method due to the dense annulus particle layer at the wall, the understanding of clusters hydrodynamics properties is still lacking. The numerical simulation method is an important way to study the gas-solid flow behavior in a complex dense gas-solid flow, which can effectively overcome the shortage of the existing experimental conditions and measurement, and simulate the flow structure and the details of the gas-solid flow. There are two primary modelling approaches for the typical fluidization system, consisting of Eulerian-Eulerian method and Eulerian-Lagrangian method. In two-fluid models (TFM), the gas and solid phases are both considered as continuous mediums, described in terms of separate sets of conservation equations and coupling by the interaction terms between the gas and solid phase. It provides a convenient and simple method to calculate the gas-solid behaviour. However, the traditional TFM cannot provide detailed information of particle movement, the discrete character of solid phase at microscopic level lose due to its continuum assumptions[3].

The Eulerian−Lagrangian (EL) method treats particles as separate, solid objects and their behaviours are modelled by the Newtonian equations of motion. The traditional Eulerian-Lagrangian approach, CFD-DEM (computational fluid dynamics-discrete element method), can track each discrete particle and compute particle-particle collision. However, the high computational cost limits the application of this method in large dense solid gas flow system

Due to the limitation of computational resources and the complexities of flow characteristics in simulation of full loop circulating fluidized bed, most the early simulations of fast fluidized bed are conducted for the riser part or in separate structure. However, as the downer maintain the pressure balance and realize a self-equilibrium

of the loop[1], thus the simulation result from separated part of the circulating fluidized bed may be quite different from the experimental results. The simulation of full-loop fast fluidized bed could capture the flow behaviour of the whole circulation system efficiently and obtain detail information of gas-solid flow[2], which has got wide attention recently. Moreover, with the development of computing capability and the improvement of simulation method, more and more studies have been proposed on flow behaviour of fast fluidized bed by full-loop simulation method.

Recently, another Eulerian-Lagrangian approach, multiphase particle-in-cell (MP-PIC) method, proposed by Andrews et al.[4] has attracted much attention because of its specific advantages at the extremely efficient calculation. In MP-PIC scheme, the particle-particle collision is not calculated directly by CFD-DEM, but through the particle stress gradient based on the Eulerian grid. Meanwhile, the real particles are grouped into computational particles (parcel) each including one or a certain amount of particles with uniform size, density, velocity, etc. On the basis of the computational particles, the dense gas-solid fluidization system at large scale can be analysed through a reasonable amount of particles [5-6].

Based on the multi-phase particle-in-cell (MP-PIC) methodology and experimental set-up in chapter 2, a three-dimensional Eulerian-Lagrangian numerical model, boundary conditions and numerical method were developed for fast fluidized bed handling Geldart B particles. The sensitivity of some crucial modelling parameters, including grid resolution, the number of particle per parcel, the drag force model and the particle close pack volume fraction have been systematically analysed, and optimized. The full-loop numerical simulation of three-dimensional fast fluidized bed, including riser, two-level cyclones, downer and J-type back-feeder was achieved.

5.2 Mathematical model

5.2.1 Governing equations of gas phase

In MC-PIC approach, the gas phase is described as continuous phase and calculated by Eulerian computational grids. The movement of gas phase is described by Navier-Stokes equations.

The mass and momentum equations are given as follows:

$$\frac{\partial(\varepsilon_g \rho_g)}{\partial \mathrm{t}} + \nabla \cdot \left(\varepsilon_g \rho_g \boldsymbol{u}_g\right) = 0 \text{(5-1)}$$

$$\frac{\partial(\rho_g \varepsilon_g \boldsymbol{u}_g)}{\partial \mathrm{t}} + \nabla \cdot \left(\rho_g \varepsilon_g \boldsymbol{u}_g \boldsymbol{u}_g\right) = -\nabla p - \boldsymbol{F} + \nabla \cdot \left(\varepsilon_g \tau_g\right) + \rho_g \varepsilon_g \boldsymbol{g} \text{(5-2)}$$

where$\boldsymbol{u}_g$and p are gas velocity vector and pressure,τ_g and ε_g are gas stress tensor and solid volume fraction, respectively,$\boldsymbol{F}$ is the momentum exchange rate between gas and solid phases per unit volume.

$$\boldsymbol{F} = \iint fm(D_p\left(\boldsymbol{u}_g - \boldsymbol{u}_p\right) - \frac{1}{\rho_p}\nabla p) dm dv \text{(5-3)}$$

Where$\boldsymbol{u}_p$ and $\rho_p$is the particle velocity and density, D_p is the drag function for particle in the position.

5.2.2 Turbulence model

In this study, the large eddy simulation (LES) method was used as turbulence model, which is the combination of the direct simulation and the Reynolds mean method. The LES model decomposes the turbulence into the large vortices and the small vortices. The large eddy motion (larger than the grid scale) is directly calculated by the numerical solution of the Navier-Stokes equation, while the effect of small vortex on large eddy motion is simulated by establishing a model.

In LES, a mathematical filter function is established to decompose the motion equation of large scale vortex from the instantaneous equation of turbulence, while the vortex is filtered out by the smaller scale than the filter function. The influence of the small eddy

on the large eddy is introduced by the equation of the large eddy flow field. The stress term is similar to the Reynolds stress term in the Reynolds average method, which is called sub grid scale stress. The corresponding model is sub grid scale stress (SGS)model.

The physical space filtering is essentially an application of an average operation, which uses a given filter function G to decompose the flow variable $f(x_i)$ into a large grid scale variable $\bar{f}(x_i)$ and a small grid scale variable $f'(x_i)$.

$$\begin{cases} \bar{f}(x_i) = G(x_i - x_i')f(x_i)dx_i' \\ f'(x_i) = f(x_i) - \bar{f}(x_i) \end{cases} \quad (5\text{-}4)$$

Three filter functions are most commonly used: the box filter function, the rich phase filter function and the Gauss filter function. Among the three functions, the Gauss filter function has the best performance, but it costs a lot computation resource, while the box filter function is the most popular filter function.

The expression of the box filter function is:

$$G(x_i - x_i') = \begin{cases} \frac{1}{\Delta_i} & |x_i - x_i'| \le \frac{\Delta_i}{2} \\ 0 & |x_i - x_i'| \ge \frac{\Delta_i}{2} \end{cases} \quad (5\text{-}5)$$

The expression of therich phase filter function is:

$$G(x_i - x_i') = \frac{sin(\pi|x_i - x_i'|/\Delta_i)}{\pi|x_i - x_i'|/\Delta_i} \quad (5\text{-}6)$$

The expression of the Gauss filter function is:

$$G(x_i - x_i') = \left(\frac{6}{\pi\Delta_i^2}\right)^{1/2} exp\left[\frac{-6(x_i - x_i')^2}{\Delta_i^2}\right] \quad (5\text{-}7)$$

5.2.3 Equation of particle motion

In MC-PIC method, the transport equation of particle distribution function (PDF) is used to predicting the dynamic of the particle phase. PDF is a function of particle position $\boldsymbol{x}_p$, velocity $\boldsymbol{u}_p$, mass m_p and time t. The function $f(\boldsymbol{x}_p,\boldsymbol{u}_p,m_p,t)dm_p d\boldsymbol{u}_p$ is the average particle number in per unit volume with time t in the interval $(\boldsymbol{x}_p,\boldsymbol{x}_p+d\boldsymbol{x}_p)$, velocity in the interval $(\boldsymbol{u}_p,\boldsymbol{u}_p+d\boldsymbol{u}_p)$, mass in the interval (m_p,m_p+dm_p) [6]. The transport equation for f is:

$$\frac{\partial f}{\partial t}+\nabla\cdot\left(f\boldsymbol{u}_p\right)+\nabla\cdot\left(f\frac{d\boldsymbol{u}_p}{dt}\right)=\left(\frac{\partial f}{\partial t}\right)_{col} \quad (5\text{-}8)$$

$$\left(\frac{\partial f}{\partial t}\right)_{col}=\frac{f_D-f}{\tau_D}+\frac{f_G-f}{\tau_G} \quad (5\text{-}9)$$

where f_D is the particle distribution function, τ_D is the collision damping time. O'Rourke et al.[13]considered the influences of particle recovery efficient and velocity distribution of the non-equilibrium particles on the particle collision time. The second term on the right of the equation includes the effect that velocity of collision particles tend to the isotropic Gauss distribution, where τ_G、f_G refers to the distribution function of the particle collision relaxation time and particle equilibrium state under that effect, respectively.

The solid phase is simulated by Lagrangian method, calculating the effect of numerical particle on the gas-solid flow efficiently. Each numerical particle contains n_p real particles with the same particle properties (e.g. particle density, particle size) at position $\boldsymbol{x}_p(x_p,y_p,z_p)$.

The motion equation of particle movement is:

$$\frac{d\boldsymbol{x}_p}{dt}=\boldsymbol{u}_p \quad (5\text{-}10)$$

The particle acceleration is:

$$\frac{\mathrm{d}\boldsymbol{u}_\mathrm{p}}{\mathrm{d}t} = D_\mathrm{p}\left(\boldsymbol{u}_\mathrm{g} - \boldsymbol{u}_\mathrm{p}\right) - \frac{1}{\rho_\mathrm{p}}\nabla p + \boldsymbol{g} - \frac{1}{\varepsilon_\mathrm{p}\rho_\mathrm{p}}\nabla\boldsymbol{\tau}_\mathrm{p} + \boldsymbol{F}_\mathrm{f} \quad (5\text{-}11)$$

where $\boldsymbol{u}_\mathrm{p}$ is particle velocity, ρ_p is the particle density, $\boldsymbol{\tau}_\mathrm{p}$ is the particle contact normal stress, $\boldsymbol{F}_\mathrm{f}$ is the particle friction force, which plays an important role in dense particle flow.

The particle friction force $\boldsymbol{F}_\mathrm{f}$ can be express by:

$$\boldsymbol{F}_\mathrm{f} = c_\mathrm{f}\boldsymbol{F}_\mathbf{N} \quad (5\text{-}12)$$

where c_f is the coefficient of friction ratio and $\boldsymbol{F}_\mathbf{N}$ is the average normal stress of particles, calculating the average friction force on each mesh[14].

5.2.2.1 Collision model

The particle-particle force is calculated by a spring-damper model and direct particle contact in DEM method [15, 16], while the collision forces between particles calculated by particle stress gradient in MC-PIC method.

The normal stress τ_p of particle, representing particle-to-particle collisions is modeled with spatial gradients. The discrete particle volume is mapped to the grid cell and then the derived solid volume fraction is used to calculate the particle stress gradient on Eulerian grid. Finally, the contact normal stress is applied to discrete particles. The stress model used here is proposed by Harris and Crighton[17].

$$\tau_\mathrm{p}\left(\varepsilon_\mathrm{p}\right) = \frac{P_\mathrm{s}\varepsilon_\mathrm{p}^{\gamma}}{max\left[\varepsilon_\mathrm{cp}-\varepsilon_\mathrm{p},\theta\left(1-\varepsilon_\mathrm{p}\right)\right]} \quad (5\text{-}13)$$

where P_s, $\gamma$and $\theta$are model constants, and ε_cp is the particle volume fraction at close pack.

5.2.2.2Particle damping collision model

The damping effect of collision between particles are calculated by Bhatnagar-Gross-Krook (BGK) collision model, which model the relaxation of profile of particle velocity toward the equilibrium state[18, 19].

In the BGK collision model, the collision damping time τ_{D} has a positive correlation with particle collision time, which is calculated by the correlation derived by O'Rourke et al. [13, 20]:

$$\frac{1}{\tau_{\mathrm{D}}}=\frac{8\sqrt{2}}{3\pi}\frac{\sum_{\mathrm{p}} n_{\mathrm{p}}\left(r_{\mathrm{p}}+r_{32}\right)^{4}\left(u_{\mathrm{p,i}}-\overline{u_{\mathrm{i}}}\right)^{2}}{\sum_{\mathrm{p}} n_{\mathrm{p}}\left(r_{\mathrm{p}}+r_{32}\right)^{2}\sqrt{\left(u_{\mathrm{p,i}}-\overline{u_{\mathrm{i}}}\right)^{2}}}g_{0}\left(\varepsilon_{\mathrm{p}}\right)\eta(1-\eta) \quad (5\text{-}14)$$

where $g_{0}\left(\varepsilon_{\mathrm{p}}\right)=\frac{\varepsilon_{\mathrm{cp}}}{\varepsilon_{\mathrm{cp}}-\varepsilon_{\mathrm{p}}}$, $\eta=\frac{1+e_{\mathrm{p}}}{2}$, e_{p} is the particle-particle restitution coefficient, is the Sauter mean radius of the cell.

5.2.4 Particle-gas interaction

Drag force model has brought out the significance in modelling the hydrodynamic characteristics in CFB risers. The drag force models adopted in Barracuda software are as follows:

(1)Wen-Yu model

This model is an appropriate choice for the gas-solid flow with solid volume fraction ranges between 0.01 to 0.61[21]:

$$D_{\mathrm{p}}=\frac{3}{4}C_{\mathrm{d}}\frac{\rho_{\mathrm{g}}\left|\boldsymbol{u}_{\mathrm{g}}-\boldsymbol{u}_{\mathrm{p}}\right|}{d_{\mathrm{p}}\rho_{\mathrm{p}}} \quad (5\text{-}15)$$

where the drag force coefficient is defined by

$$C_{\mathrm{d}}=\begin{cases}\frac{24}{Re}\varepsilon_{\mathrm{g}}^{-2.65} & Re<0.5\\ \frac{24}{Re}\varepsilon_{\mathrm{g}}^{-2.65}\left(1+0.15Re^{0.687}\right) & 0.5\leq Re\leq 1000\\ 0.44\varepsilon_{\mathrm{g}}^{-2.65} & Re>1000\end{cases} \quad (5\text{-}16)$$

(2) Ergun model

This model is a suitable for the gas-solid flow with solid volume fraction ranges between 0.47 to 0.7[22]:

$$D_{\mathrm{p}} = \left(\frac{C_1 \varepsilon_{\mathrm{p}}}{\varepsilon_{\mathrm{g}} Re} + C_2\right) \frac{|\boldsymbol{u}_{\mathrm{g}} - \boldsymbol{u}_{\mathrm{p}}|}{d_{\mathrm{p}} \rho_{\mathrm{p}}} \quad (5\text{-}17)$$

where the coefficient of viscous term $C_1 = 150$, and the coefficientof inertialterm $C_2 = 1.75$.

(3) Gidaspow model

This drag model is a combination of Wen-Yu and Ergun models，which is applicable to the gas-solid flow ranges from dilute flow to dense flow[23]：

$$D_{\mathrm{p}} = \begin{cases} D_{\mathrm{Wen-Y}} & \varepsilon_{\mathrm{p}} < 0.75\varepsilon_{\mathrm{cp}} \\ \left(D_{\mathrm{Ergun}} - D_{\mathrm{Wen-Yu}}\right)\left(\frac{\varepsilon_{\mathrm{p}} - 0.75\varepsilon_{\mathrm{cp}}}{0.85\ \varepsilon_{\mathrm{cp}} - 0.75\ \varepsilon_{\mathrm{cp}}}\right) + D_{\mathrm{Wen-Yu}} & 0.75\varepsilon_{\mathrm{cp}} \le \varepsilon_{\mathrm{p}} \le 0.85\varepsilon_{\mathrm{cp}} \\ D_{\mathrm{Ergun}} & \varepsilon_{\mathrm{p}} > 0.85\varepsilon_{\mathrm{cp}} \end{cases} \quad (5\text{-}18)$$

(4)Strokes model

$$D_{\mathrm{p}} = \frac{9}{2} \frac{\mu_{\mathrm{g}}}{r_{\mathrm{p}}^2 \rho_{\mathrm{p}}} \quad (5\text{-}19)$$

(5) Turton-Levenspiel model

$$D_{\mathrm{p}} = \frac{3}{4} C_{\mathrm{d}} \frac{\rho_{\mathrm{g}} |\boldsymbol{u}_{\mathrm{g}} - \boldsymbol{u}_{\mathrm{p}}|}{d_{\mathrm{p}} \rho_{\mathrm{p}}} \quad (5\text{-}20)$$

$$C_{\mathrm{d}} = \frac{24}{Re}\left(1 + 0.173 Re^{0.657}\right)\varepsilon_{\mathrm{g}}^{-2.65} + \frac{0.413}{1 + 16300 Re^{-1.09}} \varepsilon_{\mathrm{g}}^{-2.65} \quad (5\text{-}21)$$

(6) Richardson model

$$D_{\mathrm{p}} = \frac{3}{4} C_{\mathrm{d}} \frac{\rho_{\mathrm{g}} |\boldsymbol{u}_{\mathrm{g}} - \boldsymbol{u}_{\mathrm{p}}|}{d_{\mathrm{p}} \rho_{\mathrm{p}}} \quad (5\text{-}22)$$

5.2.5 Boundary condition and initial condition

The no-slip boundary can be specified for the gas phase, a bounce-back condition for the particle-wall collision is used[24]:

$$\boldsymbol{n}\cdot\boldsymbol{u}_{\mathrm{p}}=-e_{\mathrm{wn}}\boldsymbol{n}\cdot\boldsymbol{u}_{\mathrm{p}}^{(0)} \quad (5\text{-}23)$$

$$\tau\cdot\boldsymbol{u}_{\mathrm{p}}=e_{\mathrm{w}\tau}\tau\cdot\boldsymbol{u}_{\mathrm{p}}^{(0)} \quad (5\text{-}24)$$

where e_{wn} and $e_{\mathrm{w}\tau}$ are the normal and tangential particle-wall restitution coefficients, respectively,$\boldsymbol{u}_{\mathrm{p}}^{(0)}$is the particle velocity before collision.

The mass flow rate and the volume fraction of the gas phase and solid phase at the inlets were set according the gas mass flow rate and solid mass flux. The pressure boundary condition was adopted at the outlets. The initial condition the riser was filled with air and the gas velocity was zero.

5.2.5 Numerical solution

In the MP-PIC method, the particle properties are mapped from particle location to the Eulerian grid to obtain grid-based properties, and used to further calculation. The particle volume fraction at cell ξ can be calculated:

$$\varepsilon_{\mathrm{p}\xi}=\frac{1}{V_{\xi}}\sum_{1}^{N_{\mathrm{p}}}n_{\mathrm{p}}V_{\mathrm{P}}S_{\mathrm{p}\xi} \quad (5\text{-}25)$$

where $\mathrm{V_P}$ is the volume of particle，V_{ξ} is the volume of cell，n_{p} is the number of the real particles in a numerical particle,N_{p} is the number of numerical particle and $S_{\mathrm{p}\xi}$ is the interpolation operator. The total volume of particle phase and gas phase is 1, namely $\varepsilon_{\mathrm{p}}+\varepsilon_{\mathrm{g}}=1$.

The velocity of particle is updated by integration of the particle acceleration equation:

$$\boldsymbol{u}_{\mathrm{p}}^{\mathrm{n}+1}=\frac{\boldsymbol{u}_{\mathrm{p}}^{\mathrm{n}}+\Delta\left[D_{\mathrm{p}}\boldsymbol{u}_{\mathrm{g,p}}^{\mathrm{n}+1}-\frac{1}{\rho_{\mathrm{p}}}\nabla p_{\mathrm{p}}^{\mathrm{n}+1}-\frac{1}{\varepsilon_{\mathrm{p}}\rho_{\mathrm{p}}}\nabla\tau_{\mathrm{p}}^{\mathrm{n}+1}+\boldsymbol{g}+\frac{\overline{\boldsymbol{u}_{\mathrm{p}}^{\mathrm{n}}}-\boldsymbol{u}_{\mathrm{p}}^{\mathrm{n}}}{\tau_{\mathrm{D}}}\right]}{1+\Delta tD_{\mathrm{p}}} \quad (5\text{-}26)$$

where $\boldsymbol{u}_{\mathrm{g,p}}^{\mathrm{n+1}}$is the interpolated implicit gas velocity at the position of particle, $\boldsymbol{\nabla} p_{\mathrm{p}}^{\mathrm{n+1}}$is the interpolated implicit pressure gradient at the position of particle and $\boldsymbol{\nabla}\tau_{\mathrm{p}}^{\mathrm{n+1}}$ is the interpolated particle stress gradient at the position of particle.

The position of particle at the next time step can be expressed by:

$$\boldsymbol{x}_{\mathrm{p}}^{\mathrm{n+1}} = \boldsymbol{x}_{\mathrm{p}}^{\mathrm{n}} + \boldsymbol{u}_{\mathrm{p}}^{\mathrm{n+1}}\Delta t \quad (5\text{-}27)$$

The gas phase and the particle phase are coupled through the interphase momentum exchange implicitly in the fluid momentum equation. In cell ξ, the interphase momentum transfer function can be expressed by:

$$F_{\xi}^{\mathrm{n+1}} = \frac{1}{V_{\xi}}\sum_{\mathrm{pP}} S_{\xi}\left[D_{\mathrm{p}}\left(u_{\mathrm{g,p}}^{\mathrm{n+1}} - u_{\mathrm{P}}^{\mathrm{n+1}}\right) - \frac{1}{\rho_{\mathrm{P}}}\boldsymbol{\nabla} p_{\mathrm{p}}^{\mathrm{n+1}}\right] n_{\mathrm{P}} m_{\mathrm{P}} \quad (5\text{-}28)$$

where m_{P} is the mass of a particle, and the interphase drag force D_{p} is calculated by a drag model with the drag coefficientC_{d}.

$$D_{\mathrm{p}} = \frac{3}{4} C_{\mathrm{d}} \frac{\rho_{\mathrm{g}}|\boldsymbol{u}_{\mathrm{g}} - \boldsymbol{u}_{\mathrm{p}}|}{d_{\mathrm{p}}\rho_{\mathrm{p}}} \quad (5\text{-}29)$$

In MP-PIC method, the gas phase equations are discrete in finite volume form with staggered scalar and momentum nodes. A SIMPLE solution scheme is used to adjust pressure and gas velocity to satisfy gas continuity [25]. The momentum, energy and pressure equations are solved with a conjugate gradient solver, and each particle momentum, motion and energy ordinary differential equations are solved directly.

5.3 Computational model

The simulated three-dimensional full-loop fast fluidized bed is shown in Fig.5-1, with the riser of 3.0 m in height and 0.1 m in inner diameter. At the top of riser, the gas and solids passed through a smooth elbow and then first separated in the primary cyclone, then further gas-solid separated and collected by secondary cyclone and bag filter. The solid mass flux is monitored at eight points, including riser exit, the inlet and outlet of

the cyclones, the top and bottom of the riser, the downer and the feedback valve as seen in Fig.5-1.

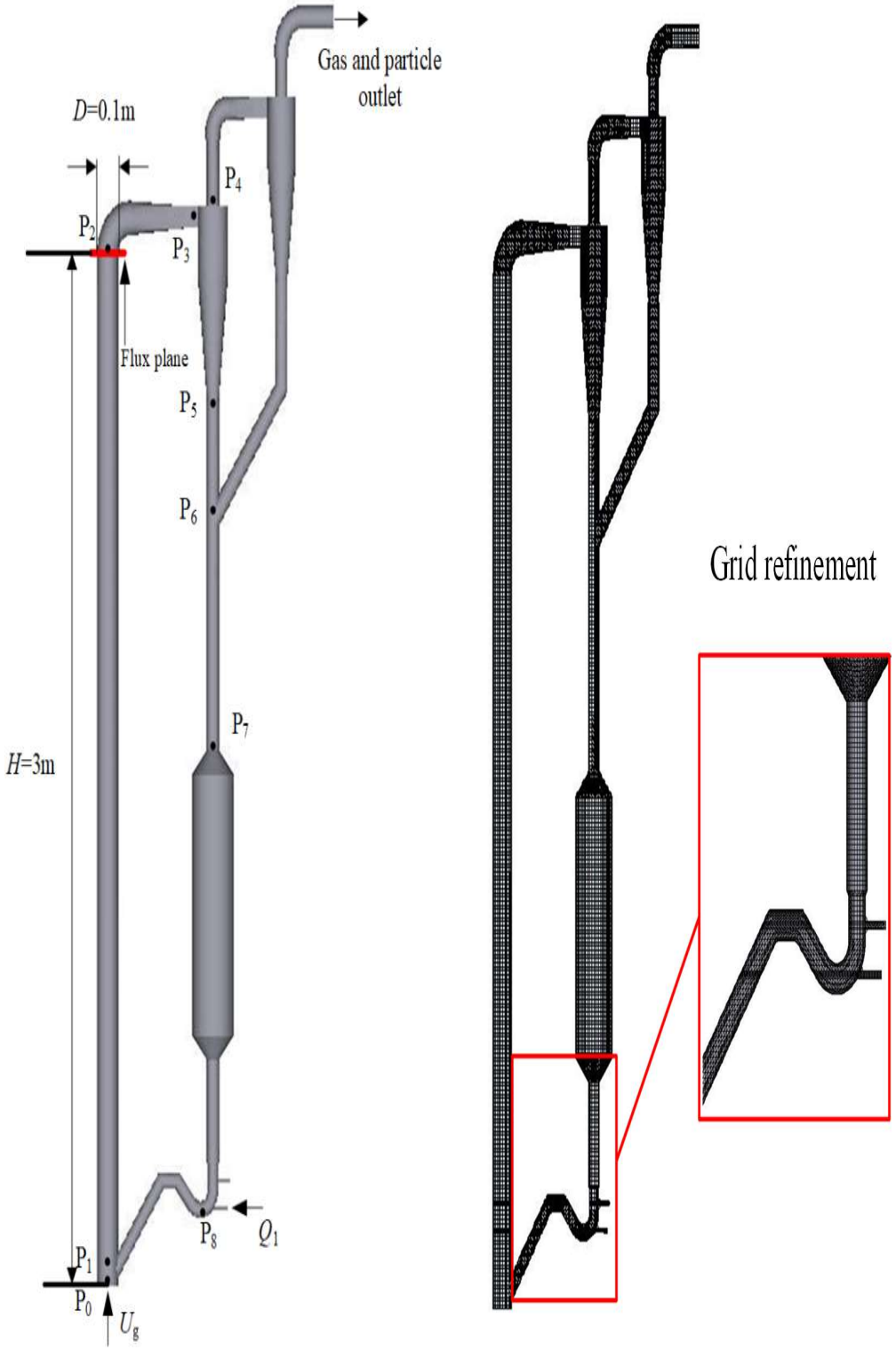

Fig.5-1 Schematic diagram of the simulated three-dimensional full-loop fast fluidized bed.

Fig.5-2 Grid representation of the simulated three-dimensional full-loop fast fluidized bed.

The pressure balance in the circulation loop can be represented as follow equation:

$$(P_1 - P_2) + (P_2 - P_3) + (P_3 - P_6) + (P_6 - P_7) + (P_7 - P_8) + (P_8 - P_1) = 0 \quad (5\text{-}30)$$

where (P_1-P_2)refers to the pressure drop between the exit $P_2$and the feedback point P_1 in the riser, (P_2-P_3) refers to the pressure loss due to the turning of the exist, (P_3-P_6) refers to the cyclone pressure drop between the inlet of the cyclone$P_3$and the exit of the cyclone P_6, (P_6-P_7) refers to the pressure drop from the free surface to top of loop seal of the downer, (P_7-P_8) refers to the pressure of the loop seal.

5.4 Initial and boundary conditions

The experimental data in this study are collected from chapter 3 and chapter 4 in a three-dimensional full-loop fast fluidized bed. Computational domain is based on the pilot scale experimental set-up seen in Fig.5-1. Grid representation of the simulated three-dimensional full-loop fast fluidized bed is shown in Fig.5-2. Other simulation conditions are based on the experimental work in Chapter 3 and summarized in table 5-1.

Table 5-1 Simulation conditions based on the experimental work in Chapter 3

Parameters	Value	Parameters	Value
Diameter of riser (D)	0.1 m	Pressure	Atmospheric
Height of riser (H)	3.0 m	Normal particle-wall restitution coefficient (e_{wn})	0.3[29] [31]
Particle size (d_p)	0.25 mm	Tangential particle-wall	0.99

		restitution coefficient ($e_{w\tau}$)	
Particle density (ρ_p)	2650 kg/m^3	Turbulent model	LES
Random close pack (ε_{cp})	0.58	Grid size	14.3 mm+8 mm
gas viscosity(μ_g)	1.84×10^{-5} Pa/s	Time step (Δt)	1×10^{-4} s
Superficial gas velocity(u_g)	5.28 m/s	Drag model	Wen-Yu-Ergun
Solid mass flux (G_s)	20 kg/m^2·s		

5.5 Determination of simulation parameters

5.5.1 Grid size

The grid size impact the accuracy of simulation directly, the size need be small enough to depict the small bubbles in the gas-solid flow accurately in the Eulerian-Eulerian method[1], which is quite different from that in MC-PIC method. The requirement of grid size in MC-PIC method is likely lower than that in the Eulerian-Eulerian method, but the determination of grid size is mostly by depending experience at present.

In this work, different grid sizes were taken into account in the grid dependence tests, from coarse size, to medium size then to fine. The influence of grid size on the distribution of pressure, solid volume fraction distribution and solid mass flux are discussed. The grid size used in simulation is shown in Table 5-2.

Table 5-2 Grid size in simulation

Case	Grid size	refinement	Number of cells	Simulation particle n_p
Case 1	10.0 mm	-	10837	1390
Case 2	12.5 mm	-	61762	1390
Case 3	14.3 mm	-	44361	1390
Case 4	16.7 mm	-	30299	1390
Case 5	20.0 mm	-	19639	1390
Case 6	14.3 mm	8.0 mm	103525	1390

Fig.5-3 shows the instantaneous distribution of solid volume fraction in fast fluidized bed under different grid size. As seen in Fig.5-3, with the increase of grid number, the inhomogeneous axial distribution of solid volume fraction in the riser occurs, and the slug in the packing region of the downer decreases. When the number of real particles in a simulation particle is kept constant, the flow characteristics can be better predicted with increasing grid number. However, when the grid size is smaller than 14.3 mm, the flow structure in the riser changes very little.

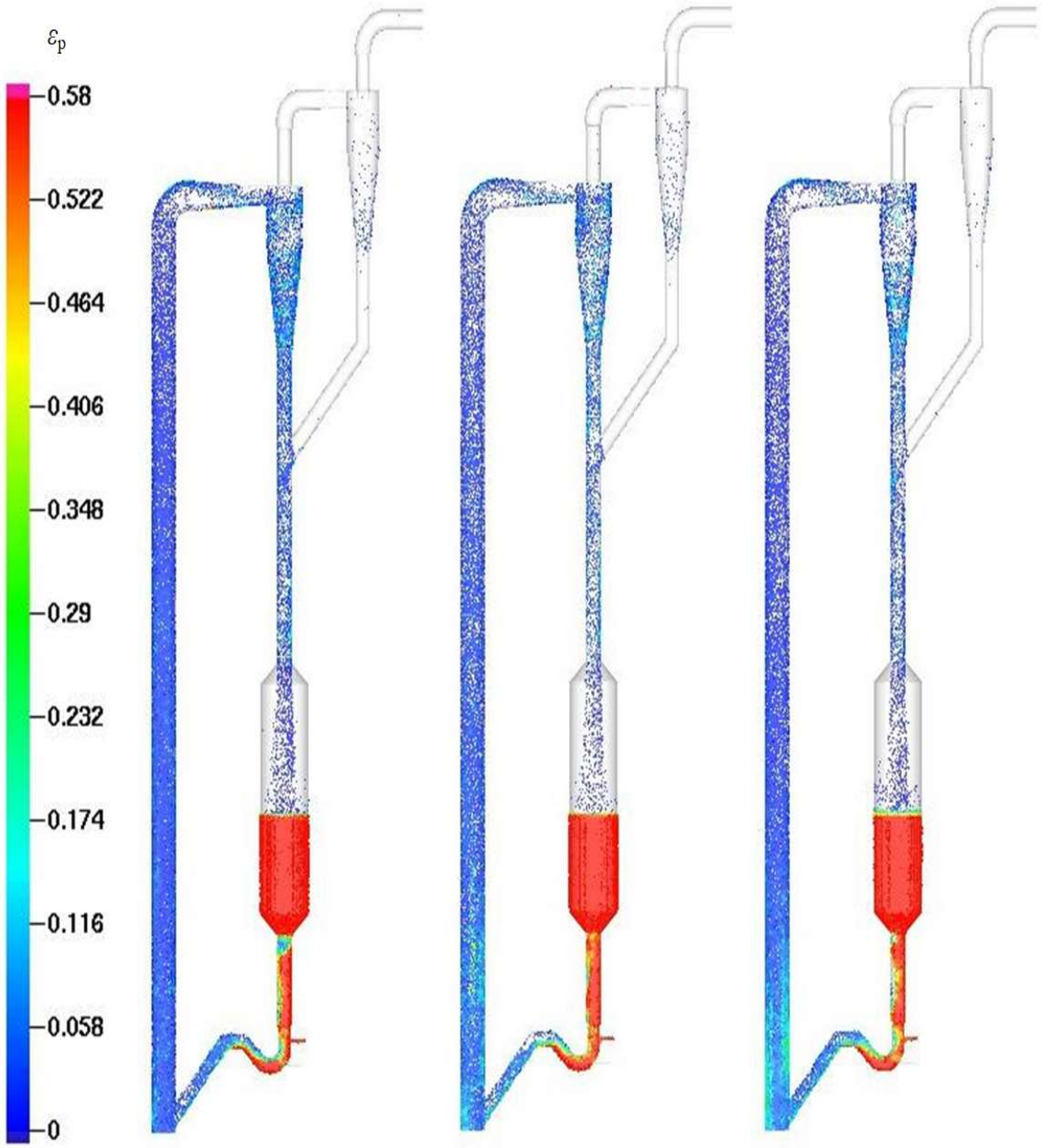
ε_p
0.58
0.522
0.464
0.406
0.348
0.29
0.232
0.174
0.116
0.058
0

(a) (b) (c)

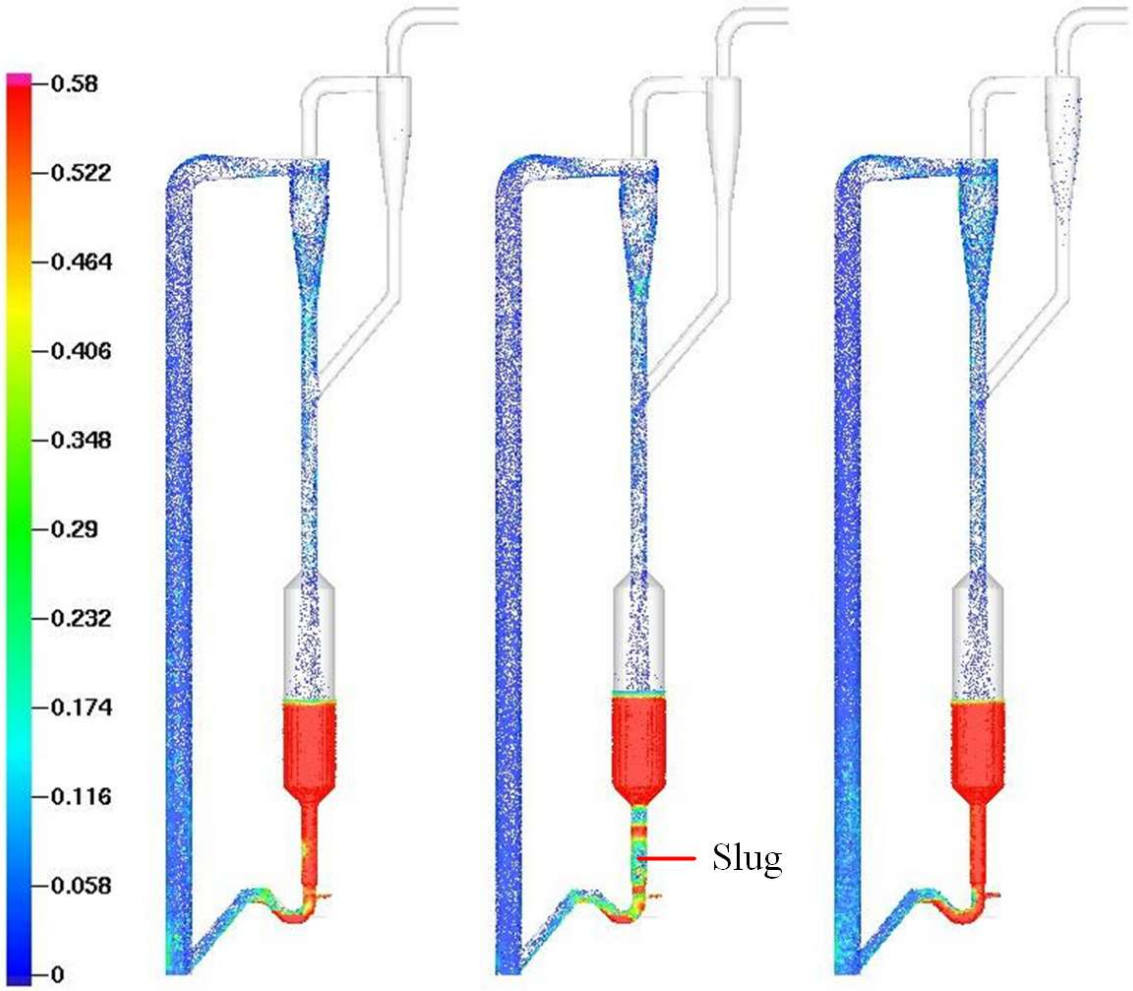

(d) (e) (f)

Fig.5-3 Influence of the grid size on instantaneous solid volume fraction distribution in the fast fluidized bed:

(a) Case 1;(b) Case 2; (c) Case 3; (d) Case 4; (e) Case 5; (f) Case 6.

Fig.5-4 illustrates the influence of grid size on the pressure drop. With the decrease of the grid size, the pressure drop in the riser declines gradually, while the pressure drop in the downer increases, and the particle packed height decreases. It can be explained that when the grid size is large, the slug likely occurs in the packing region, decreasing the pressure in the downer. Consequently, the balance in the fast fluidized bed is broken, the solid circulation is disrupted, and the solid mass flux decreases.

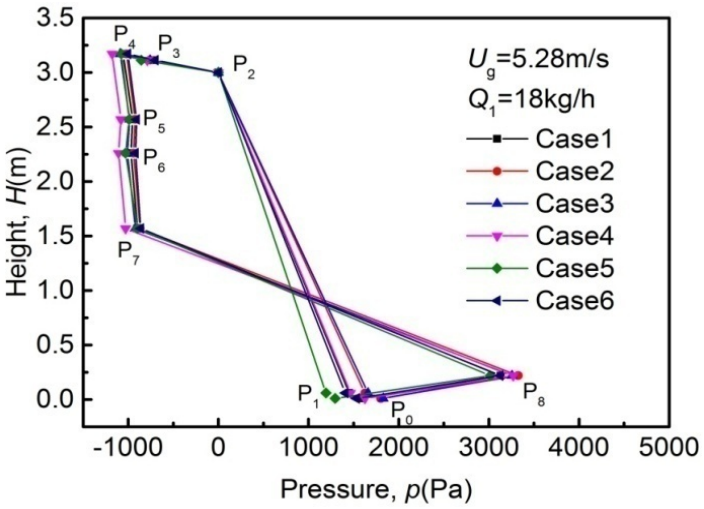

Fig.5-4 Influence of grid size on the pressure drop in a fast fluidized bed.

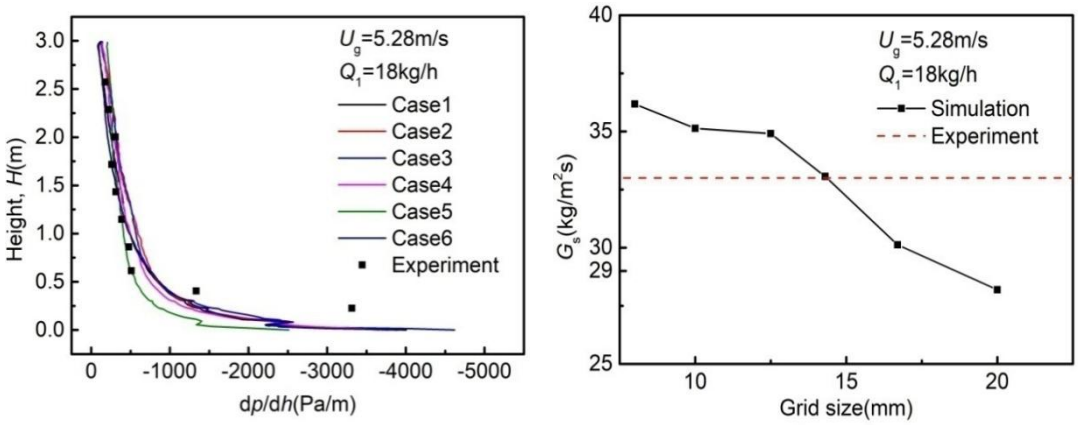

(a) (b)

Fig.5-5 (a)Influence of grid size on the pressure distribution in the riser of a fast fluidized bed; (b) Influence of grid size on solid mass flux in a fast fluidized bed.

Fig.5-5 (a) shows the pressure distribution in the riser of the fast fluidized bed with different grid size. The simulation result in case 5 shows a larger difference than the other cases compared to the experimental result. It may be due to the grid size set in case 5 was too large. It can be seen from Fig.5-5 (b) that the increase of grid size leads to lower solid mass flux. As the grid size decreasing, the slug in the packing region of the downer disappears, and the number of bubbles in that region decreases rapidly. When the grid size is lower than 14.3mm, the further decrease of grid size shows little influence on the solid mass flux and the pressure distribution of the riser. Refine the

mesh in the packing region of the riser, the bubbles in the packing region is gone. Moreover, when the grid size in the packing region of the riser is 8mm, the pressure distribution of the riser and the solid mass flux is in good agreement with the experimental result.

In MP-PIC method, n_p refers to the real particles in each simulation particle, the value of n_p affect the accuracy and efficiency of the simulation directly. The lower the n_p is, the more accuracy the simulation result is. However, if the n_p is set too small, the cost of computation resource will increase significantly. The influence of n_p on the simulation is also discussed, when the n_p is 2780，1853，1390 and 950. The grid size is 14.3 mm and the refined grid is set at the packing region of the downer of 8 mm.

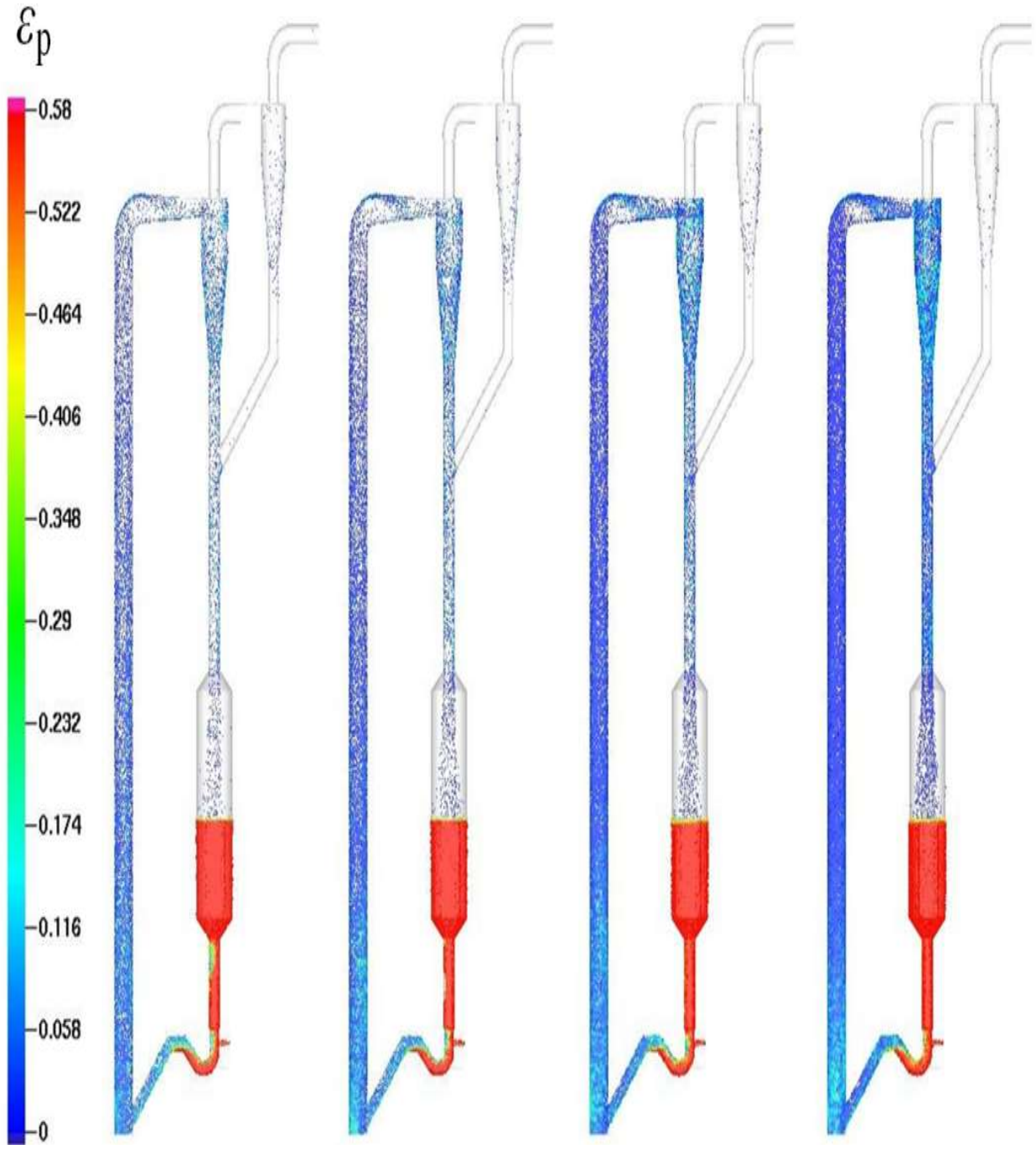

Fig.5-6 Influence of n_p on instantaneous solid volume fraction distribution in fast fluidized bed:(a) n_p=2780; (b) n_p=1853; (c) n_p=1390; (d) n_p=950.

It can be seen from Fig.5-6, with the increase of real particle number in a simulation particle, especially when n_p=2780 and n_p=1853, large slugs emerges in the downer.

The slugs disappear with decreasing n_p, while the solid volume fraction in the riser changes very little.

Fig.5-7 shows the influence of n_p on the pressure drop in a fast fluidized bed. As n_p decreases, the pressure drop in the riser and downer increase slightly, but the influence on the pressure drop in the riser is greater. It can be seen that the influence of n_p on the flow structure is less significant than that of grid size.

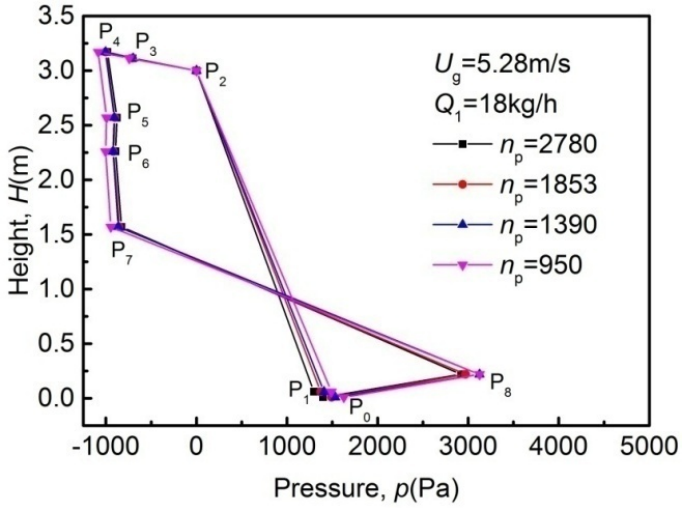

Fig.5-7 Influence of n_p on the pressure drop in a fast fluidized bed.

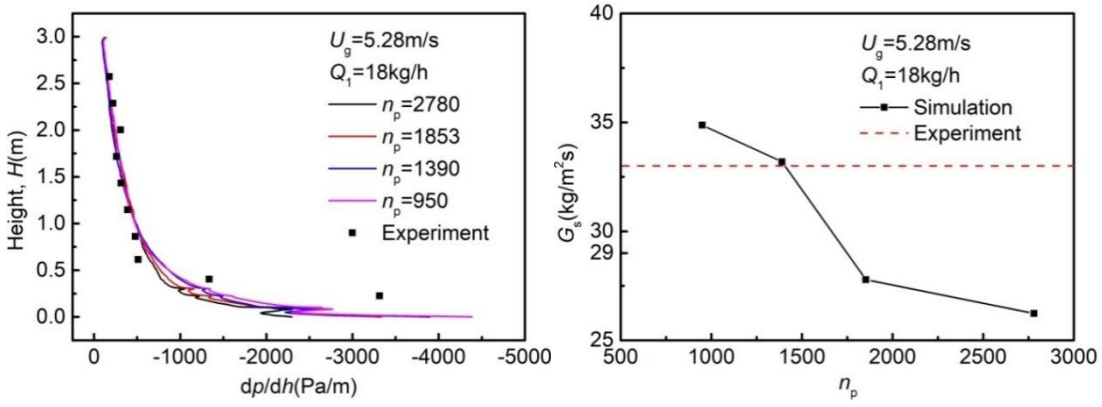

(a) (b)

Fig.5-8 (a) Influence of n_p on the pressure distribution in the riser of a fast fluidized bed; (b) Influence of n_p on the solid mass flux in a fast fluidized bed.

As seen in Fig.5-8(a), the lower n_p leads to higher solid volume fraction in the bottom of the riser, and the simulation prediction is in better agreement with the experiment

result. From Fig.5-8(b), the solid mass flux increases significantly and then gradually with lower n_p, when n_p=1390, the solid mass flux can be well predicted.

5.5.2 Close pack volume fraction

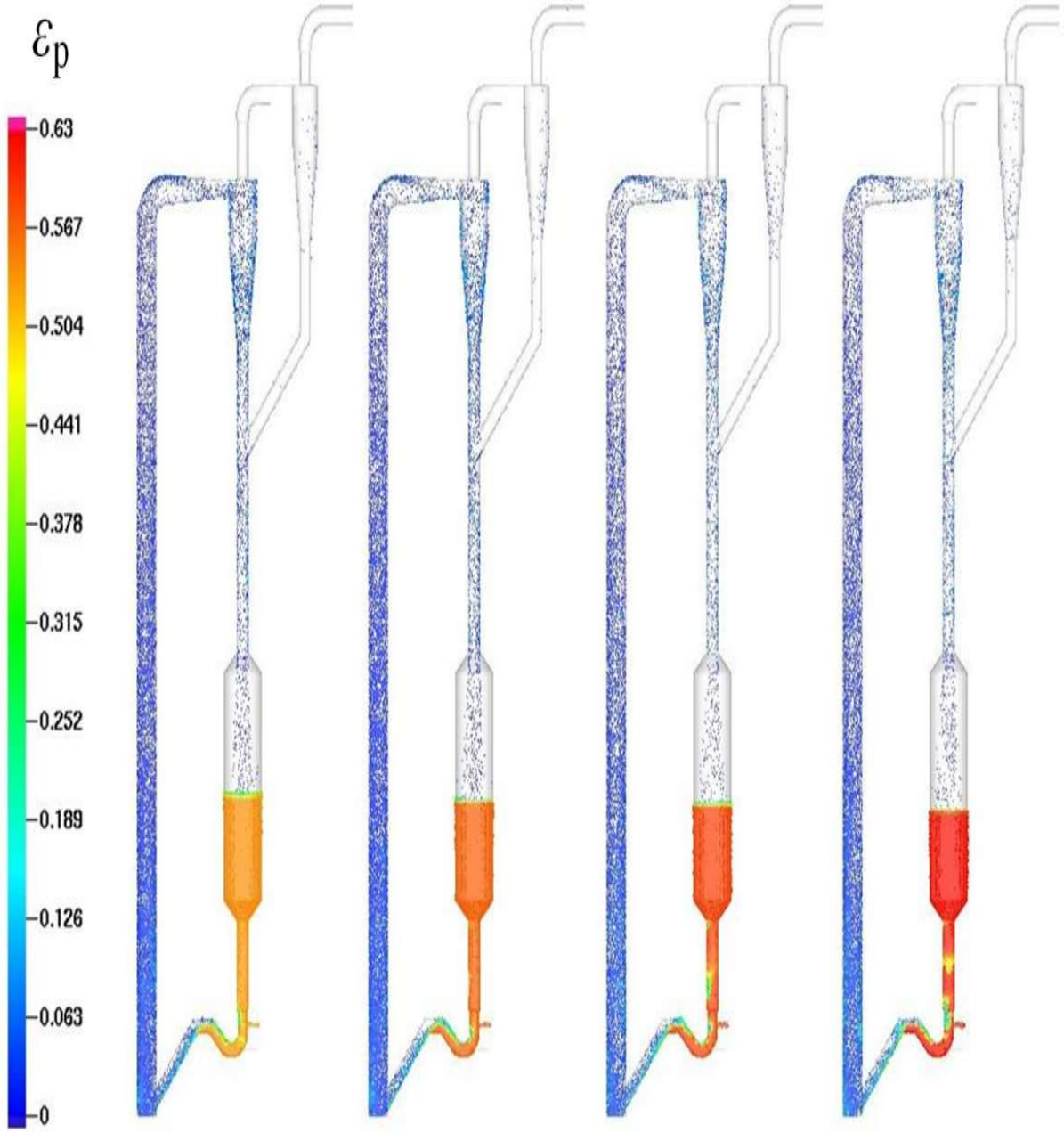

Fig.5-9 Influence of random close pack ε_{cp} on instantaneous particle distributions in a fast fluidized bed: (a)ε_{cp} =0.55; (b)ε_{cp} =0.58; (c)ε_{cp} =0.60; (d)ε_{cp} =0.63.

The random close pack ε_{cp} is the maximum particle volume fraction when they are randomly packed. It is obvious that the particles in the lower part of downer and the loop seal are packing particles, thus the determination of the random close pack is crucial to the particle packing status. Moreover, the ε_{cp} could affect the simulation of gas-solid drag coefficient, the profile of pressure gradient and the solid mass flux[1]. The influence of ε_{cp} on gas-solid flow in fast fluidized bed is studied, with superficial gas velocity u_g=5.28m/s，seal loop aeration rate Q_1=10 kg/h，and the bed inventory M_0=20 kg. The transient particle volume fraction profiles with various ε_{cp} at steady simulation are presented in Fig.5-9.

It is notable that the ε_{cp} affects the solid volume fraction profile in the riser, but the influence of the ε_{cp} is more obvious in the downer. It can be explained by that the downer is the packing zone at the beginning while the solid volume fraction in the riser is lower, but when the ε_{cp} is too high, bubbles start to arise in the downer. Moreover, The influence of ε_{cp} on the inner circulation is lower than result of Wang *et al.*[1], which is because the J valve adopted in our simulation is applicable to circulation system.

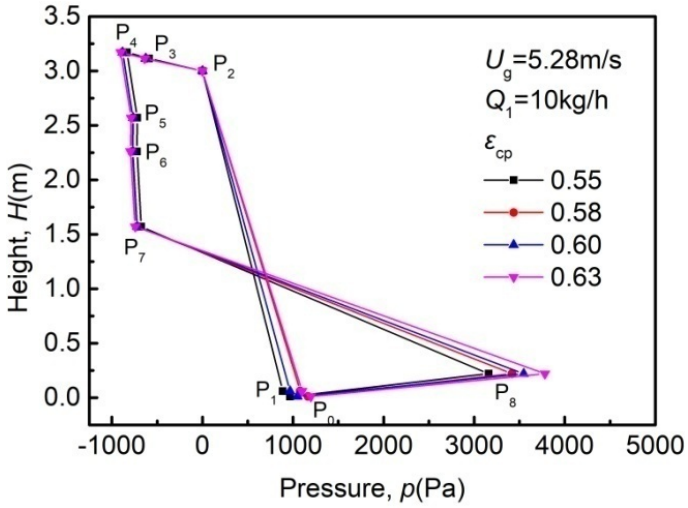

Fig.5-10 Influence of random close packε_p on the pressure distributions.

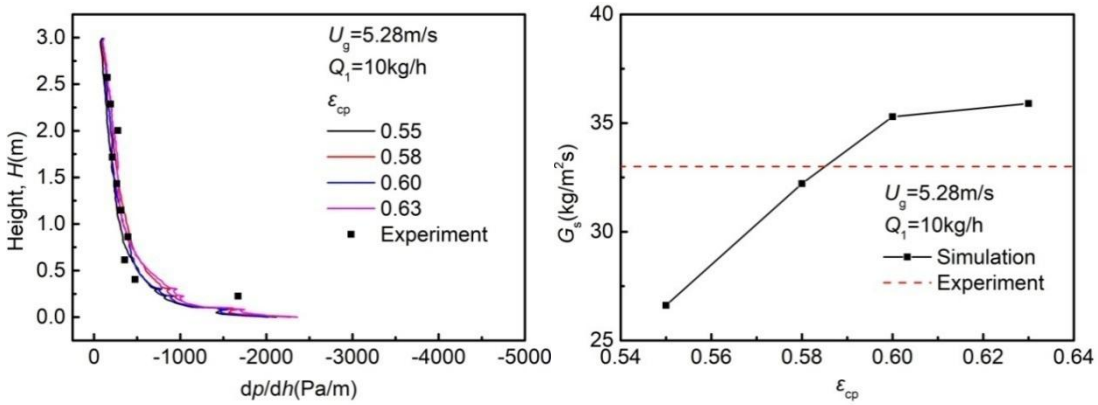

(a) (b)

Fig.5-11 (a) The influence of ε_{cp} on pressure distribution of the riser in a fast fluidized bed; (b) The influence of ε_{cp} on the solid mass flux in a fast fluidized bed.

It can be seen that ε_{cp} influences the particle packed height in the downer, pressure distribution and solid mass flux significantly. Fig.5-10 shows that ε_{cp} affects the pressure drop in the riser and downer and influences the solid mass flux. With higher $\varepsilon_{cp,}$ the pressure drop in the riser and the downer are significantly increased. As shown in Fig.5-11(b), the influence of ε_{cp} on G_s first increases and then slows down. It can be seen that the influence of ε_{cp} on the solid volume fraction in the upper riser is very small, while influence is greater for the solid volume fraction in the bottom, as seen in Fig.5-11(a). It is notable that when ε_{cp}=0.58, the predicted G_s and the pressure distribution in the riser are in good agreement with experimental results.

5.5.3 Drag models

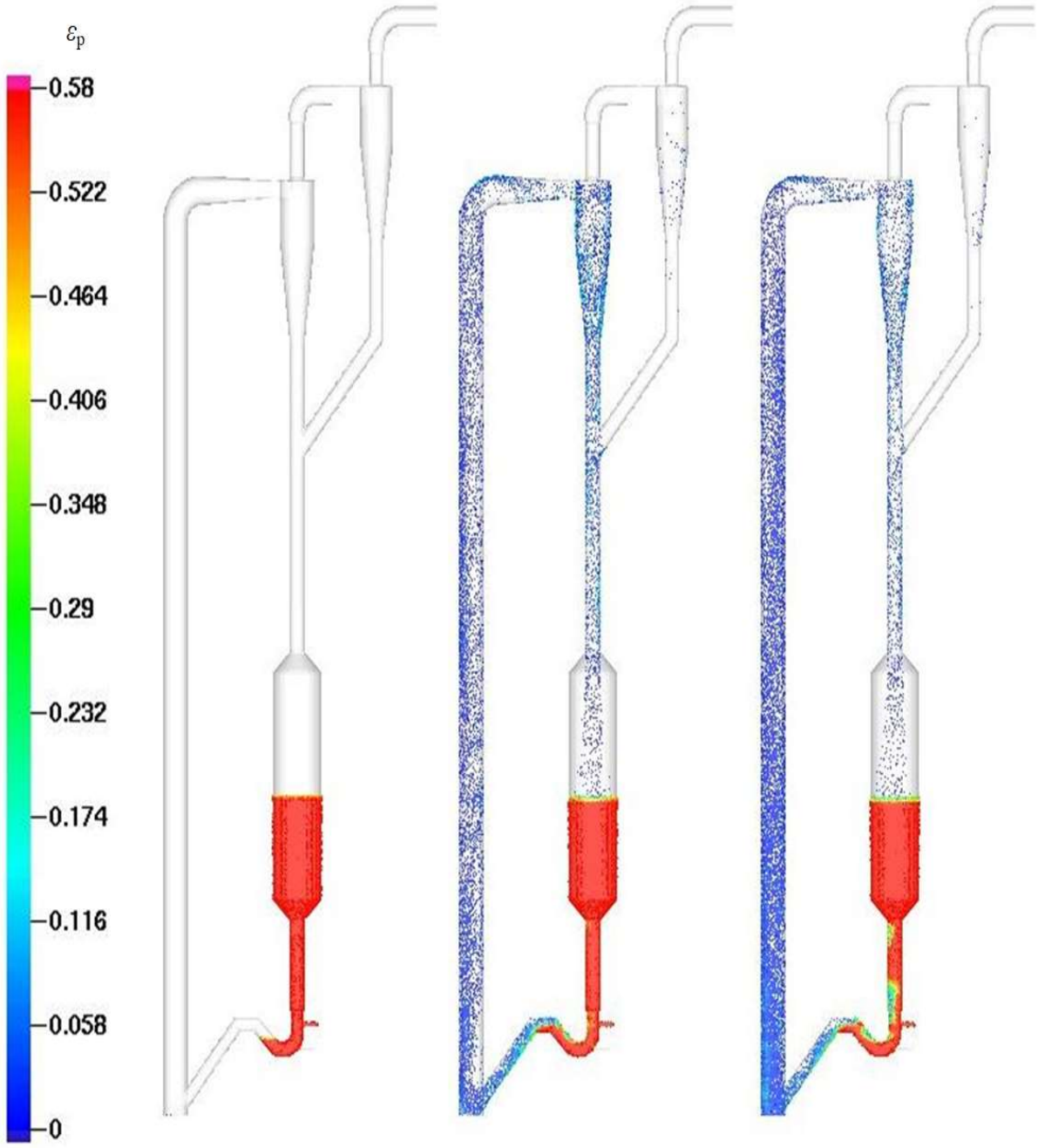

(a) (b) (c)

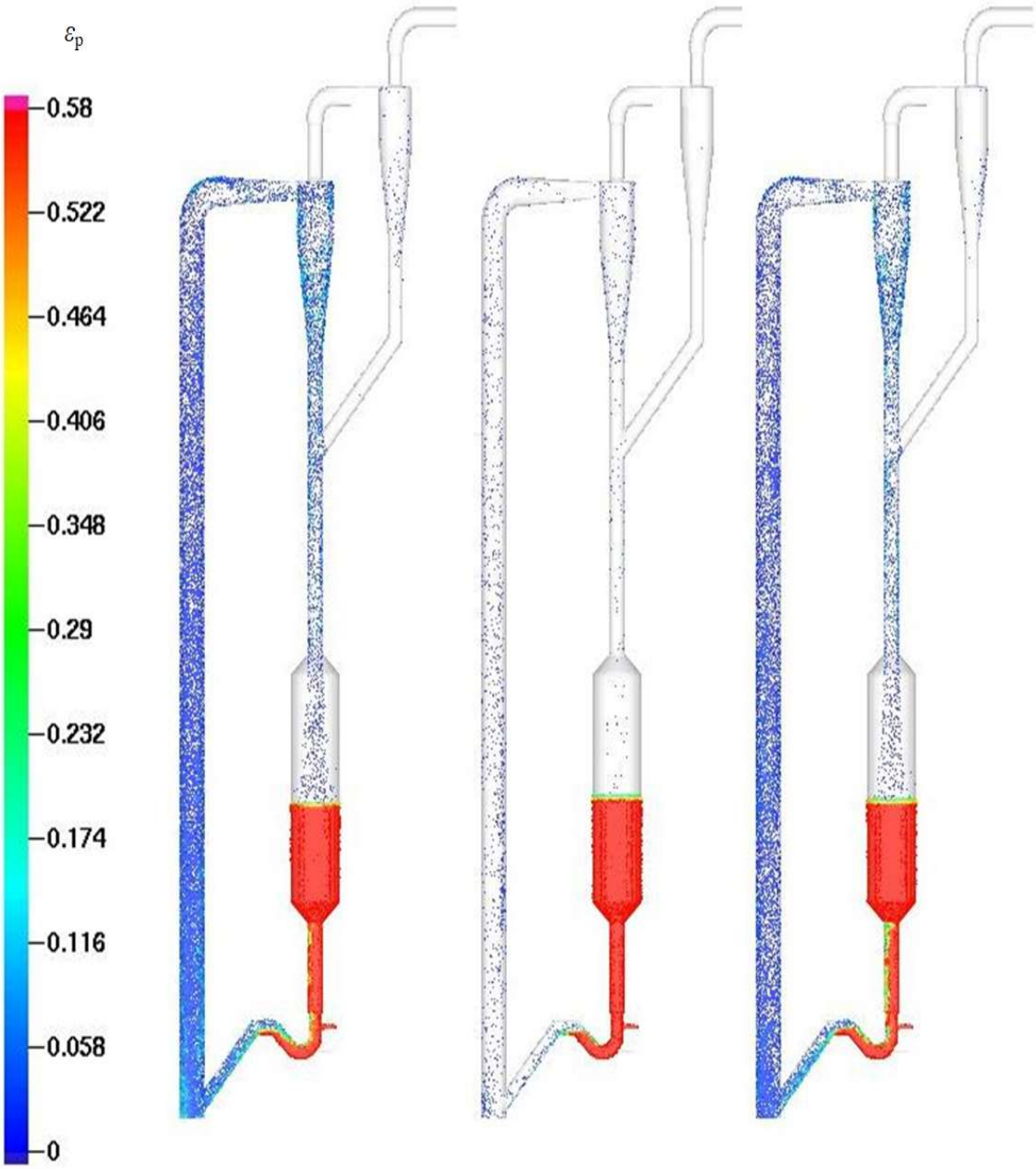

Fig.5-12 Influence of drag model on instantaneous particle volume fraction distributions in fast fluidized bed:(a) the Strokes model; (b) the Ergun model; (c) the Wen-Yu model; (d) the Wen-Yu-Ergun model; (e)the Richardson model; (f) the Turton-Levenspiel model.

In MP-PIC method, the interaction between the gas phase and particle phase is coupled through gas-solid drag model [4]. Moreover, the drag force is the primary force in the vertical direction, and the gas-solid interphase momentum exchange is significantly affected by drag force [26], which has influence on solid volume fraction in the riser directly. Thus, the determination of drag model is of significance to the simulation accuracy [27].

In our study, the most common drag model, e.g. the Strokes model, the Ergun model, the Wen-Yu model and the Wen-Yu-Ergun model are used in the simulation of the fast fluidized bed. Moreover, the drag coefficient and the profile of solid volume fraction vary with different drag models.

The drag models are proposed for very different operating conditions, e.g. the Wen-Yu model is usually used for the solid volume fraction ranges from 0.01 to 0.61[21], while the Ergun model is limited to the solid volume fraction from 0.47 to 0.7[22], and the Strokes model is appropriate for the dilute slow flow of low Reynolds number[28]. The Gidaspow model is the combination of the Wen-Yu and Ergun models, which could cover a wide range of gas-solid flow from dilute flow to dense flow [23]. The flow structure of different gas-solid flow system changes with operating conditions, thus it is crucial to find a accurate drag model for the fast fluidized bed.

In this case, the superficial gas velocity u_g=5.28m/s, the seal loop aeration rate Q_1=10 kg/h, and the bed inventoryM_0=20 kg. The transient solid volume fraction profiles under different drag models in a fast fluidized are shown in Fig.5-12. The simulation results of the Wen-Yu model and the Wen-Yu-Ergun model are similar, which predicts the solid volume fraction profile and the solid mass flux well for the fluidized bed. However, the fast fluidized bed is unlikely to achieve a stable flow using the Strokes model or Richardson model, as seen in Fig.5-12 (a) and (c).It is notable that big bubbles

can be observed in the loop seal of the downer in the Wen-Yu model and Turton-Levenspiel model. When drag force is increasing, the gas carrying capacity is enhanced, resulting in higher solid volume fraction and solid mass flux in the riser. Meanwhile, it is easier for the gas flows into the riser form big bubbles, which impede the circulation of the system [29]. It is obvious that different drag models exert various influences on pressure drop in the riser. It can be seen that Wen-Yu-Ergun model predicts higher solid volume fraction in the riser and higher pressure in the loop seal of the downer. The drag coefficient varies with different drag models. It is found that the increase in drag force leads to more solid inventory in the loop seal while the solid mass flux is still the same. Moreover, the Strokes model and the Richardson model are derived from the analysis of a single particle[28, 30], the prediction of drag coefficient of the two models are irrelevant to solid volume fraction.

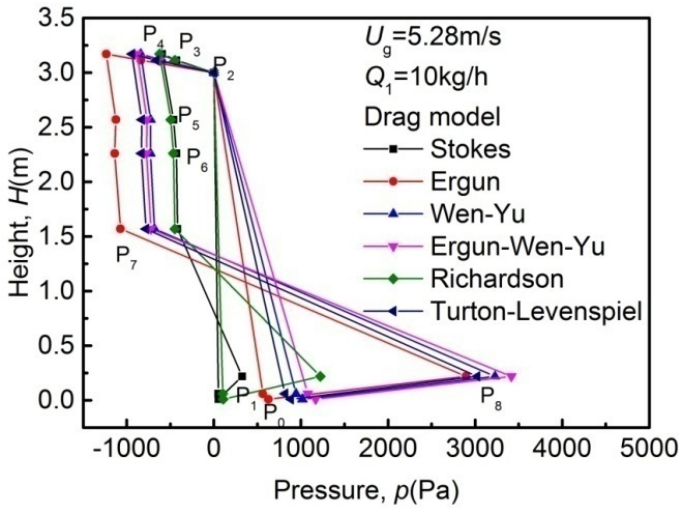

Fig. 5-13 Influence of drag model on the pressure drop in a fast fluidized bed.

The influence of drag model on pressure drop in the fast fluidized bed is shown in Fig.5-13. It can be observed that the simulation results with Richardson and Stokes model underestimated the pressure drop in the riser. The pressure distribution by different drag models in the riser of a fast fluidized is shown in Fig.5-14(a), it can be seen that the Wen-Yu and Ergun-Wen-Yu model give the best prediction for the

simulation pressure distribution compared with the experimental results, while the Turton-Levenspiel model and the Ergun model underestimate the pressure drop. The Wen-Yu model, the Ergun-Wen-Yu model and the Ergun model has close prediction to the experimental result. Fig.5-14(b) shows that the simulation results with Stokes and Richardson model have a great difference from the experimental result, which is in agreement with the results in Fig.5-13 and Fig.5-14(a). The solid mass fluxes predicted by Turton-Levenspiel model, Ergun-Wen-Yu model, Wen-Yu model and Ergun model fit well with the experimental result. In summary, the Ergun-Wen-Yu model is the most appropriate drag model in prediction gas-solid flow in the fast fluidized bed.

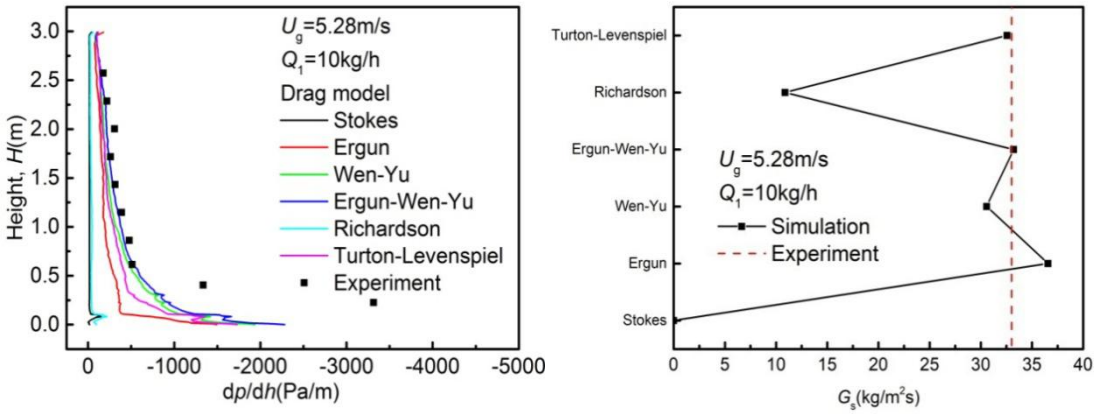

(a) (b)

Fig.5-14 (a) Influence of drag model on the pressure distribution in the riser of a fast fluidized bed; (b) Influence of drag model on the solid mass flux in a fast fluidized bed.

5.6 Conclusions

A Eulerian-Lagrangian approach based on MP-PIC method was applied in the simulation of a fast fluidized bed with seal loop. The modelling parameters, including grid resolution, the number of particles per parcel, the drag model and the particle

close pack volume fraction have been systematically analysed and optimized. The conclusions are as follows:

(1) The LES model was used as the turbulence model, while the particle phase is modelled as discrete particles, where the particle momentum equation is base the MP-PIC method. The real particles with the same properties are packed into computational particles (parcel), thus the dense gas-solid fluidization system can be analysed through a reasonable amount of particles.

(2) Compared with the Eulerian-Eulerian method, the grid size adopted in MP-PIC method is larger. It is found that when the grid size is 14.3mm and the grid of the downer have been refined, the further decrease of grid size shows little influence on the pressure drop, solid volume fraction and solid mass flux.

(3) When n_p=1390, the prediction of the flow structure and the pressure distribution of the fast fluidized bed is reasonable agree with the experimental results. Moreover, the further decrease of n_p has little influence on the simulation result. Therefore, n_p=1390 is used in further simulation.

(4) Different drag models show certain influence on the flow behaviour of fast fluidized bed. It shows that both Wen-Yu model and Wen-Yu-Ergun model can well predict the solid volume fraction and the solid mass flux, but big bubbles are observed in the downer for the Wen-Yu model. Therefore, the Wen-Yu-Ergun model is proved to be the optimum choice.

5.7 Reference

[1] Wang Q, Yang H, Wang P, et al. Application of CPFD method in the simulation of a circulating fluidized bed with a loop seal, part I-Determination of modeling parameters[J]. *Powder Technology* 2014, 253: 814-821.

[2] Zhang N, Lu B, Wang W, et al. Virtual experimentation through 3D full-loop simulation of a circulating fluidized bed[J]. *Particuology* 2008, 6(6): 529-539.

[3] Feng Y Q, Yu A B. Microdynamic modelling and analysis of the mixing and segregation of binary mixtures of particles in gas fluidization[J]. *Chemical Engineering Science* 2007, 62: 256-268.

[4] Andrews M J, O'Rourke P J. The multiphase particle-in-cell (MP-PIC) method for dense particulate flows[J]. *International Journal of Multiphase Flow 1996,* 22(2): 379-402.

[5] Snider D M, O'Rourke P J, Andrews M J. An imcompressible two-dimensional multiphase particle-in-cell model for dense particle flows[R]. Los Alamos National Lab, 1997.

[6] Snider D M, Clark S M, O'Rourke P J. Eulerian-Lagrangian method for three-dimensional thermal reacting flow with application to coal gasifiers[J]. *Chemical Engineering Science*2011, 66(6): 1285-1295.

[7] SmagorinskyJ. General circulation experiments with the primitive equations, part I: the basic experiment[J]. Monthly Weather Review. 1963, 91: 99-164.

[8] Kim W W M S. A new dynamic one-equation subgrid-scale model for large eddy simulations[C]. AIAA: 1995. 356.

[9] Pierre S. Simulations of separated flows with subgrid models[J]. *La Recherche Aerospatiable*1996, 1: 51-61.

[10] Metais O, Lesieur M. Spectral large-eddy simulation of isotropic and stably stratified turbulence [J]. *Journal of Fluid Mechanics***1992**, 239: 157-194.

[11] Snider D M, O'Rourke P J. The multiphase particle-in-cell (MP-PIC) method for dense particle flow[M]. Computational Gas-Solids Flows and Reacting Systems, New York:Engineering Science Reference Press, 2009, 282-284.

[12] Amsden A A, O'Rourke P J, D B T. KIVA-Ⅱ: A computer program for chemically reactive flows with sprays[M]. Los Alamos: Los Alamos National Lab, 1989.

[13] O'Rourke P J, Snider D M. An improved collision damping time for MP-PIC calculations of dense particle flows with applications to polydisperse sedimenting beds and colliding particle jets[J]. *Chemical Engineering Science***2010**, 65(22): 6014-6028.

[14] Snider D M. Three fundamental granular flow experiments and CPFD predictions[J]. *Powder Technology***2007**, 176(1): 36-46.

[15] Tsuji Y, Kawaguchi T, Tanaka T. Discrete particle simulation of 2-dimensional fluidized bed[J]. *Powder Technology***1993**, 77(1): 79-87.

[16] Hoomans B, Kuipers J, Briels W J, et al. Discrete particle simulation of bubble and slug formation in a two-dimensional gas-fluidised bed: A hard-sphere approach[J]. *Chemical Engineering Science***1996**, 51(1): 99-118.

[17] Harris S E, Crighton D G. SOLITONS, Solitary waves, and voidage disturbances in gas-solid fluidized beds [J]. *Journal of Fluid Mechanics***1994**, 266: 243-276.

[18] Struchtrup H. The BGK-model with velocity-dependent collision frequency[J]. *Continuum Mechanics and Thermodynamics***1997**, 9(1): 23-31.

[19] Tang H, Xu K, Cai C. Gas-Kinetic BGK Scheme for Three Dimensional Magnetohydrodynamics[J]. *Numerical Mathematics-Theory Methods and Applications***2010**, 3(4): 387-404.

[20] O'Rourke P J, Zhao P P, Snider D. A model for collisional exchange in gas/liquid/solid fluidized beds[J]. *Chemical Engineering Science***2009**, 64(8): 1784-1797.

[21] Wen C, Yu Y. Mechanics of fluidization[J]. *Chemical Engineering Progressing symposium series***1966**, 62: 100-111.

[22] Ergun S. Fluid flow through packed columns[J]. *Chemical Engineering and Progressing***1952**: 89-94.

[23] Gidaspow D. Multiphase flow and fluidization: continuum and kinetic theory description[M]. San Diego: Academic Press, 1994.

[24] Galimov A Y, Drew D A, Lahey R T, et al. The analysis of interfacial waves[J]. *Nuclear Engineering and Design* **2005**, 235(10-12): 1283-1292.

[25] Ferziger J H, Peric M. Computational methods for fluid dynamics[M]. New York: Spriger-Verlag, 1996.

[26] Ranade V. Computational flow modeling for chemical reactor engineering[M]. New York: Academic Press **2002**: 85-117.

[27] van Wachem B, Schouten J C, van den Bleek C M, et al. Comparative analysis of CFD models of dense gas-solid systems[J]. *AIChE Journal***2001**, 47(5): 1035-1051.

[28] White F M. Viscous fluid flow[M]. New York: McGraw-Hill, 1991.

[29] Yin S.Y. Experimental and Modeling Study on a Pressurized High-Density Circulating Fluidized Bed [D]. Nanjing: Southeast University, 2014.

[30] Richardson J F. Fluidization[M]. Davidson J F, Harrison D, New York: Academic Press, 1971.

[31] Xie J.. [D]. Three-dimensional Numerical Simulation of Combustion/Pyrolysis/Gasification Processes of Combustible Solid Waste/Coal. Nanjing: Southeast University, 2014.

CHAPTER 6 Simulation of Hydrodynamics in the Three-dimensional Full-loop Fast Fluidized Bed

6.1 Introduction

Only few simulation studies were presented for three-dimensional full-loop fast fluidized bed, and most of the simulations were for the Geldart A particles[1-4].Moreover, the influence of operating conditions on the flow behaviour should be further illustrated. A series simulation studies of particle clusters were proposed based on Eulerian-Eulerian method and Eulerian-Lagrangian method[5-7] Tsuji *et al.*[8]compared the simulation results of gas-solid flow in the riser based on DSMC method and two-fluid model, and found that the cluster number is larger in the DSMC method than in the two-fluid model. Moreover, the clusters size may increase with the riser size in DSMC method while disappear in the riser in two-fluid model.. However, due to the limitation of computational sources, most of the previous studies were conducted in two dimensional riser[3, 9-11]. Berrouk et al.[12] discussed the severe disadvantage of the phase coupling scheme used in the context of a two-dimensional DPM. The two-phase coupling scheme underestimated the pressure drop and result in erroneous prediction of the minimum fluidization velocity. Capecelatro et al.[13] found that the simulation of two dimensional riser may lead to unphysical accumulation of particles due to the restriction of particle motion in a plane, which may lead to an over-predict in volume fraction and velocity fluctuations. The radial motion of particles to avoid falling clusters is increased in the riser. Moreover, most of previous studies focus on the cluster structures, the study on the evolutionary processes of the clusters is limited.

The MP-PIC method was applied in the simulation of a three-dimensional full-loop fast fluidized bed in this chapter, and the effect of operating conditions including superficial gas velocity u_g, seal loop aeration rate $Q_1$and bed inventory M_0 on gas-solid flow characteristics was investigated. Moreover, the typical clusters structures were well

predicted, further illustrated the evolutional processes of particle cluster in the fast fluidized bed. The flow behaviour of particle cluster was studied by simulation method, revealing the distribution of solid volume fraction and the velocity of particle clusters.

6.2 Flow behavior in three-dimensional full-loop fast fluidized bed

In current study, the Eulerian-Lagrangian approach based on the multi-phase particle-in-cell (MP-PIC) methodology was applied in the simulation of the effect of operating conditions on the gas-solid flow behaviour of three-dimensional (3D) full-loop fast fluidized bed handling Geldart B particles. The model is validated with experimental data and acceptable agreement has achieved.

Based on the experiment in Chapter 3, a simulated model of three-dimensional full-loop fast fluidized bed is established as shown in Fig.5-1. The influence of operating conditions on the flow behaviour of a fast fluidized bed is systematically studied. The simulation conditions are shown in Table 6-1

Table 6-1 Simulation conditions

Case	u_g (m/s)	Q_1(kg/h)	M_0(kg)	d_p	Particle size
Case 1	3.5	20	20	0.25 mm	PSD
Case 2	5.5	20	20	0.25 mm	PSD
Case 3	6.5	20	20	0.25 mm	PSD
Case 4	7.5	20	20	0.25 mm	PSD
Case 5	5.28	5	20	0.25 mm	PSD
Case 6	5.28	15	20	0.25 mm	PSD
Case 7	5.28	20	20	0.25 mm	PSD
Case 8	5.28	30	20	0.25 mm	PSD
Case 9	5.28	7.5	18	0.25 mm	PSD

Case 10	5.28	10	18	0.25 mm	PSD
Case 11	5.28	20	18	0.25 mm	PSD
Case 12	5.28	30	18	0.25 mm	PSD

Table 6-2Key parameters and simulation conditions

Parameters	Value	Parameters	Value
Diameter of riser (D)	0.1 m	Maximum momentum redirection from collision(α_{max})	40%
Height of riser (H)	3 m	Normal particle-wall restitution coefficient (e_{wn})	0.3
Particle size (d_p)	0.25 mm	Tangential particle-wall restitution coefficient ($e_{w\tau}$)	0.99
Particle density (ρ_p)	2650 kg/m^3	Turbulent model	LES
gas density (ρ_g)	ideal gas law	Grid size	14.3 mm+8 mm
gas viscosity(μ_g)	1.84×10^{-5} Pa/s	Grid number	103525
Superficial gas velocity(u_g)	3.5-7.5 m/s	The number of simulation particles(N_p)	664004
Solid mass flux (G_s)	10-50 kg/m^2·s	The number of real particle per parcel(n_p)	1390
Random close pack (ε_{cp})	0.58	Time step (Δt)	1×10^{-4} s
Drag model	Wen-Yu-Ergun		

6.2.1 Influence of superficial gas velocity

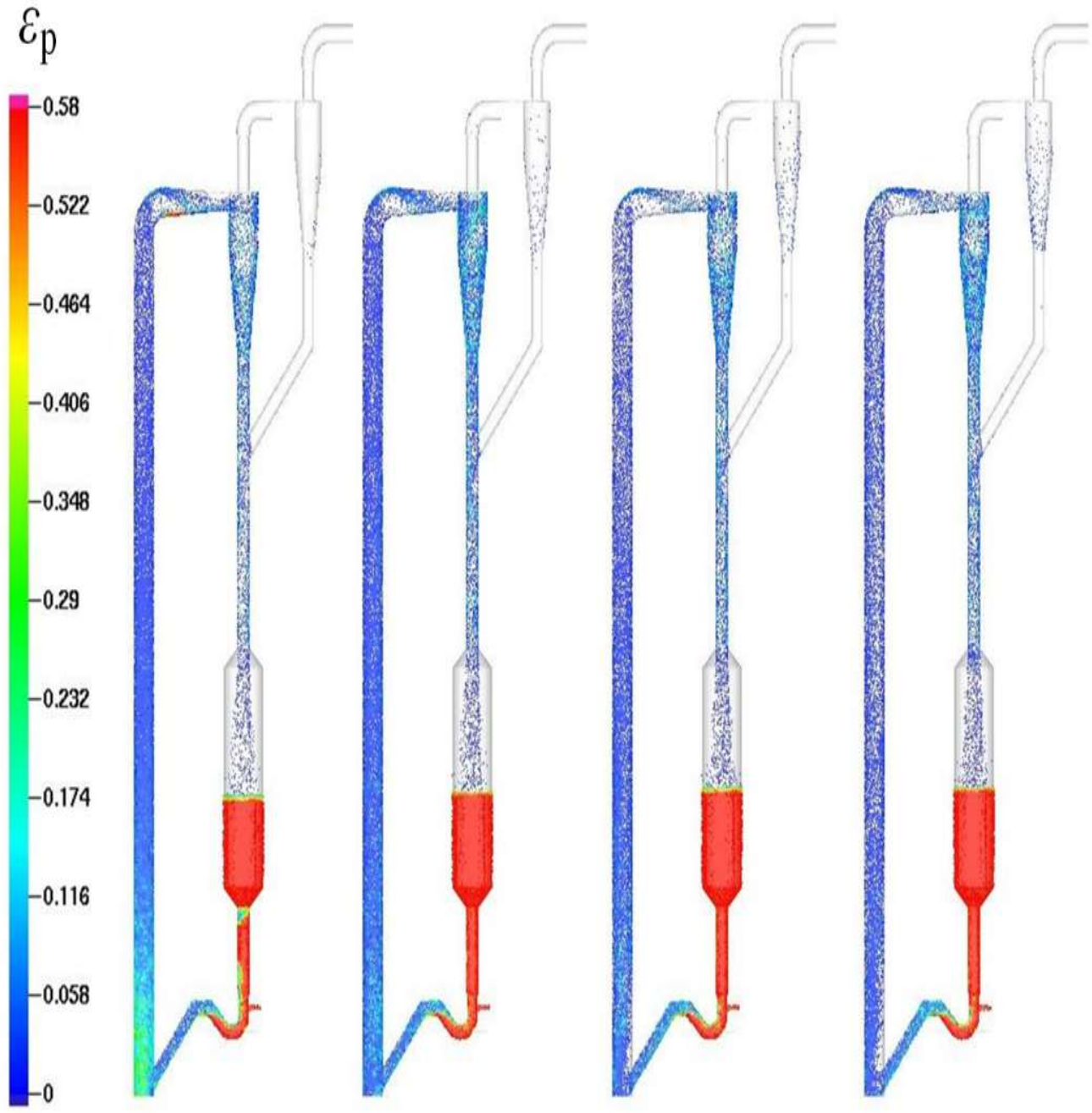

(a) (b) (c) (d)

Fig.6-1Influence of the superficial gas velocity on transient solid volume fraction distribution in the fast fluidized bed (Q_1=20 kg/h, M_0=20 kg)

(a)u_g=3.5 m/s; (b)u_g=5.5 m/s; (c)u_g=6.5 m/s; (d)u_g=7.5 m/s.

Fig.6-1 shows the transient solid volume fraction distribution in the fast fluidized bed under various superficial gas velocities. When superficial gas velocity u_g=3.5 m/s, big bubbles form in the loop seal of the downer, which results in the instability of the circulation system. With the increasing of superficial gas velocity, the bubbles in the loop seal disappear. It can be explained by that higher superficial gas velocity leads to stronger carrying capacity of the gas flow, more and more particles are blew out of the riser, decreasing the solid volume fraction in the riser, especially for the dense bottom zone. Meanwhile, the distribution of solid volume fraction in the riser becomes more uniform. The increase of superficial gas velocity enhances the solid flow rate entrained into the downer, and the separation efficiency of primary cyclone declines, so more particles need be separated in the secondary cyclone. Moreover, the higher superficial gas velocity leads to higher slip velocity in the downer.

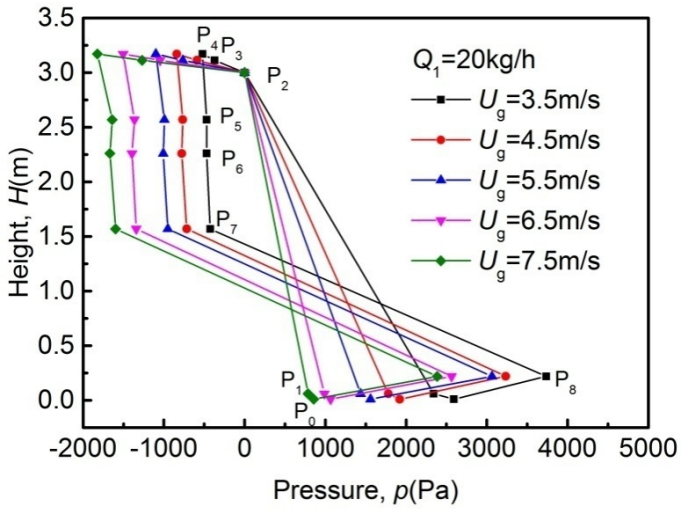

Fig.6-2Influence of superficial gas velocity on the distributions of pressure in the whole loop (Q_1=20 kg/h, M_0=20 kg).

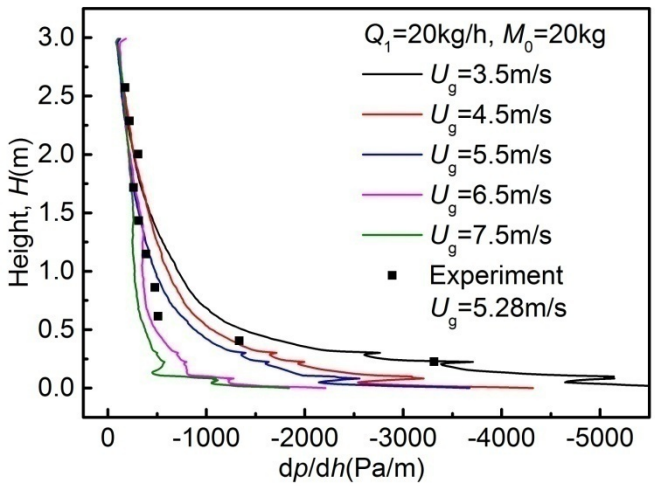

Fig.6-3Influence of superficial gas velocity on the distributions of pressure drop in the riser (Q_1=20 kg/h, M_0=20 kg).

It can be seen from the Fig.6-2 that the pressure drop in the riser declines with increasing superficial gas velocity, due to the increase of pressure drop caused by the exit and the cyclones. With higher superficial gas velocity, the carrying capacity of gas flow is increasing. More particles are blew out of the riser and be separated by the cyclone into the downer, which leads to the decline of pressure drop in the riser. At lower superficial gas velocity, the increase of superficial gas velocity enhances the solid mass flux in the fast fluidized bed significantly. However, with further increasing superficial gas velocity, the increase in solid mass flux is slow down. When the u_g is higher than 6.5 m/s, the increase of u_g has very little influence on solid mass flux. The maximum solid mass flux is reached. Since the limitation of loop seal aeration rate Q_1 , the carrying capacity of gas flow is limited. Fig.6-3 shows the distribution of pressure in the riser under different superficial gas velocities. The higher the superficial gas velocity is, the stronger the carrying capacity of gas flow is, and more particles can be blew out from the riser. Thus, the solid volume fraction in the riser was reduced with a more uniform distribution. Moreover, the higher superficial gas velocity resulted in

higher solid flow rate in the downer, when the loop seal aeration rate was kept constant, the slip velocity in the downer decreases.

Fig.6-4 shows the radial distributions of time-averaged solid volume fraction under different superficial gas velocities. It was obvious that the solid volume fraction increased from the core region to the wall in the riser, which may be the result of formation of particle clusters in the wall region. When the superficial gas velocity increased from 3.5 m/s to 7.5 m/s, the core-annulus structure can always be observed in the riser of the fast fluidized bed. At lower superficial gas velocity, e.g. u_g=3.5 m/s, a dense zone forms in the bottom of the riser, and the solid volume fraction in the riser decreases with riser height. Meanwhile, the core-annulus structure is obvious, but the radial distribution of solid volume fraction becomes more even gradually with riser height. With the increase of superficial gas velocity, the solid volume fraction in the center of the riser slowly declines, but the change along the riser weakens gently. It is notable that when u_g=6.5 m/s and u_g=7.5 m/s, clear core-annular structure and strong particle back-mixing can be observed in the top of the riser, which is inconsistent with previous study [14], this may be due the studies being conducted under different flow patterns.

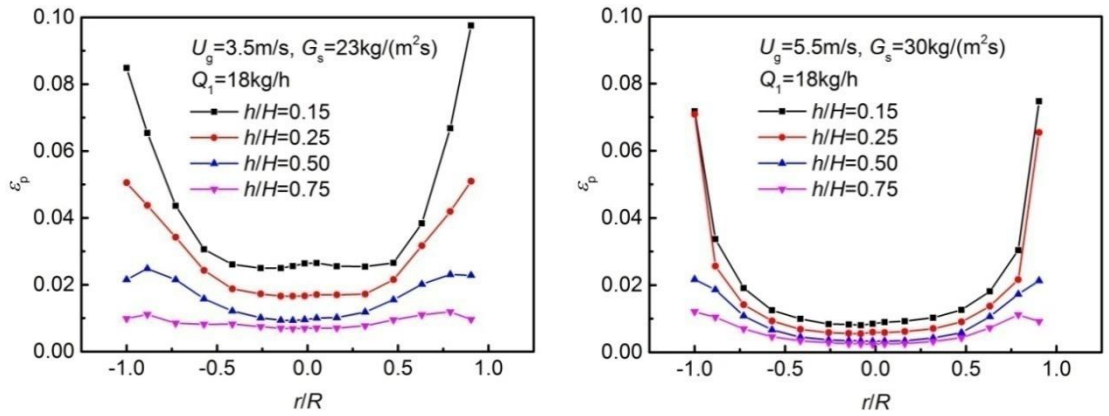

(a) (b)

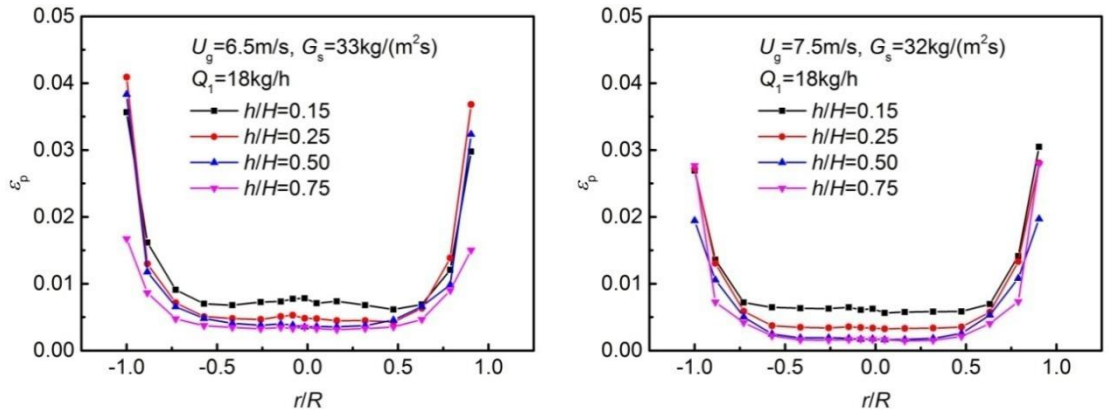

(c) (d)

Fig.6-4Influence of superficial gas velocities on radial profiles of the time-averaged solid volume fraction for different riser height (Q_1=20 kg/h, M_0=20 kg):

(a) u_g=3.5 m/s;(b) u_g=5.5 m/s;(c) u_g=6.5 m/s;(d) u_g=7.5 m/s.

Fig.6-5 shows the predicted spatial distribution of the transient axial particle velocity at various superficial gas velocities, the particles have been magnified by six times in the images. In Fig.6-5, when the superficial gas velocity u_g=3.5 m/s, a large amount of falling particles can be observed in the bottom (h/H=0.15-0.25) of the riser, promoting the back-mixing of the particles. Moreover, the number of falling particles declines with increasing riser height. It is because that the gas-solid slip velocity increases with increasing superficial gas velocity, results in stronger acceleration in particles, enhancing the average particle velocity of the riser.

It is obvious that the solid volume fraction in the lower part of the riser declines sharply and tends to be evenly with increasing superficial gas velocity. The back-mixing of particles weakens at higher superficial gas velocity, especially when u_g=7.5m/s, only few falling particles can be observed, a small amount of high velocity particles appears in the top of the riser, which results in the inhomogeneous distribution of particle velocity.

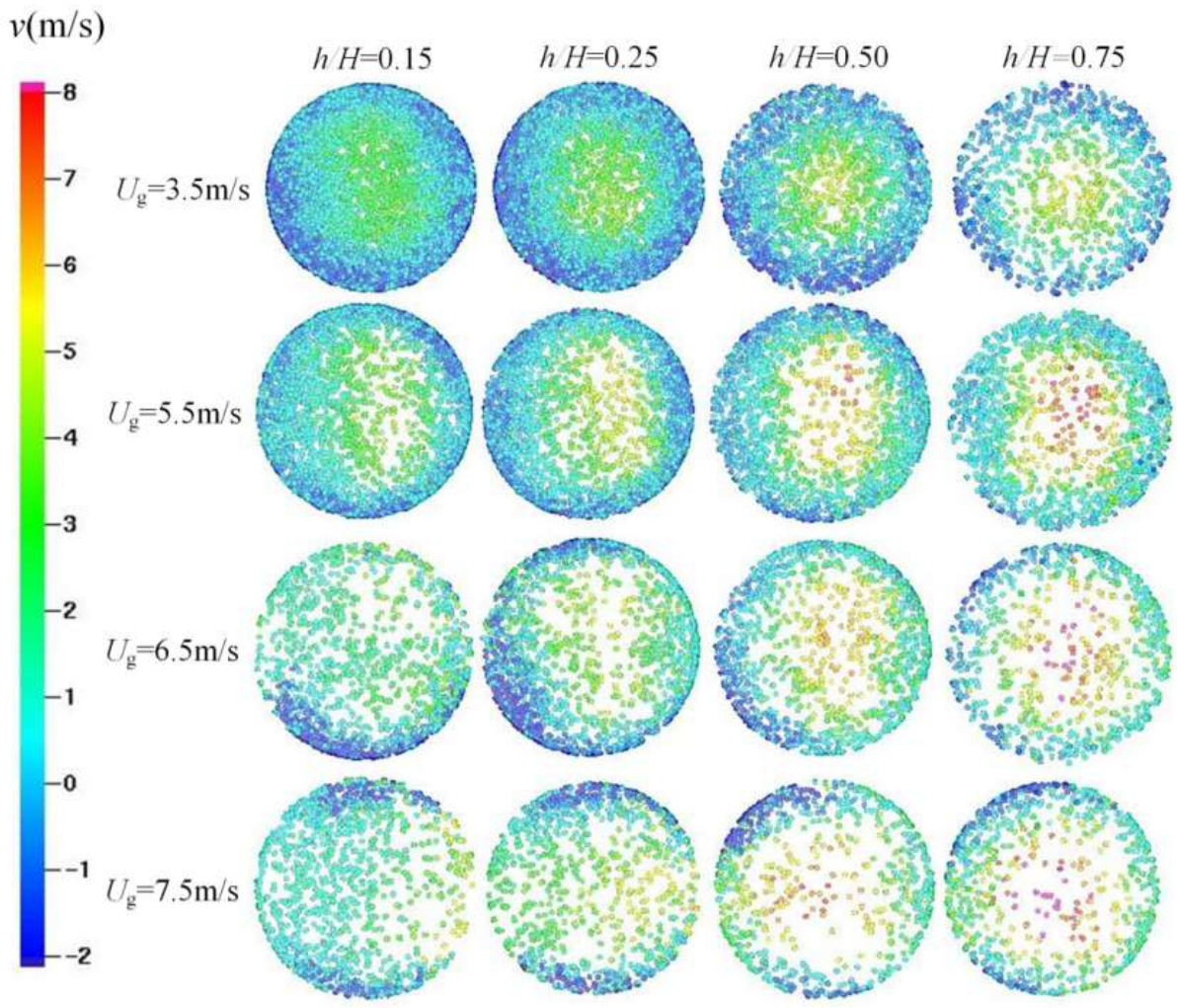

Fig.6-5 Spatial distribution of the instantaneous axial particle velocity at various superficial gas velocities (Q_1=20 kg/h, M_0=20 kg).

6.2.2 Influence of seal loop aeration rate

The loop seal in the downer provides the pressure for the particles to feed back into the riser, and to avoid the gas flow in the riser entering the downer. To keep the stable circulation of particles, the pressure drop of loop seal of the downer should be large enough. The variation of loop seal aeration rates can change the solid circulation behaviours in the fast fluidized bed effectively. The loop seal aeration rate Q_1 should be high enough to provide the energy for the particles to feed back into the riser, and keep a stable solid circulation. However, the Q_1 should be kept under a maximum value or

the particles in the loop would start to fluidized. A series studies on the effect of aeration rate have been conducted by the researchers in and abroad [15,23-25]. In this work the flow structure of the fast fluidized bed at u_g=5.28m/s is studied, with the aeration rate ranges from 5 kg/h to 30 kg/h.

The effect of loop seal aeration rate on transient solid volume fraction distribution in the fast fluidized bed is shown in Fig.6-6. As shown in Fig.6-6, more and more particles have been entrained into the riser when the Q_1 increases from 5kg/h to 15kg/h, and the solid volume fraction in the riser enhances remarkably. When further increases the aeration rate, the influence of aeration rate on the solid volume fraction in the riser weakens.

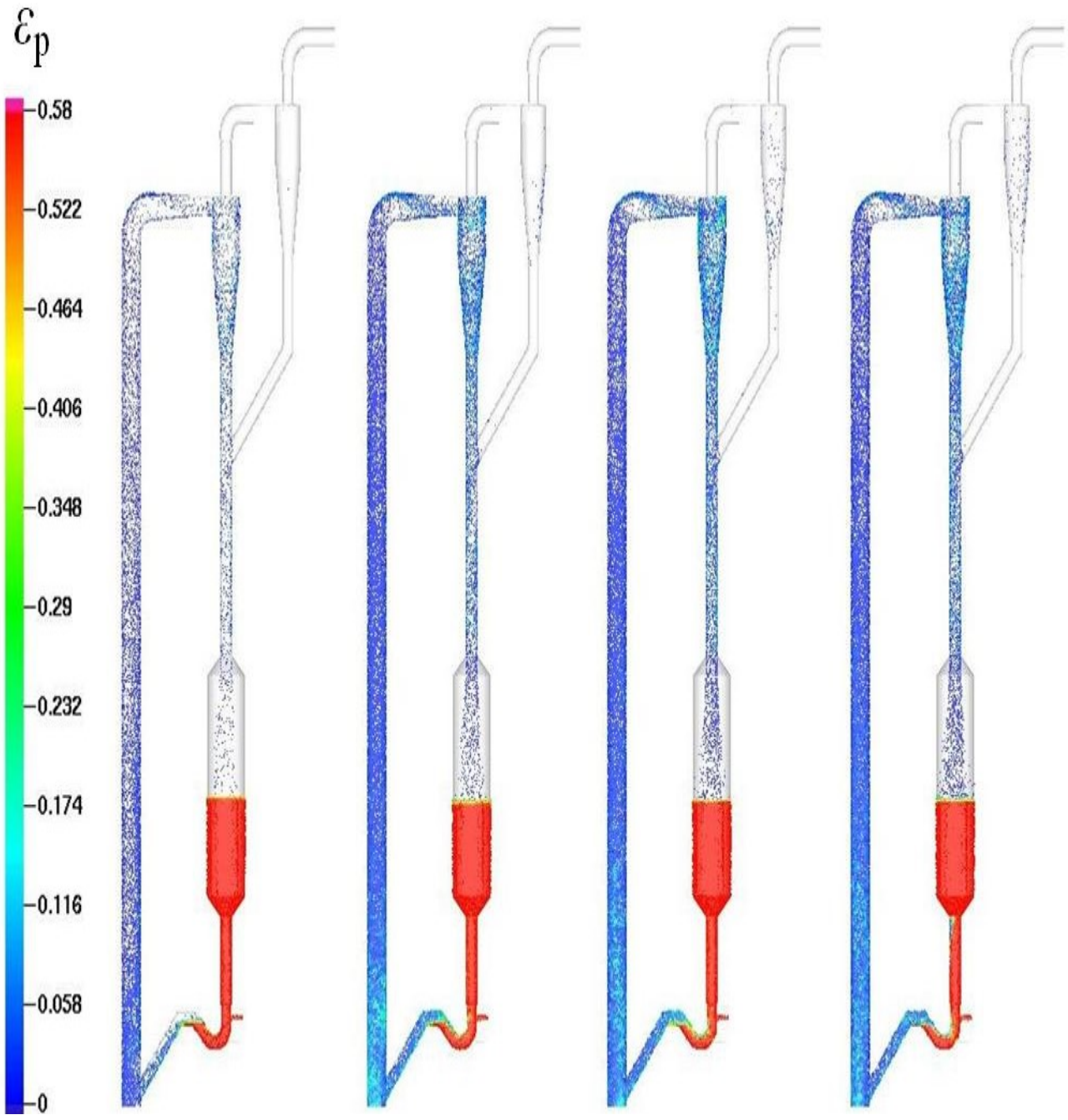

Fig.6-6Influence of the loop seal aeration rate on instantaneous solid volume fraction distribution in the fast fluidized bed:

(a)Q_1=5 kg/h; (b)Q_1=15 kg/h; (c)Q_1=20 kg/h; (d)Q_1=30 kg/h.

The higher aeration rate leads to higher solid mass flux in the fast fluidized bed, and more particles are fed back into the riser. With the increase of solid volume fraction in

the riser, the pressure drop P_1-P_2 is increasing, as shown in Fig.6-7. Meanwhile, the pressure drop in the downer is enhanced, so a larger pressure drop provided by loop seal is needed to turn the particles into the circulation of the riser. As the number of particles in the riser is increasing, the slip velocity and the height of loop seal in the downer declines. Accordingly, the higher loop seal aeration rate is, the higher the pressure drop of the loop seal is, but the changes is decreasing.

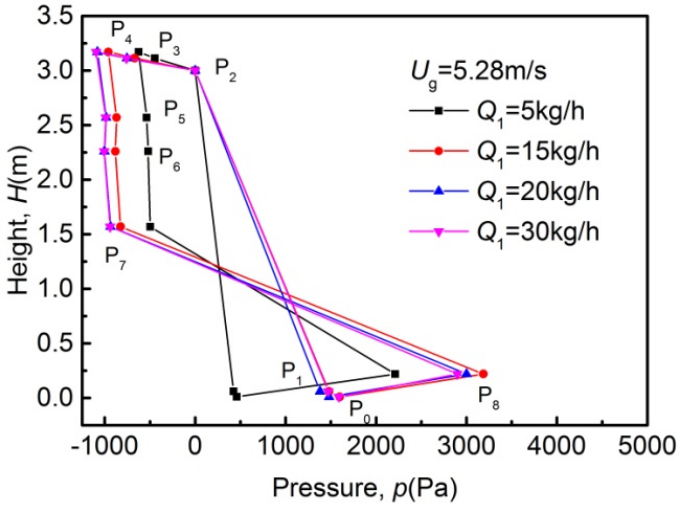

Fig.6-7Influence of seal loop aeration rate on the distributions of pressure in the whole loop.

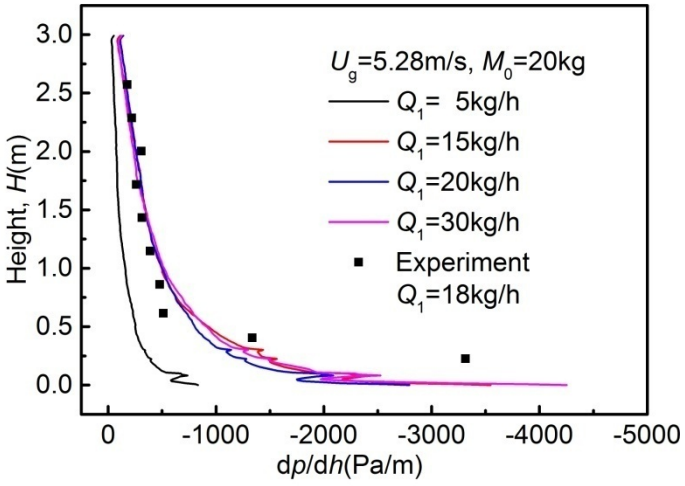

Fig.6-8Influence of seal loop aeration rate on the distributions of pressure drop in the riser.

The distributions of pressure drop in the riser under different loop seal aeration rates are shown in Fig.6-8. In the lower part of the riser, i.e. $h<0.5$ m, the solid volume fraction is relatively high, while the particles are loosely dispersed in the upper part of the riser ($h>0.5$ m). With Q_1 increases from 5kg/h to 15kg/h, the solid volume fraction in the riser increasing remarkably. When further increase the aeration rate, the solid volume fraction in the lower part of the riser still increases, while the solid volume fraction in the upper part changes very little.

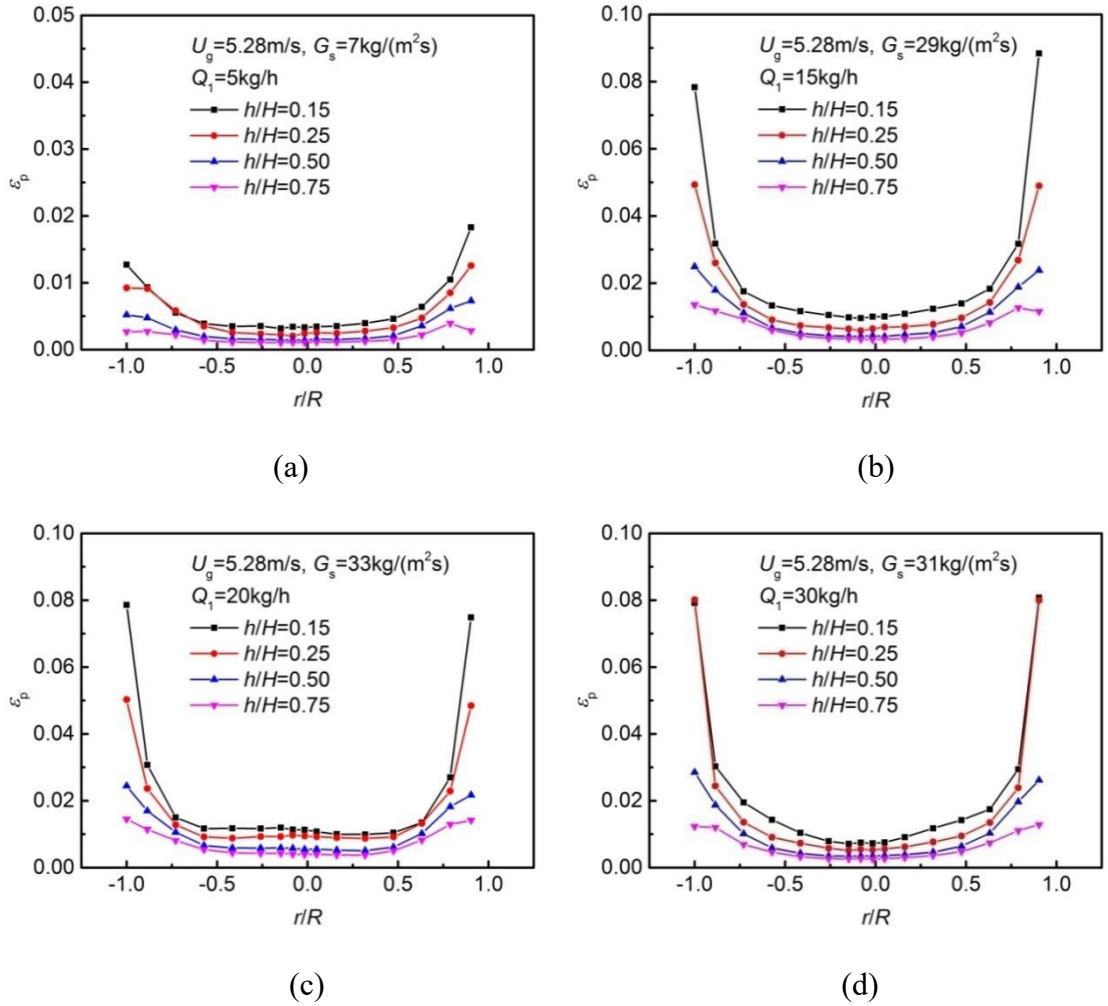

Fig.6-9 Influence of loop seal aeration rate on radial profiles of the time-averaged solid volume fraction for different riser height:

(a) Q_1=5 kg/h;(b) Q_1=15 kg/h;(c) Q_1=20 kg/h;(d) Q_1=30kg/h.

As shown in Fig.6-9, the typical core-annulus solid volume fraction in the riser can be observed, but when the aeration rate is lower, e.g. Q_1=5 kg/h, the solid volume fraction is distributed more evenly. With the increase of aeration rate, the solid volume fraction of the lower riser increases, especially for the wall region of the lower part. Meanwhile, the solid volume fraction also increases, this trend become more obviously with the riser height. When the aeration rateis further increased, the solid mass flux increases slightly, results in less obvious increase in solid volume fraction in the riser. When the Q_1 is increased to 30 kg/h, the dense zone in the bottom of the riser expands, but the increase of solid volume fraction is declining along the riser.

Fig.6-10 shows the spatial distribution of the transient axial particle velocity at various loop seal aeration rate, and the particles have been magnified by six times in the images. When Q_1=5 kg/h, the back-mixing of particles is not notable since the amount of falling particles is small. However, as the aeration rate is increased to 15 kg/h, the number of falling particles increases significantly, but the number of falling particles decreasing along the riser. Meanwhile, the velocity of the particles in the centre of the riser is increased. When further increase the aeration rate, the back-mixing particles observed in the higher position of the riser, and the particles in the centre are accelerated significantly. It can be explained that the increase of aeration rate results in higher solid mass flux, which leads to more back-mixing particles.

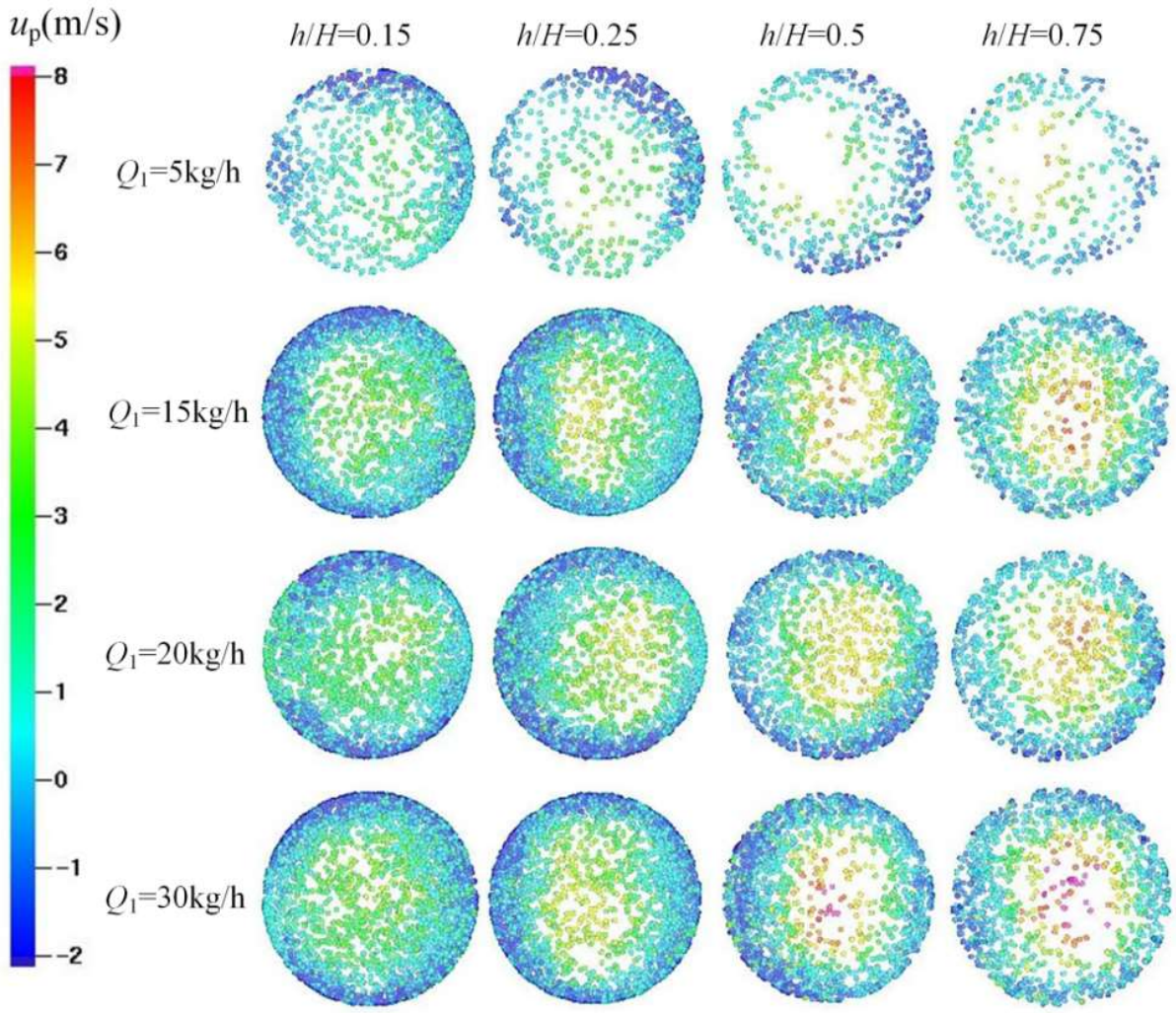

Fig.6-10 Spatial distribution of the instantaneous axial particle velocity under various loop seal aeration rates.

6.2.3 Influence of bed inventory

Basu et al.[16]and Yanget al.[17] proposed that the bed inventory is crucial to the pressure balance in the circulation of fast fluidized bed, and affects the solid mass flux significantly. When the bed inventory increases, the pressure drops in the riser, the exit, the cyclones and the loop seal will all increases accordingly. As a consequence, a larger pressure drop in the downer is needed to balance the pressure variations in the circulation system. In this section, the effect of the bed inventory on the flow structure of the fast fluidized bed is studied. Fig.6-11 shows the effect of the bed inventory on transient solid volume distribution in the fast fluidized bed at fixed superficial gas

velocity and loop seal aeration rate. With increasing bed inventory, the solid volume fraction and the particle packed height increases, which is consistent with the result of Wang et al.[15] However, Kim et al.[18] found that the particle packed height decreases with increasing bed inventory. Moreover, Yin [19] found that when the bed inventory is too large, the connection between the downer and the cyclone may be blocked, which impedes the particle circulation of the system. The increase of pressure drop of the downer sends more particles into the riser to balance the pressure in the system.

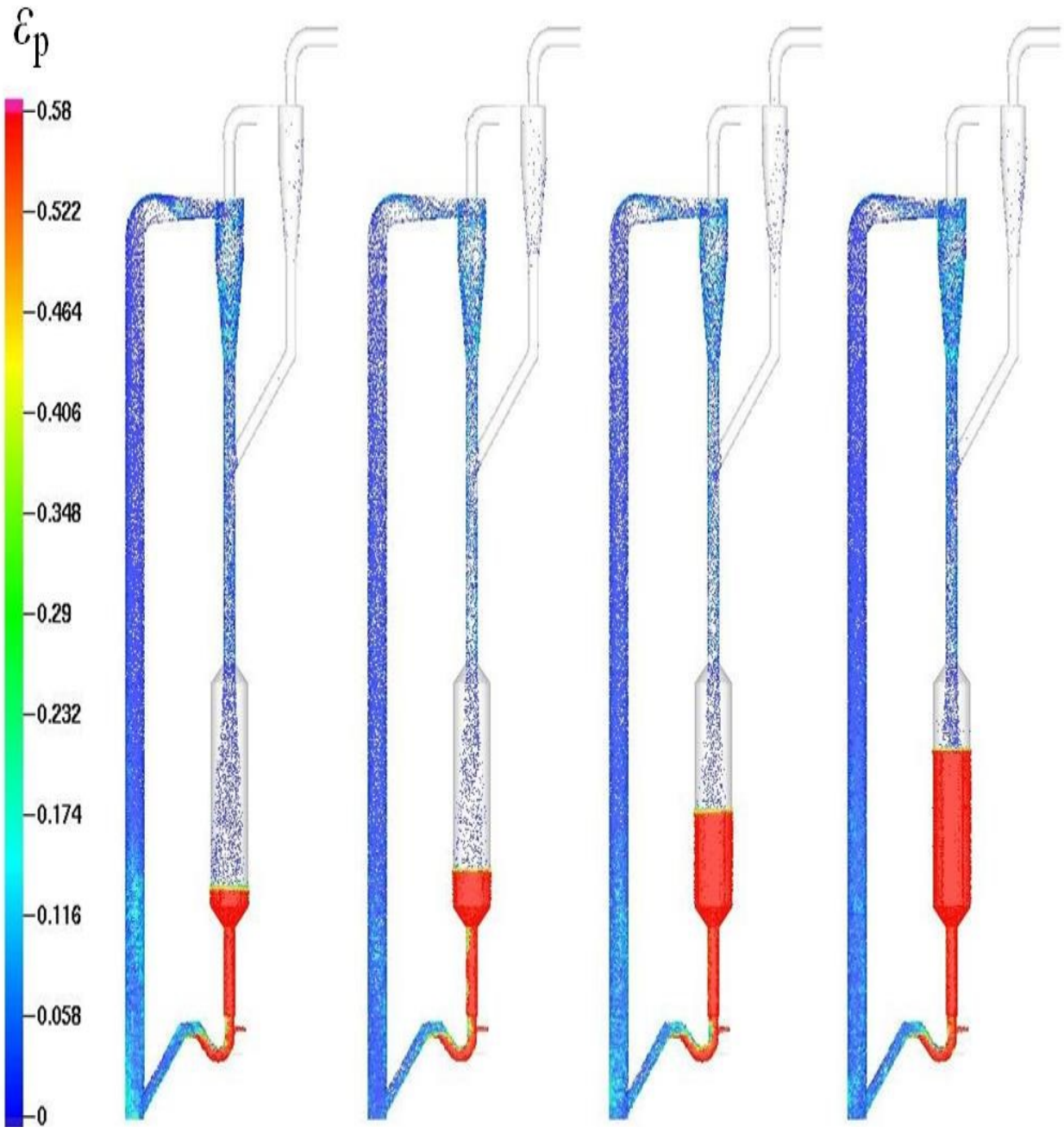

Fig.6-11Influence of the bed inventory on instantaneous solid volume fraction distribution in the fast fluidized bed:

(a) M_0=7.5 kg; (b)M_0=10 kg; (c)M_0=20 kg; (d)M_0=30 kg.

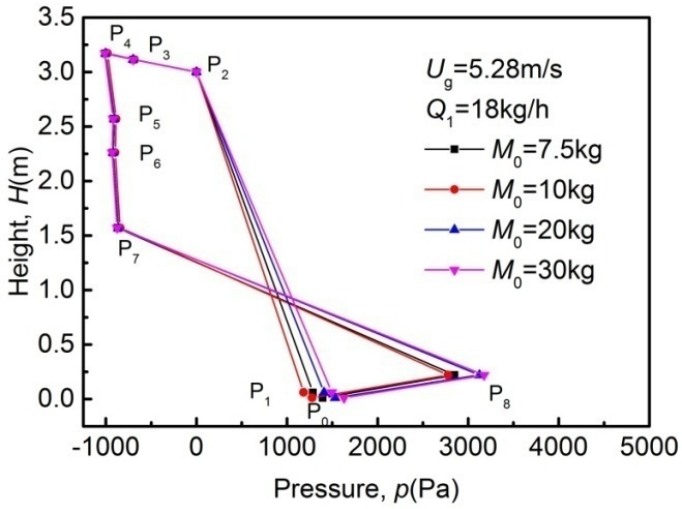

Fig.6-12 Influence of bed inventory on the distributions of pressure in the whole loop.

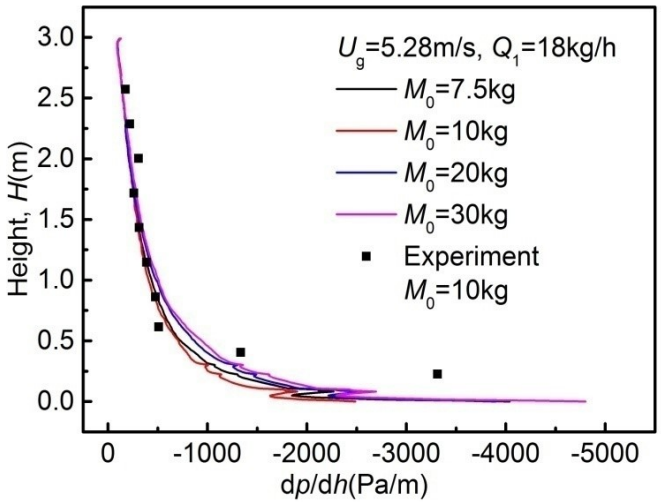

Fig.6-13 Influence of bed inventory on the distributions of pressure drop in the riser.

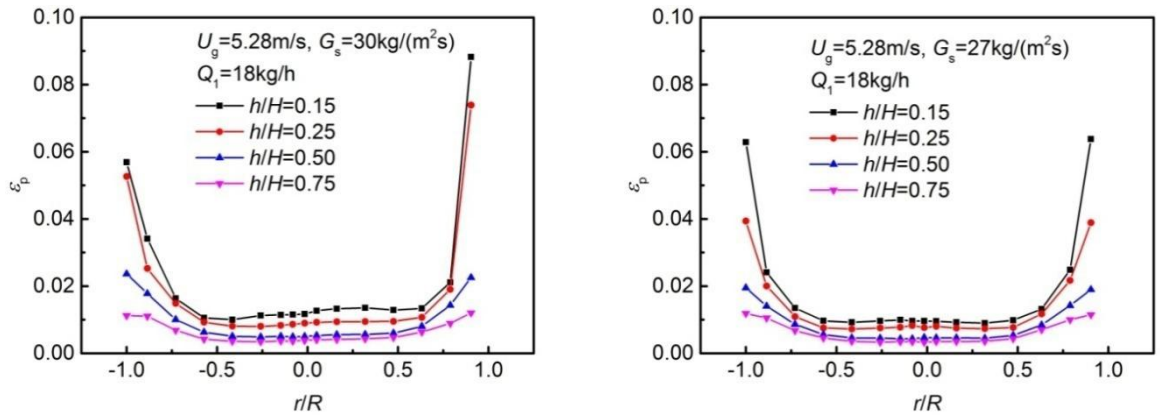

(a) (b)

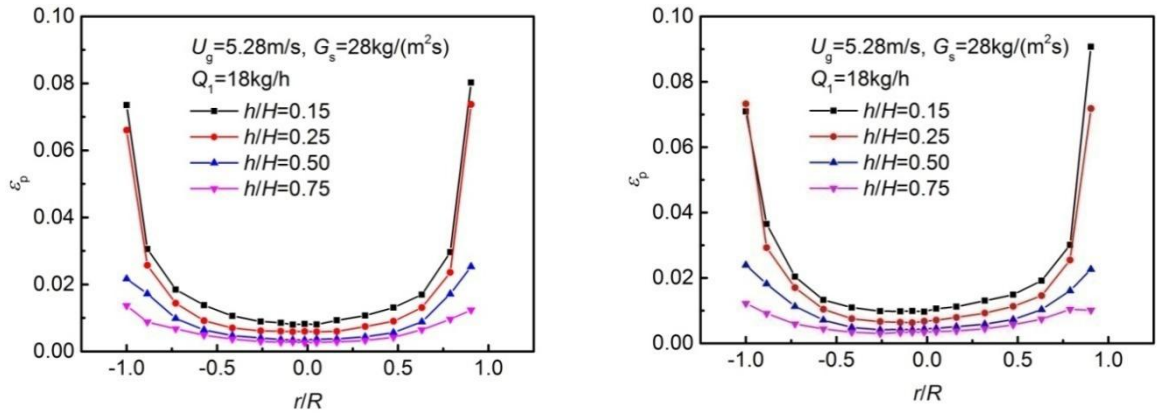

(c) (d)

Fig.6-14Influence of bed inventory on the radial profiles of the time-averaged solid volume fraction for different riser height under:

(a)M_0=7.5 kg;(b)M_0=10 kg;(c)M_0=20 kg;(d)M_0=30 kg.

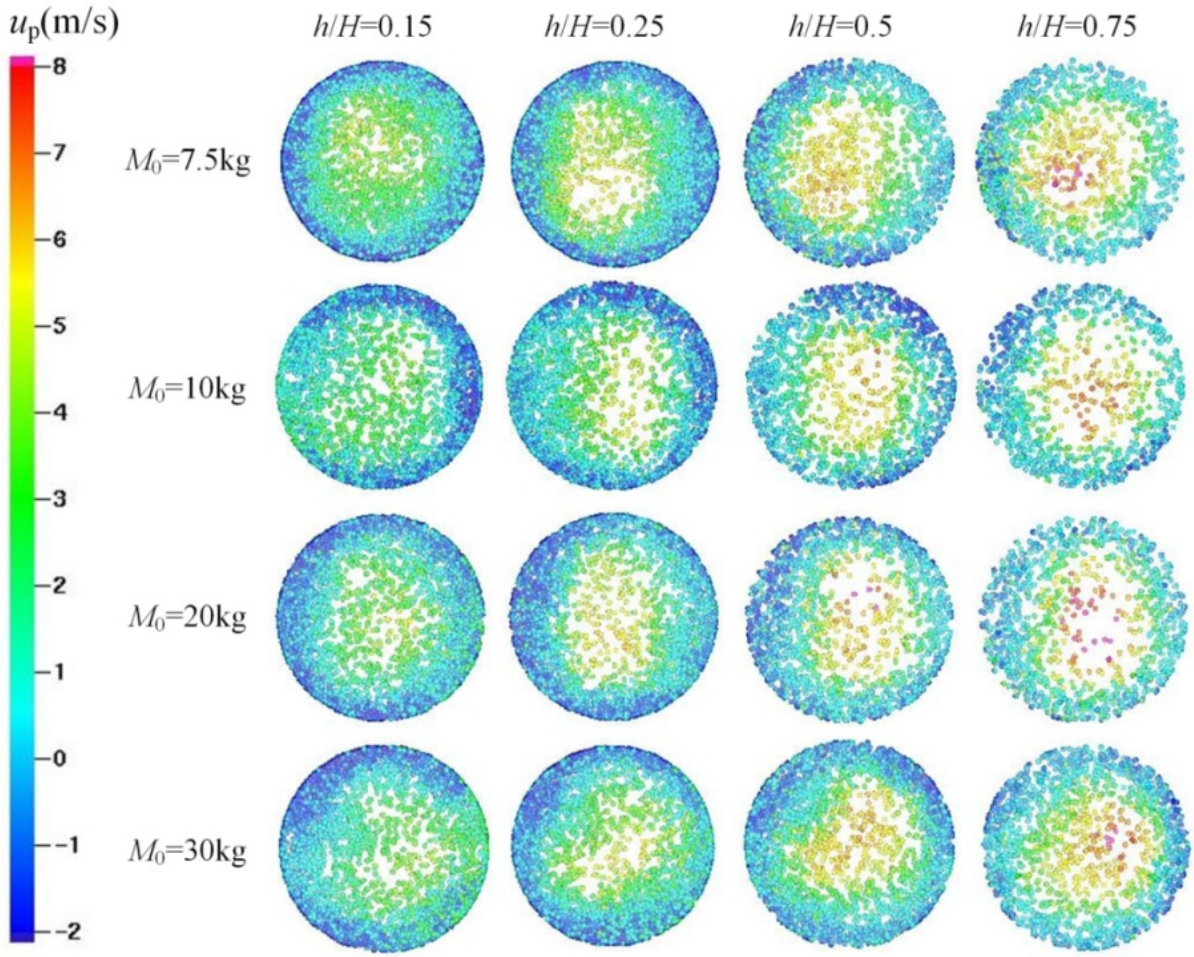

Fig.6-15 Spatial distribution of the instantaneous axial particle velocity under various bed inventories.

It can be seen from Fig.6-12 that the pressure drop in the riser changes very little with bed inventories. The pressure drop of the loop seal and solid mass flux varies constantly to keep the pressure balance of the fast fluidized bed system. At fixed superficial gas velocity and loop seal aeration rate, the increase of bed inventory leads to the enhancement of loop seal of the downer. Meanwhile, the P_8 at the bottom of the downer increases, driving more and more particles to circle back to the riser. Consequently, the pressure drop of the riser and the solid mass flux increase. However, when the solid mass flux reaches the maximum, the further increase of the bed inventory has no influence on the solid mass flux, and the stable circulation in the fast fluidized bed is destroyed[19]. As shown in Fig.6-13, the solid volume fraction varies very little with different bed inventories when the superficial gas velocity is kept constant. With the increase of bed inventory, the solid volume fraction in the wall region of lower riser increases. However, the solid mass flux changes little with increasing bed inventory, therefore the axial distribution of solid volume fraction have little difference, as shown in Fig.6-14. Fig.6-15 shows the spatial distribution of the transient axial particle velocity under various bed inventories. It is notable that when the bed inventory increase, the velocity of particles in the middle of the riser increases, especially when h/H=0.75.

6.3 Modeling of particle clusters in the fast fluidized bed

The geometry of the riser (H=1.5m) is shown in Fig.6-16, and the key parameters and simulation conditions are listed in Table 6-3.

Table 6-3 Key parameters and simulation conditions

Parameters	Value	Parameters	Value
Diameter of riser (D)	0.1m	Maximum momentum redirection from collision(α_{max})	40%
Height of riser (H)	1.5 m/3.0 m	Normal particle-wall restitution coefficient (e_{wn})	0.3
Particle size (d_p)	0.25 mm	Tangential particle-wall restitution coefficient ($e_{w\tau}$)	0.99
Particle density (ρ_p)	2650kg/m^3	Turbulent model	LES
gas density (ρ_g)	ideal gas law	Grid size	6 mm
gas viscosity(μ_g)	1.84×10^{-5} Pa/s	Grid number	51840
Superficial gas velocity(u_g)	5.28m/s	The number of simulation particles(N_p)	622080
Solid mass flux (G_s)	57.5 kg/m^2·s	The number of real particle per parcel(n_p)	65
Random close pack (ε_{cp})	0.58	Time step (Δt)	1×10^{-4} s
Drag model	Wen-Yu-Ergun		

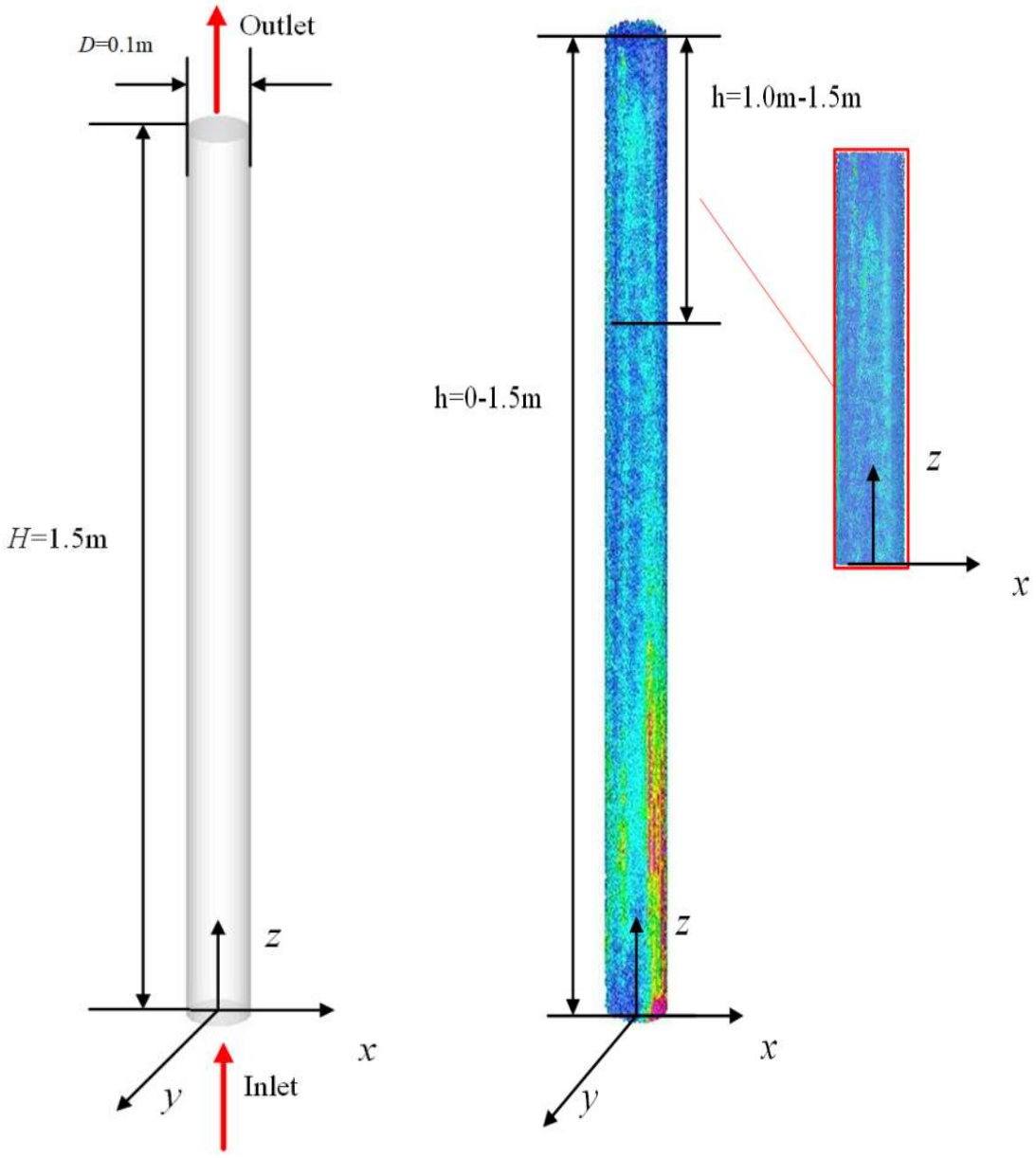

(a) (b)

Fig.6-16 (a) Geometry of the riser in fast fluidized bed;

(b) Snapshot of particle cluster in the simulation.

6.3.1 Validation of simulation

Fig.6-17 shows the comparison of simulation results and the experimental cluster structures in the riser: (a) Stripe-shaped cluster, (b) Saddle-shaped cluster and (c) U-shaped cluster, where the simulation images are from the riser at h=1.15-1.4 m, and the experimental images are from the results in chapter 3. The simulation results are in

good agreement with the experiments. That is, the simulation method can well predict the clusters in the fast fluidized bed.

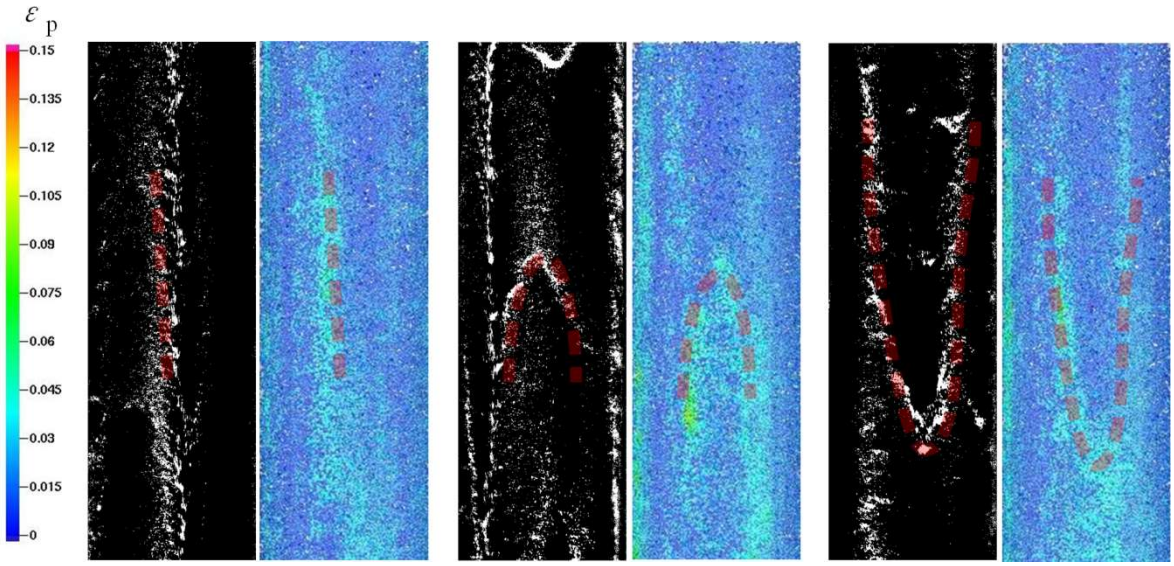

(a) (b) (c)

Fig.6-17 Comparison of simulated and experimental of cluster structures:

(a)u_g=5.28 m/s,G_s=57.5 kg/(m^{2}s),d_p=0.25 mm ; (b)u_g =5.28 m/s,G_s=57.5kg/(m^{2}s),d_p=0.25 mm ;(c)u_g =5.28 m/s,G_s=57.5 kg/(m^{2}s),d_p=0.25 mm.

6.3.2 Cluster structures and evolutionary processes

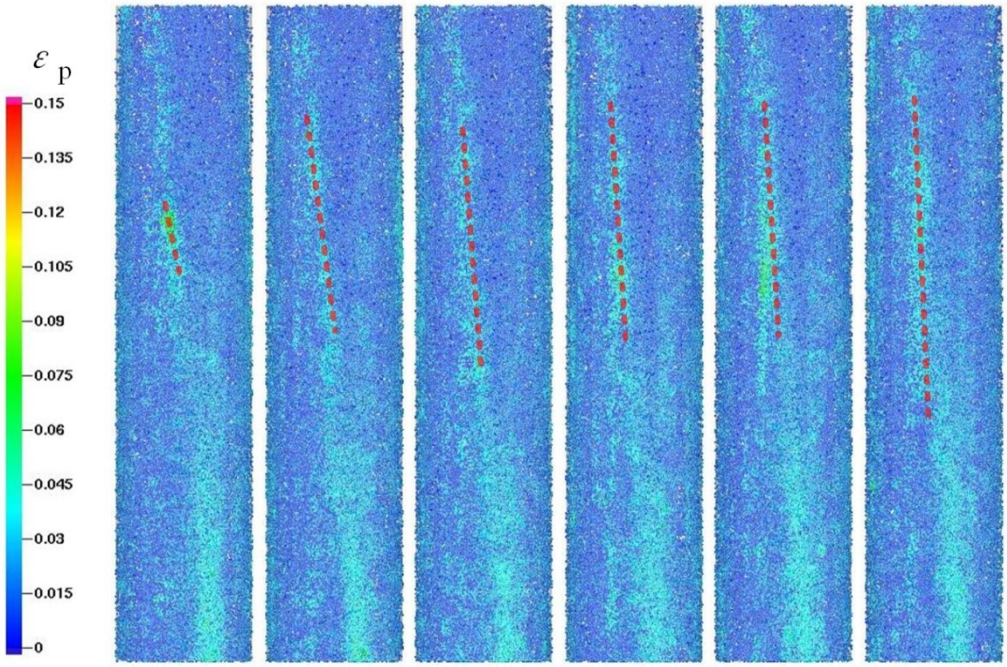

(a) (b) (c) (d) (e) (f)

Fig. 6-18 The simulated evolutionary processes of the stripe-shaped cluster (Δt=0.1s, u_g =5.28 m/s,G_s=57.5 kg/(m^{2}s),d_p=0.25 mm).

Fig.6-18 shows the simulated evolutionary processes of the stripe-shaped cluster at wall region of h=1.0 m to1.5 m of the riser. The stripe-shaped cluster is the most common cluster in the wall region of the riser. As shown in Fig.6-18, the length of the stripe-shaped cluster in the simulation is in good agreement with the experimental results, ranging from 300mm to 1000mm. In Fig.6-18 (a), the micro clusters encounter the upward particles and interact with the upward particle flow due to the instability of particle flow. As shown in Fig.6-18 (b)(c), The particle streams move upward continuously and interact with the micro clusters. The disperse particles aggregate with the micro cluster at the interface, forming stripe-shaped dense particle zone where stripe-shaped clusters start to take shape, as seen in Fig.6-18 (d). Meanwhile, the particles are further compacted and the solid volume fraction of particle clusters increases, the upward particle streams accumulate at the interfaces where they

encounter with stripe-shaped clusters, which promote the development of the saddle shaped clusters, as seen in Fig.6-18 (e) and (f).

Fig.6-19 shows the simulated evolutionary processes of the stripe-shaped cluster at the wall region of the riser. As seen in Fig.6-19 (a), the micro clusters on the left side are entrained by the gas-solid flow. Meanwhile, the upward micro clusters encounter the particle streams on the right side, resulting in energy dissipation of the particles in the micro cluster and aggregating with the stripe-shaped cluster, as seen in Fig.6-19 (b). Due to the particle aggregation, the pressure around the particle clusters is decreased. Consequently, the disperse particles move toward the particle clusters and aggregate with them, which enhance the solid volume fraction of particle clusters. As the momentum of the downward particle stream is larger than that of the upward particle stream, the saddle-shaped cluster will move downward with a slow velocity, as shown in Fig.6-19 (c) (d). Meanwhile, the saddle-shaped cluster collapses and coalesces with strip-shaped cluster constantly, thus the energy of particles decreases and form a low-pressure area, which draw the surrounding particles toward saddle-shaped cluster, as in Fig.6-19 (e), further increases the solid volume fraction of particle clusters. Shown in Fig.6-19 (f), when particle stream with large momentum crashes the saddle-shaped cluster, the cluster is then carried by the particle stream until it is destroyed.

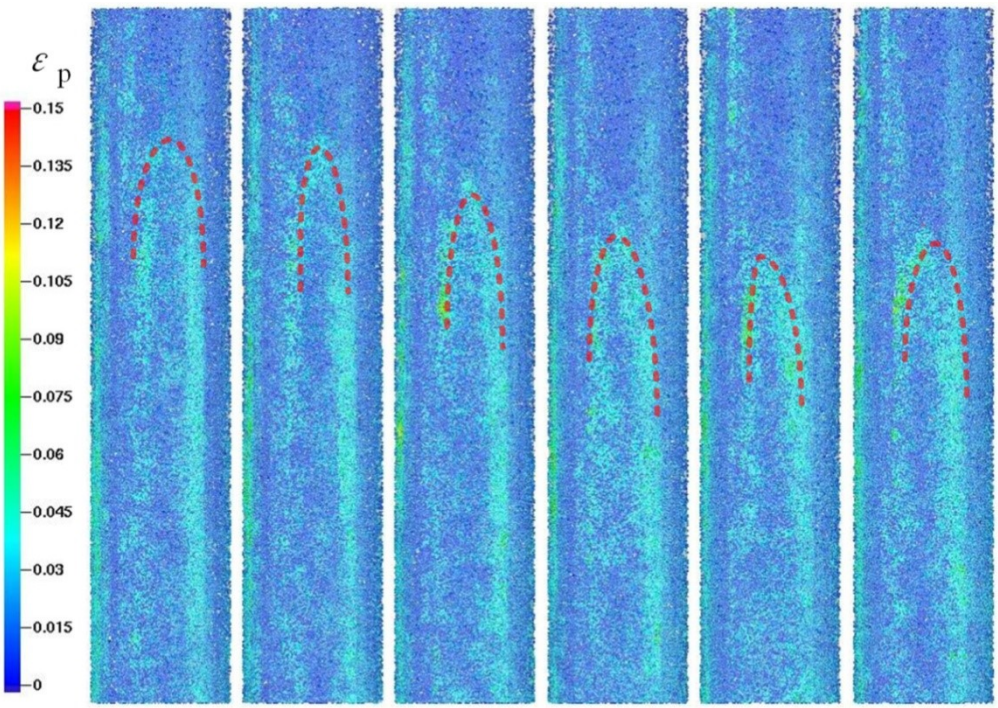

(a) (b) (c) (d) (e) (f)

Fig. 6-19 The simulated evolutionary processes of the saddle-shaped cluster (Δt=0.1s, u_g =5.28 m/s,G_s=57.5 kg/(m^{2}s),d_p=0.25 mm).

Fig.6-20 demonstrates the simulated evolutionary processes of the U-shaped cluster at the wall region of the riser. As seen in Fig.6-20 (a), when some particle clusters grow to a large size and overbalance the carrying capacity of the gas flow, they collapse from the clusters and fall down. The falling particles encounter the particle cluster on the right side, the U-shaped cluster begin to take shape, as in Fig.6-20 (b). However, the gas-solid jet on the left side keeps crashing the particle cluster and decreases the solid volume fraction of it, which slows down the dropping of the particle cluster, as in Fig.6-20 (c). It can been from Fig.6-20 (d) that as the disperse particles accumulate in the low-pressure region of the inner U-shaped cluster, the solid volume fraction of U-shaped clusters keep increasing. When the particle cluster overbalances the carrying capacity of gas flow, the U-shaped cluster will restart falling and develop, as in Fig. 6-20 (e) (f).

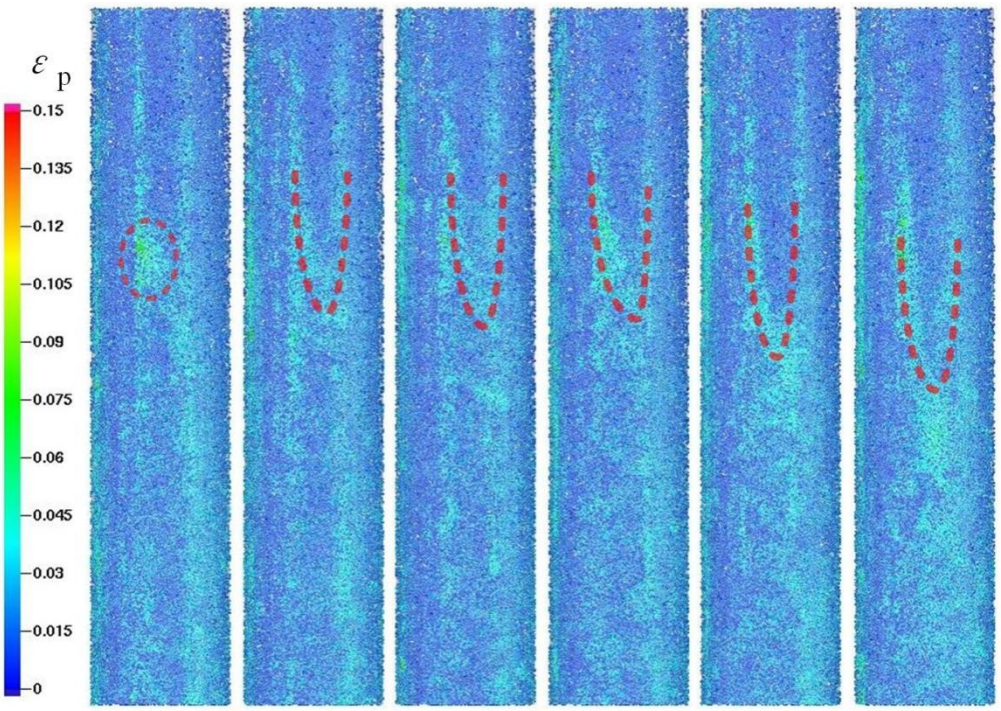

(a) (b) (c) (d) (e) (f)

Fig. 6-20 The simulated evolutionary processes of the U-shaped cluster

(Δt=0.1s, u_g =5.28 m/s,G_s=57.5 kg/(m^{2}s),d_p=0.25 mm).

6.4 Flow characteristics of particle clusters

The identification of particle cluster is developed from the criterion proposed by Soonget al.[20] and Sharmaet al.[21], which is:

$$\varepsilon_{cl} = \overline{\varepsilon_{ave}} + 2\sigma \quad (6\text{-}1)$$

Fig.6-21 is the distributions of average solid volume fraction and average velocity of particle clusters under different riser height. It can be seen from Fig.6-21 (a) (b), the average solid volume fraction of particle clusters increases from the center of the riser to the wall region, which is consistent with previous study [5] . In Fig.6-21 (c) (d), it can be seen that the average velocity of particle cluster increases with higher riser height. The velocity of particle cluster in the center is positive, while the velocity of the particle cluster in the wall region is negative.

6.4.1Radial distribution of solid volume fraction and velocity of particle cluster

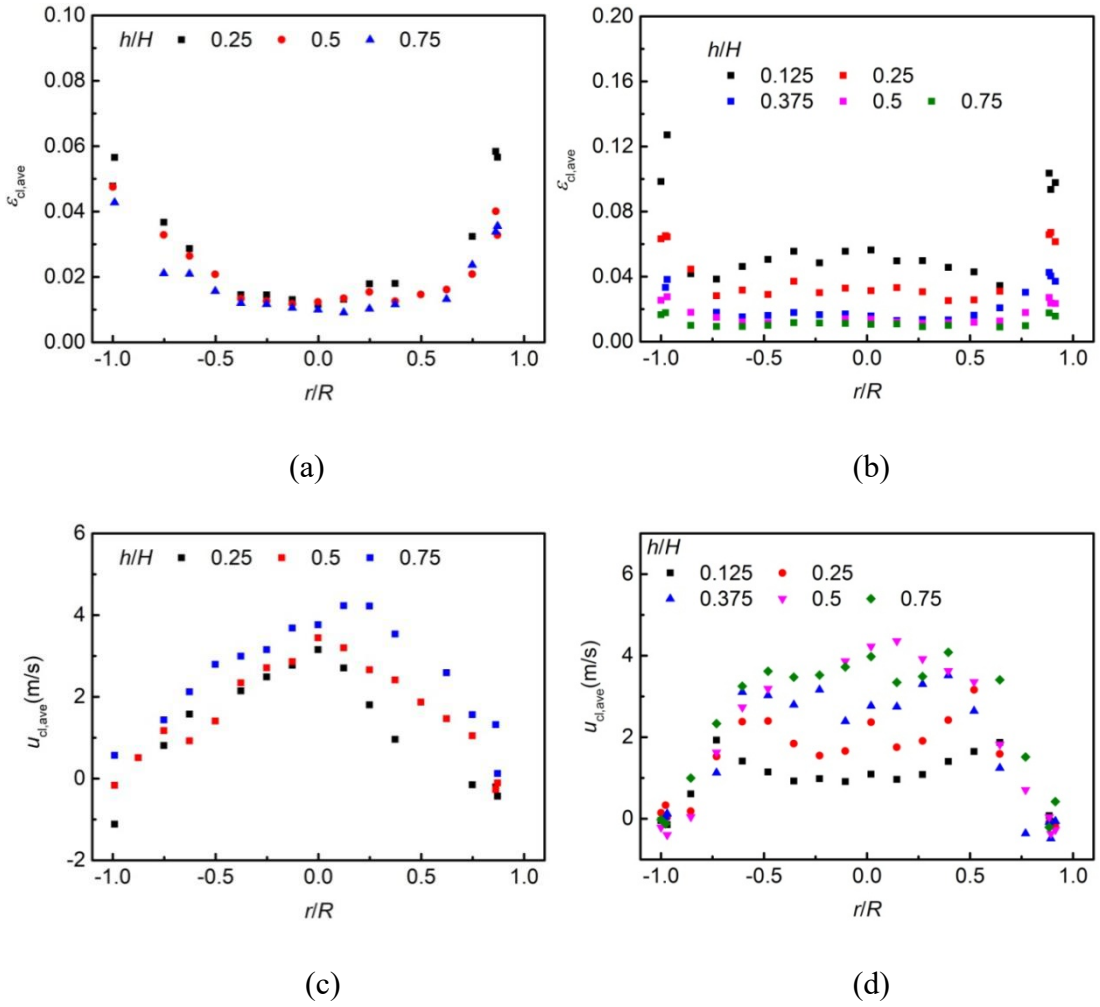

Fig.6-21 Radial distribution of average solid volume fraction of particle cluster:

(a) H =1.5 m, u_g =5.28 m/s,G_s=57.5 kg/(m^{2}s),d_p=0.25 mm;

(b)H =3.0 m, u_g =5.28 m/s,G_s=57.5 kg/(m^{2}s),d_p=0.25 mm;

Radial distribution of average velocity of particle cluster:

(c)H =1.5 m, u_g =5.28 m/s,G_s=57.5 kg/(m^{2}s),d_p=0.25 mm;

(d) H =3.0 m, u_g =5.28 m/s,G_s=57.5 kg/(m^{2}s),d_p=0.25 mm.

Moreover, the descending velocity of particle clusters is lower than 1m/s, which is very close to the experiment result in chapter 3, and consistent with previous simulation study by Liu et al.[22]. It is obvious that most of the particle clusters are carried by the upward gas flow under the operating condition, while only small account of particle

clusters in the wall region may move upward and downward from time to time. As shown in Fig.6-21(b), when increase the length of the simulated riser, the solid volume fraction of particle clusters become more evenly distributed at the axial direction, particle cluster with high solid volume fraction can only observed in the wall region. Meanwhile, the distribution of particle clusters solid volume fraction for different height riser follow similar trend, but the solid volume fraction at the same position is higher of 3.0m riser than that of 1.5m riser. The average velocity particle cluster in longer riser at certain position is lower than that in the short riser at the same position.

6.4.2 Axial distribution of solid volume fraction and velocity of particle cluster

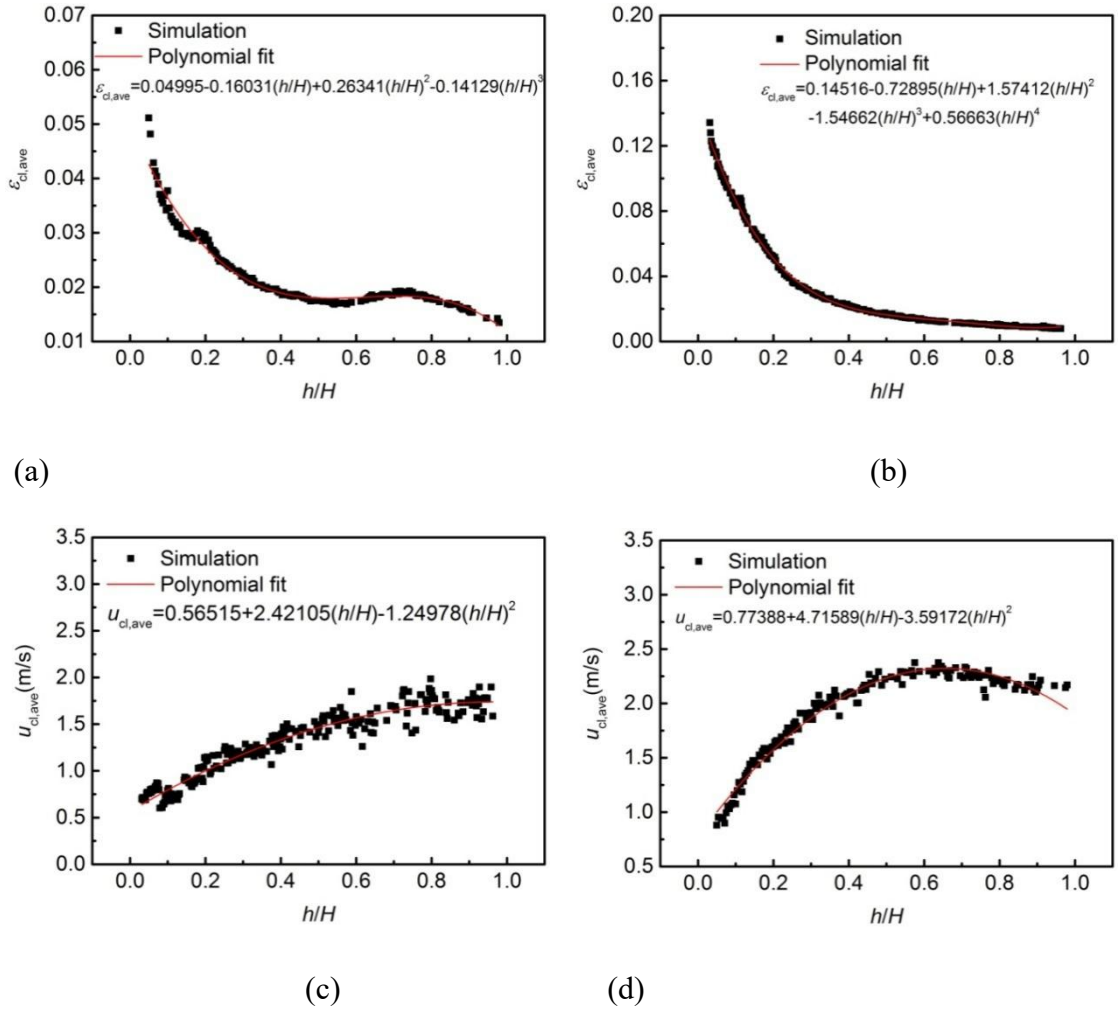

Fig. 6-22 Axial distribution of average solid volume fraction of particle cluster:

(a)H =1.5 m, u_g =5.28 m/s,G_s=57.5 kg/(m^{2}s),d_p=0.25 mm;

(b)H =3.0 m, u_g =5.28 m/s,G_s=57.5 kg/(m^{2}s),d_p=0.25 mm;

Axial distribution of average velocity of particle cluster:

(c)H =1.5 m, u_g =5.28 m/s,G_s=57.5 kg/(m^{2}s),d_p=0.25 mm;

(d)H =3.0 m, u_g =5.28 m/s,G_s=57.5 kg/(m^{2}s),d_p=0.25 mm.

Fig.6-22 is the axial distribution of cross-sectional average solid volume fraction and velocity of particle clusters. The average solid volume fraction decreases with increasing riser height, as seen in Fig.6-22 (a)(b). Moreover, it can be seen that the solid volume fraction of particle clusters in the lower riser increases with the increasing length of the riser, while that in the upper riser changes very little. As in Fig.6-22 (c)(d), the average velocity of particle clusters increases rapidly at first and then become stable with riser height, while the result of Liu et al.[22]shows that the velocity of particle clusters increases with the riser height gradually, which may be explained by that the simulation is conducted in a two-dimensional geometry.

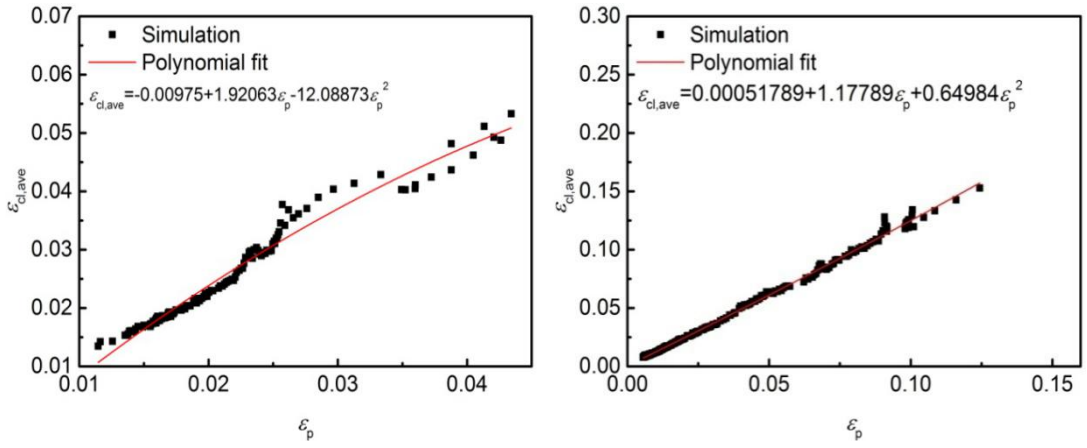

(a) (b)

Fig.6-23 Influence of average cross-sectional solid volume fraction on solid volume fraction of particle cluster:

(a)H =1.5 m, u_g =5.28 m/s,G_s=57.5 kg/(m^{2}s),d_p=0.25 mm;

(b)H =3.0 m, u_g =5.28 m/s,G_s=57.5 kg/(m^{2}s),d_p=0.25 mm.

Fig.6-23(a)(b) are the effect of average cross-sectional solid volume fraction on solid volume fraction of particle cluster for different riser length. It is obvious that the solid volume fraction of particle clusters has a positive relationship with the average cross-sectional solid volume fraction, which is in good agreement with the prediction of experiment by Harris et al.[23].

6.5 Conclusions

The MP-PIC method was applied in the simulation of a three-dimensional full-loop fast fluidized bed in this chapter, and the effect of operating conditions including superficial gas velocity u_g, seal loop aeration rate $Q_1$and bed inventory M_0 on gas-solid flow characteristics were investigated. Moreover, the typical clusters structures were well predicted, further illustrated the evolutional processes of particle cluster in the fast fluidized bed. The flow behavior of particle cluster was studied by simulation method, revealing the distribution of solid volume fraction and the velocity of particle clusters. The follow conclusions can be drawn:

(1) The superficial gas velocity plays the dominant role on the gas-solid flow characteristics among three factors. The increase of superficial gas velocity leads to remarkably decrease in the solid volume fraction of the riser. Meanwhile, the solid volume fraction of the riser becomes better distributed axially and radially.

(2) With the increase of seal loop aeration rate, the solid mass flux and the solid volume fraction are increasing, and the increase become more visible with riser height. Meanwhile, the particle velocity in the center of the riser is enhanced while that in the wall region is declined.

(3) As the bed inventory increases, the solid volume fraction of the lower riser is increasing, and the particle velocity is also increased. When the bed inventory increases

at fixed superficial gas velocity, the solid mass flux has little change. Notably, the connection between the downer and the cyclone may be blocked by excessive bed inventory, which impedes the solid circulation of the system.

(4) Based on MP-PIC method, the meso-scale flow structure of the fast fluidized bed is studied. Three typical patterns of particle clusters, i.e. stripe-shaped cluster, saddle-shaped cluster and U-shaped cluster were identified, revealing the evolutional processes of particle clusters.

(5) The distribution of cross-sectional average solid volume fraction and solid volume fraction of particle clusters shows similar trend in the shaped of U, while the distribution of velocity of particle clusters shows a reverse trend. With the increase of riser height, the volume fraction of particle clusters decreases gradually while the velocity of particle clusters is increasing, but the changes slow down with the riser height.

6.6 Reference

[1] Wu Y, Peng L, Qin L, et al. Validation and application of CPFD models in simulating hydrodynamics and reactions in riser reactor with Geldart A particles[J]. *Powder Technology***2018**, 323: 269-283.

[2] Luo K, Wu F, Yang S, et al. High-fidelity simulation of the 3-D full-loop gas-solid flow characteristics in the circulating fluidized bed[J]. *Chemical Engineering Science***2015**, 123: 22-38.

[3] Lu L, Xu J, Ge W, et al. EMMS-based discrete particle method (EMMS-DPM) for simulation of gas-solid flows[J]. *Chemical Engineering Science* **2014**, 120: 67-87.

[4]Wang S, Luo K, Hu C, et al. CFD-DEM study of the effect of cyclone arrangements on the gas-solid flow dynamics in the full-loop circulating fluidized bed[J]. *Chemical Engineering Science***2017**, 172: 199-215.

[5]Chalermsinsuwan B, Gidaspow D, Piumsomboon P. Comparisons of particle cluster diameter and concentration in circulating fluidized bed riser and downer using computational fluid dynamics simulation[J]. *Korean Journal of Chemical Engineering* **2013**, 30(4): 963-975.

[6] Lu H, Wang S, He Y, et al. Numerical simulation of flow behavior of particles and clusters in riser using two granular temperatures[J]. *Powder Technology* **2008**, 182(2): 282-293.

[7] Lu H L, Sun Q Q, He Y R, et al. Numerical study of particle cluster flow in risers with cluster-based approach[J]. *Chemical Engineering Science***2005**, 60(23): 6757-6767.

[8] Tsuji Y, Tanaka T, Yonemura S. Cluster patterns in circulating fluidized beds predicted by numerical simualtion (discrete particle model versus two-fluid model)[J]. *Powder Technology***1998**, 95: 254-264.

[9] Carlos V A E, Peters E A J F, Kuipers J A M. CFD-DEM simulations and experimental validation of clustering phenomena and riser hydrodynamics[J]. *Chemical Engineering Science***2017**, 169(Supplement C): 246-258.

[10] Liu H, Lu H. Numerical study on the cluster flow behavior in the riser of circulating fluidized beds[J]. *Chemical Engineering Journal* **2009**, 150(2): 374-384.

[11] Liu H P, Liu D Y, Liu H. Study of cluster behavior in the riser of CFB by the DSMC method[M]. AIP Conference Proceedings, Guo L J, Joseph D D, Matsumoto Y, et al, 2010: 1207, 951-956.

[12] Berrouk A S, Wu C L. Two-dimensional discrete particle model: Comment on the numerical simulation of cluster flow behavior in the riser of circulating fluidized beds by Liu and Lu[J]. *Chemical Engineering Journal***2010**, 160(2): 810-811.

[13] Capecelatro J, Pepiot P, Desjardins O. Numerical characterization and modeling of particle clustering in wall-bounded vertical risers[J]. *Chemical Engineering Journal***2014**, 245(Supplement C): 295-310.

[14] Luo K, Wang S, Yang S, et al. Computational Fluid Dynamics–Discrete Element Method Investigation of Pressure Signals and Solid Back-Mixing in a Full-Loop Circulating Fluidized Bed[J]. *Industrial & Engineering Chemistry Research***2017**, 56(3): 799-813.

[15] Wang Q, Yang H, Wang P, et al. Application of CPFD method in the simulation of a circulating fluidized bed with a loop seal Part II-Investigation of solids circulation[J]. *Powder Technology***2014**, 253: 822-828.

[16] Basu P, Cheng L. An analysis of loop seal operations in a circulating fluidized bed[J]. 2000, 78(7): 991-998.

[17] Yang S, Yang H, Zhang H, et al. Impact of operating conditions on the performance of the external loop in a CFB reactor[J]. *Chemical Engineering and Processing* **2009**, 48(4): 921-926.

[18] Kim S W, Namkung W, Kim S D. Solids flow characteristics in loop-seal of a circulating fluidized bed[J]. *Korean Journal of Chemical Engineering***1999**, 16(1): 82-88.

[19] Yin S.Y. Experimental and Modeling Study on a Pressurized High-Density Circulating Fluidized Bed [D]. Nanjing: Southeast University, 2014.

[20] Soong C, Tuzla K, Chen J. Identification of particle clusters in circulating fluidized bed[M]. Circulating Fluidized Bed Technology Ⅳ, Avidan A A. ed; New York:AIChE, 1994, 615-620.

[21] Sharma A K, Tuzla K, Matsen J, et al. Parametric effects of particle size and gas velocity on cluster characteristics in fast fluidized beds[J]. *Powder Technology* **2000**, 111(1-2): 114-122.

[22] Liu H, Lu H. Numerical study on the cluster flow behavior in the riser of circulating fluidized beds[J]. *Chemical Engineering Journal***2009**, 150(2): 374-384.

[23] Harris A T, Davidson J F, Thorpe R B. The prediction of particle cluster properties in the near wall region of a vertical riser (200157)[J]. *Powder Technology***2002**, 127(2): 128-143.

[23] Ma Q, Lei F L∗, Xu X, Xiao Y H. Three-dimensional full-loop simulation of a high-density CFB with standpipe aeration experiments[J]. *Powder Technolog***2017,** 320: 574–585.

[24] Li T W, Dietiker J F, Shadle L. Comparison of full-loop and riser-only simulations for a pilot-scale circulating fluidized bed riser[J]. *Chemical Engineering Science1***2014,** 20:10–21.

[25] Guan Y J, Chang J, Zhang K, Wang B D, Sun Q, Wen D S. Three-dimensional full loop simulation of solids circulation in an interconnected fluidized bed. *Powder Technology***2016,** 289:118–125.

CHAPTER 7 Conclusion Remarks and Recommendations for Future Work

7.1 Conclusions remarks

The thesis focused on revealing the flow meso scale in fast fluidized bed, i.e. the flow structures and transitions, the cluster structures and behaviour.

The thesis investigated flow behaviour under various operating conditions and particle properties and developed the flow regime map for fast fluidized bed handling Geldart B particles. Moreover, the cluster characteristics including cluster structures, size, velocity and distribution feature have been investigated, four types of particle cluster and their typical evolutionary processes were proposed and illustrated.

The MP-PIC method was applied in the simulation of a three-dimensional full-loop fast fluidized bed in this chapter, and the effect of operating conditions including superficial gas velocity u_g, seal loop aeration rate $Q_1$and bed inventory M_0 on gas-solid flow characteristics were investigated. Moreover, the typical clusters structures were well predicted, further illustrated the evolutional processes of particle cluster in the fast fluidized bed. The flow behaviour of particle cluster was studied by numerical simulation method, which indicates the distribution of solid volume fraction and the velocity of particle clusters.

The following are the highlights of conclusions drawn from this research.

7.1.1 Experimental work

(1) The flow structures from low velocity fluidization to high velocity fluidization in a fast fluidized bed have been investigated, and five distinct flow patterns were identified. With increasing superficial gas velocity at various static bed heights, the flow patterns transit from bubbling flow (BF), to slug flow (SF) and to turbulent flow (TF). When the superficial gas velocity exceeds transition velocity u_{tr} , with increasing solid mass flux, the flow patterns transit from dilute phase flow (DPF) to fast fluidization (FF).

(2) The gas-solid slip characteristics **are** closely related to the superficial gas velocity and solid volume fraction. With increasing superficial gas velocity at constant solid volume fraction, the slip velocity increases accordingly. Moreover, the particle size shows no influence on the impact of solid volume fraction on slip velocity, and the solid volume ration shows exponential relationship with dimensionless slip velocity. The variation of slip characteristics of Geldart B particles and Geldart A particles have similar tendency and the relations between slip characteristics and operating conditions could be represented by empirical equations.

(3) The variation of pressure gradient and images captured by a high resolution digital CCD camera were used to identify and analyse the flow patterns of high velocity fluidization in a fast fluidized bed. Two flow patterns in high velocity fluidization were identified, i.e. dilute phase flow and fast fluidization, and the flow characteristics were further investigated. Moreover, a typical flow pattern diagram of a fast fluidized bed was plotted, and the equation for transition velocity was proposed to further illustrate the flow structures in high velocity fluidization.

(4)In the riser of the fast fluidized bed with Geldart B particles, four typical cluster structures, namely the macro-scale stripe-shaped cluster, saddle-shaped cluster, U-shaped cluster and the micro cluster are commonly found in the core-annulus flow regime, while only stripe-shaped cluster and micro clusters mainly forms in the dilute flow regime. Macro clusters with clear shapes start to appear in the region which is higher than about1/4 of the riser height.

(5) Particle clustering in fast fluidized bed may be due to the cohesive forces, the loss of momentum and the hydrodynamic forces. The average cluster size increases with increasing superficial gas velocity and particle size, however decreases with growing solid mass flux in the riser. When particle size is small, the effect of superficial gas

velocity on the average cluster size becomes less obvious, especially for particles less than 0.100 mm. The average cluster size usually presents a significant increase with the axial height varying from 1/5 to 1/3 of riser height, and then varies slightly with height in the higher region. It was found that for the large particles, the particles clusters changes with superficial gas velocity and solid mass flux, so the hydrodynamic forces plays an important role in promoting particle clustering. However, for the small particles, the cohesive forces may also have a significant effect on particle clustering.

(6) The cluster time fraction decreases with increasing superficial gas velocity and particle size, while it increases with rising solid mass flux. The effects of operating conditions on cluster time fraction also become less obvious for small particles. The cluster time fraction in the lower region is much higher than that of the higher bed.

7.1.2 Simulation work

(1) The superficial gas velocity plays a dominant role on the gas-solid flow characteristics in three perspectives. The increase of superficial gas velocity leads to remarkably decrease in the solid volume fraction of the riser. Meanwhile, the solid volume fraction of the riser becomes better distributed axially and radially.

(2) With the increase of seal loop aeration rate, the solid mass flux and the solid volume fraction are increased accordingly, and the increase magnitude becomes more visible with the height of the riser. Furthermore, the particle velocity in the centre of the riser is increased while that in the wall region is declined.

(3) As the bed inventory increases, the solid volume fraction of the lower riser demonstrates an increasing trend, and the particle velocity is also increased. When the bed inventory increases at fixed superficial gas velocity, the solid mass flux keeps constant. Notably, the connection between the downer and the cyclone may be blocked by excessive bed inventory, which impedes the solid circulation of the system.

(4) Based on MP-PIC method, the meso-scale flow structure of the fast fluidized bed was studied. Three typical patterns of particle clusters, i.e. stripe-shaped cluster, saddle-shaped cluster and U-shaped cluster were identified, and the evolutional processes of particle clusters were also illustrated.

(5) The distribution of cross-sectional average solid volume fraction and solid volume fraction of particle clusters shows similar trend in the shaped of U, while the distribution of velocity of particle clusters shows a reverse trend. With the increase of riser height, the volumefraction of particle clusters decreases gradually while the velocity of particle clusters is increasing, but the changes slow down with the riser height.

7.2 Future work

7.2.1 Experimental work

(1) The research of characteristics of particle clusters is conducted in a fast fluidized bed, while particle clusters can also be observed in the high-flux circulating fluidized bed. Moreover, the effect of structure of fluidized bed on particle clusters should also be considered. Therefore, the characteristics of particle clusters in the high-flux circulating fluidized bed and that under different fluidized bed should be further studied.

(2) The study of the characteristics of particle clusters are presented under atmospheric conditions, so the further study of particle clustering behaviour can be conducted at different pressures.

(3) The study on the effect of particle properties on the characteristics of particle clusters is limited, and it is notable that the formation mechanisms for particle clusters

with various particle diameters is quite different, the influence of particle properties on the particle cluster characteristics should be further investigated.

7.2.2 Simulation work

(1) The numerical simulation studies of particle clusters under different structures of riser and operating conditions could be conducted, which can provide more information for the design and optimization of fast fluidized bed system.

(2) Most of the studies on particle clusters in fast fluidized bed are simulated under atmospheric pressure conditions, the influence of temperature, pressure and chemical reactions can be coupled in the future simulations.

List of Publications

1. **Chen Dailin**, Liu Xuejiao, SunZiwen, ZhongWenqi, JinBaosheng. Experiments on particle cluster behaviors in a fast fluidized bed. ***Chinese Journal of Chemical Engineering,*** 2017, 25(9): 1153-1162. **(catalogued by SCI&EI，IF = 1.174)**
2. **Chen Dailin**, Liu Xuejiao, Zhong Wenqi,Shao Yingjuan, Jin Baosheng. Interactions of spout jets in a multiple-spouted bed. ***Canadian Journal of Chemical Engineering***, 2014, 92(6): 1150-1159. **(catalogued by SCI&EI，IF =1.356)**
3. **Chen Dailin**, Zhong Wenqi, Shao Yingjuan, Geng Chaming, Jin Baosheng. The flow pattern and transition of the fast fluidized bed. 2015, 36(11): 2403-2406. **(catalogued by EI).**
4. Sun Ziwen, **Chen Dailin**, Zhong Wenqi, Yu Aibing, MP-PIC simulation of particle clusters in fast fluidized bed risers, ***Journal of Chemical Industry and Engineering (China)***, 2018,69(8):3443-3451. **(catalogued by EI).**
5. **Chen Dailin,** Sun Ziwen, Zhong Wenqi, Jin Baosheng, Yu Aibing. Modelling on the hydrodynamics of full-loop circulating spouted bed. ***10th World Congress of Chemical Engineering International Symposium on Spouted Beds, Barcelona, Spain, 2017.***
6. **Chen Dailin**, Sun Ziwen, Zhong Wenqi, Jin Baosheng, Yu Aibing. Three-dimensional Full-loop Simulation of Hydrodynamics in the Fast Fluidized Bed. ***3rd International Symposium of Fluids and Thermal Engineering, Ningbo, China, 2017.***